

Notes for AMS Short Course on Discrete Differential Geometry **(ROUGH DRAFT)**

Keenan Crane, Yaron Lipman,
Justin Solomon, Johannes Wallner, Max Wardetzky

November 30, 2017

WARNING: This document is a *rough draft*, to be distributed to participants at the AMS Short Course on Discrete Differential Geometry in January, 2018. **There may be serious errors or omissions**, and some sections may not yet be complete.

CONTENTS

1	Introduction	3
2	Discrete Laplace Operators	5
2.1	Introduction	5
2.2	Smooth Laplacians on Riemannian manifolds	7
2.3	Discrete Laplacians	11
3	Discrete parametric surfaces	27
3.1	Introduction	27
3.2	Circular nets: a 3-system	32
3.3	K-nets: a 2-system	37
3.4	Applications: computing minimal surfaces	41
3.5	Applications: freeform architecture	46
4	Discrete Mappings	54
4.1	Overview	54
4.2	Triangulations and discrete mappings.	54
4.3	Convex combination mappings.	56

4.4	Proof of homeomorphism.	62
4.5	Variational principle.	66
4.6	Approximation of conformal mappings.	66
4.7	Surface to surface mappings.	68
4.8	Other Euclidean cone surfaces.	68
4.9	Convex combination in higher dimensions.	70
5	Discrete Conformal Geometry	73
5.1	Overview	73
5.2	Preliminaries	76
5.3	Angle Preservation	77
5.4	Circle Preservation	78
5.5	Cauchy-Riemann Equation	82
5.6	Metric Scaling	83
5.7	Conjugate Harmonic Pairs	86
5.8	Critical Points of Dirichlet Energy	87
5.9	Hodge Duality	89
5.10	Summary	90
6	Optimal Transport on Discrete Domains	94
6.1	Introduction	94
6.2	Motivation: From Probability to Discrete Geometry	96
6.3	Motivating Applications	102
6.4	One Problem, Many Discretizations	102
6.5	Beyond Transport	102

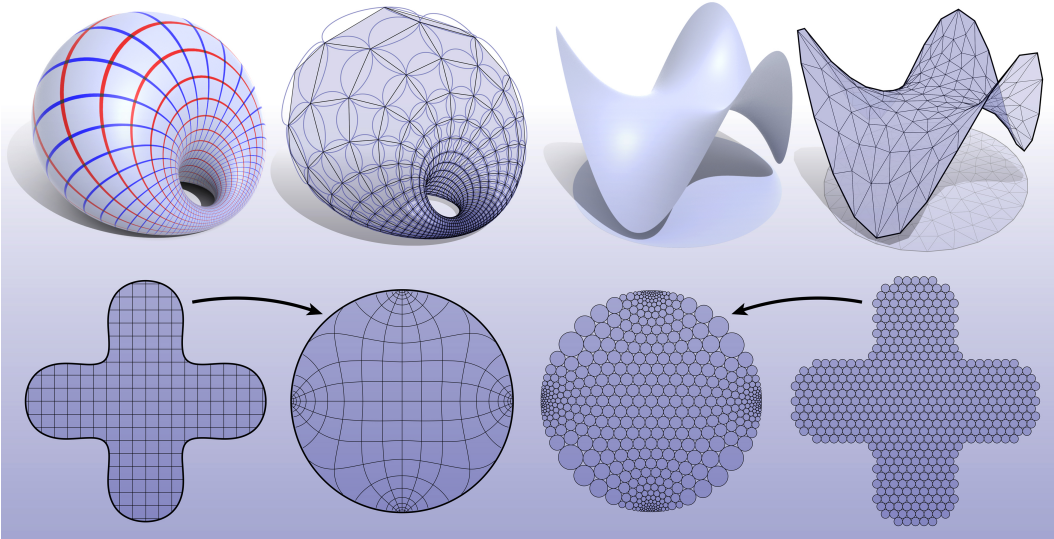


Figure 1: Discrete differential geometry re-imagines classical ideas from differential geometry without reference to differential calculus. For instance, surfaces parameterized by principal curvature lines are replaced by meshes made of circular quadrilaterals (top left), the maximum principle obeyed by harmonic functions is expressed via conditions on the geometry of a triangulation (top right), and complex-analytic functions can be replaced by so-called circle packings that preserve tangency relationships (bottom). These discrete surrogates provide a bridge between geometry and computation, while at the same time preserving important structural properties and theorems.

1 INTRODUCTION

The emerging field of *discrete differential geometry* (DDG) studies discrete analogues of smooth geometric objects, providing an essential link between analytical descriptions and computation. In recent years it has unearthed a rich variety of new perspectives on applied problems in computational anatomy/biology, computational mechanics, industrial design, computational architecture, and digital geometry processing at large.

The basic philosophy of discrete differential geometry is that a discrete object like a polyhedron is not merely an approximation of a smooth one, but rather a differential geometric object in its own right. In contrast to traditional numerical analysis which focuses on eliminating approximation error in the limit of refinement (*e.g.*, by taking smaller and smaller finite differences), DDG places an emphasis on the so-called “mimetic” viewpoint, where key properties of a system are preserved exactly, independent of how large or small the elements of a mesh might be. Just as algorithms for simulating mechanical systems might seek to exactly preserve physical invariants such as total energy or momentum, structure-preserving models

of discrete geometry seek to exactly preserve global geometric invariants such as total curvature. More broadly, DDG focuses on the discretization of objects that do not naturally fall under the umbrella of traditional numerical analysis.

The Game. The spirit of discrete differential geometry is well-illustrated by a “game” often used to develop discrete analogs of a given smooth object:

1. Write down several *equivalent* definitions in the smooth setting.
2. Apply each smooth definition to an object in the discrete setting.
3. See which properties of the original smooth object are preserved by each of the resulting discrete objects, which are invariably *inequivalent*.

Most often, no discrete object preserves *all* the properties of the original smooth one—a so-called *no free lunch* scenario. Nonetheless, the properties that are preserved often prove invaluable for particular applications and algorithms. Moreover, this activity yields some beautiful and unexpected consequences—such as a connection between conformal geometry and pure combinatorics, or a description of constant-curvature surfaces that requires no definition of curvature! These notes provide an incomplete overview of several contemporary topics in DDG—a broad overview can also be found in the recent *Notices* article, “*A Glimpse Into Discrete Differential Geometry*” by Crane & Wardetzky.

2 DISCRETE LAPLACE OPERATORS

Max Wardetzky

In this chapter¹ we review some important properties of Laplacians, smooth and discrete. We place special emphasis on a unified framework for treating smooth Laplacians on Riemannian manifolds alongside discrete Laplacians on graphs and simplicial manifolds. We cast this framework into the language of linear algebra, with the intent to make this topic as accessible as possible. We combine perspectives from smooth geometry, discrete geometry, spectral analysis, machine learning, numerical analysis, and geometry processing within this unified framework.

2.1 Introduction

The Laplacian is perhaps *the* prototypical differential operator for various physical phenomena. It describes, for example, heat diffusion, wave propagation, steady state fluid flow, and it is key to the Schrödinger equation in quantum mechanics. In Euclidean space, the Laplacian of a smooth function $u : \mathbb{R}^n \rightarrow \mathbb{R}$ is given as the sum of second partial derivatives along the coordinate axes,

$$\Delta u = - \left(\frac{\partial^2 u}{\partial x_1^2} + \frac{\partial^2 u}{\partial x_2^2} + \cdots + \frac{\partial^2 u}{\partial x_n^2} \right),$$

where we adopt the geometric perspective of using a minus sign.

2.1.1 Basic properties of Laplacians

The Laplacian has many intriguing properties. For the remainder of this exposition, consider an open and bounded domain $\Omega \subset \mathbb{R}^n$ and the L^2 inner product

$$(f, g) := \int_{\Omega} fg$$

on the linear space of square-integrable functions on Ω . Let $u, v : \Omega \rightarrow \mathbb{R}$ be two (sufficiently smooth) functions that vanish on the boundary of Ω . Then the

¹Note: this chapter is a pre-publication version of content appearing in *Generalized Barycentric Coordinates in Computer Graphics and Computational Mechanics* (CRC Press, 2017. All rights reserved.)

Laplacian Δ is a *symmetric* (or, to be precise, a formally self-adjoint) linear operator with respect to this inner product since integration by parts yields

$$(u, \Delta v) = \int_{\Omega} \nabla u \cdot \nabla v = (\Delta u, v). \quad (\text{SYM})$$

Here ∇ denotes the standard gradient operator and $\nabla u \cdot \nabla v$ denotes the standard inner product between vectors in \mathbb{R}^n . The choice of using a minus sign in the definition of the Laplacian makes this operator positive semi-definite since

$$(u, \Delta u) = \int_{\Omega} \nabla u \cdot \nabla u \geq 0. \quad (\text{PSD})$$

If one restricts to functions that vanish on the boundary of Ω , PSD implies that the only functions that lie in the kernel of the Laplacian ($\Delta u = 0$) are those functions that vanish on the entire domain. Moreover, properties SYM and PSD imply that the Laplacian can be diagonalized and its eigenvalues are nonnegative,

$$\Delta u = \lambda u \Rightarrow \lambda \geq 0.$$

Another prominent property of smooth Laplacians is the *maximum principle*. Let $u : \Omega \rightarrow \mathbb{R}$ be *harmonic*, i.e., $\Delta u = 0$. The maximum principle asserts that

$$u \text{ is harmonic} \Rightarrow u \text{ has no strict local maximum in } \Omega, \quad (\text{MAX})$$

where we no longer assume that u vanishes on the boundary of Ω . Likewise, no harmonic function can have a strict local minimum in Ω .

The maximum principle can be derived from another important property of harmonic functions, the *mean value property*. Consider a point $\mathbf{x} \in \Omega$ and a closed ball $B(\mathbf{x}, r)$ of radius r centered at \mathbf{x} that is entirely contained in Ω . Every harmonic function has the property that the value $u(\mathbf{x})$ can be recovered from the average of the values of u in the ball $B(\mathbf{x}, r)$:

$$u(\mathbf{x}) = \frac{1}{\text{vol}(B(\mathbf{x}, r))} \int_{B(\mathbf{x}, r)} u(\mathbf{y}) d\mathbf{y}.$$

A simple argument by contradiction shows that the mean value property implies property MAX.

The properties mentioned so far play an important role in applications; specifically, in the context of barycentric coordinates, they give rise to *harmonic coordinates* and *mean value coordinates*, see [26, 34, 35]. Below we discuss additional properties of Laplacians. For further reading we refer to the books [5, 25, 44] and the lecture notes [11, 16].

2.2 Smooth Laplacians on Riemannian manifolds

The standard Laplacian in \mathbb{R}^n can be expressed as

$$\Delta u = -\operatorname{div} \nabla u,$$

where div is the usual divergence operator acting on vector fields in \mathbb{R}^n . Written in integral form, the negative divergence operator is the (formal) adjoint of the gradient: If X is a vector field and $u : \Omega \rightarrow \mathbb{R}$ is a function that vanishes on the boundary of Ω , then

$$\int_{\Omega} \nabla u \cdot X = \int_{\Omega} u (-\operatorname{div} X).$$

This perspective can be generalized to Riemannian manifolds. The Laplacian plays an important role in the study of these curved spaces.

2.2.1 Exterior calculus

Although gradient and divergence can readily be defined on Riemannian manifolds, it is more convenient to work with the differential (or *exterior derivative*) d instead of the gradient and with the codifferential d^* instead of divergence.

The differential d is similar to (but not the same as) the gradient. Indeed, given a function $u : \Omega \rightarrow \mathbb{R}$, one has

$$du(X) = \nabla u \cdot X$$

for every vector field X . In particular, the differential does not require the notion of a metric, whereas the gradient does. The codifferential d^* is defined as the formal adjoint (informally, transpose) to d , in the same way as divergence is the adjoint of the gradient. In contrast to the divergence operator, which acts on vector fields, the codifferential d^* acts on 1-forms. A 1-form is a covector at every point of Ω , i.e., if X is a vector field on Ω and α is a 1-form, then $\alpha(X)$ is a real-valued function on Ω . In order to define the codifferential d^* , consider a 1-form α and a function $u : \Omega \rightarrow \mathbb{R}$ that vanishes on the boundary of Ω . Then

$$\int_{\Omega} du \cdot \alpha = \int_{\Omega} u d^* \alpha,$$

where the dot product is the inner product between covectors induced from the inner product between vectors. Notice that different from the differential d , the codifferential d^* does require the notion of a metric. The Laplacian of a function u can be expressed as

$$\Delta u = d^* du,$$

which is equivalent to the representation $\Delta u = -\operatorname{div} \nabla u$ given above.

In order to carry over this framework to manifolds, let M be a smooth orientable manifold with smooth Riemannian metric g . Suppose for simplicity that M is compact and has empty boundary. The Riemannian metric induces a pointwise inner product between tangent vectors on M , which, analogously to the above discussion, induces an inner product between 1-forms. More generally, one works with k -forms for $k \geq 0$. A 0-form, by convention, is a real-valued function on M . A 1-form can be thought of as an oriented 1-volume in the sense that applying a 1-form to a vector field returns a real value at every point. Likewise, a k -form for $k > 1$ can be thought of as an oriented k -volume in the sense of returning a real number at every point when applied to an ordered k -tuple (parallelepiped) of tangent vectors. As a consequence, k -forms can be integrated over (sub)manifolds of dimension k . In the sequel, we let Λ^k denote the linear space of k -forms on M .

Analogous to the L^2 inner product between function in \mathbb{R}^n , let

$$(\alpha, \beta)_k := \int_M g(\alpha, \beta) \operatorname{vol}_g$$

denote the L^2 inner product between k -forms α and β on M , where, by slight abuse of notation, we let $g(\alpha, \beta)$ denote the (pointwise) inner product induced by the Riemannian metric.

The differential $d : \Lambda^k \rightarrow \Lambda^{k+1}$ maps k -forms to $(k+1)$ -forms for $0 \leq k \leq \dim M$, where one sets $d\alpha = 0$ for any k -form with $k = \dim M$. One can define the differential acting on k -forms by postulating *Stokes' theorem*,

$$\int_U d\alpha = \int_{\partial U} \alpha,$$

for every k -form α and every (sufficiently smooth) submanifold $U \subset M$ of dimension $(k+1)$ with boundary ∂U . If one asserts this equality as the defining property of the differential d , then it immediately follows that $d \circ d = 0$ since the boundary of a boundary of a manifold is empty ($\partial(\partial U) = \emptyset$).

The codifferential d^* , taking $(k+1)$ -forms back to k -forms, is the (formal) adjoint of d with respect to the L^2 inner products on k - and $(k+1)$ -forms. It is defined by requiring that

$$(d\alpha, \beta)_{k+1} = (\alpha, d^*\beta)_k$$

for all k -forms α and all $(k+1)$ -forms β . Finally, the *Laplace–Beltrami operator* $\Delta : \Lambda^k \rightarrow \Lambda^k$ acting on k -forms is defined as

$$\Delta\alpha := dd^*\alpha + d^*d\alpha.$$

Notice that this expression reduces to $\Delta u = d^*du$ for 0-forms (functions) on M . It follows almost immediately from the definition of the Laplacian that a k -form α is *harmonic* ($\Delta\alpha = 0$) if and only if α is closed ($d\alpha = 0$) and co-closed ($d^*\alpha = 0$).

From a structural perspective it is important to note that properties SYM, PSD, and MAX mentioned earlier remain true (among various other properties) in the setting of Riemannian manifolds. For further details on exterior calculus and the Laplace–Beltrami operator, we refer to [44].

2.2.2 Hodge decomposition

Every sufficiently smooth k -form α on M admits a unique decomposition

$$\alpha = d\mu + d^*\nu + h,$$

known as the *Hodge decomposition* (or Hodge–Helmholtz decomposition), where μ is a $(k - 1)$ -from, ν is a $(k + 1)$ -form and h is a harmonic k -form. This decomposition is unique and orthogonal with respect to the L^2 inner product on k -forms,

$$0 = (d\mu, d^*\nu)_k = (h, d\mu)_k = (h, d^*\nu)_k,$$

which immediately follows from the fact that $d \circ d = 0$ and the fact that harmonic forms satisfy $dh = d^*h = 0$. The Hodge decomposition can be thought of as a (formal) application of the well-known fact from linear algebra that the orthogonal complement of the kernel of a linear operator is equal to the range of its adjoint (transpose) operator.

By duality between vector fields and 1-forms, the Hodge decomposition for 1-forms carries over to a corresponding decomposition for vector fields into curl-free and divergence-free components, which has applications for fluid mechanics [3] and Maxwell’s equations for electromagnetism [29].

Geometrically, the Hodge decomposition establishes relations between the Laplacian and global properties of manifolds. Indeed, the linear space of harmonic k -forms is finite-dimensional for compact manifolds and isomorphic to $H^k(M; \mathbb{R})$, the k -th cohomology of M . As an application of this fact, consider a compact orientable surface without boundary. Then the dimension of the space of harmonic 1-forms is equal to twice the genus of the surface, that is, this dimension is zero for the 2-sphere, two for the two-dimensional torus, four for a genus two surface (pretzel) and so on. Hence the Laplacian provides global information about the topology of the underlying space.

For a thorough treatment of Hodge decompositions, including the case of manifolds with boundary, we refer to [46].

2.2.3 The spectrum

One cannot speak about the Laplacian without discussing its spectrum. On a compact orientable manifold without boundary, it follows from the inequality

$$(\Delta u, u)_0 = (du, du)_1 \geq 0$$

that the spectrum is nonnegative and that the only functions in the kernel of the Laplacian are constant functions. Thus zero is a trivial eigenvalue of the Laplacian with a one-dimensional space of eigenfunctions. The next (non-trivial) eigenvalue $\lambda_1 > 0$ is much more interesting. By the min-max principle, this eigenvalue satisfies

$$\lambda_1 = \min_{(u,1)_0=0} \frac{(du, du)_1}{(u, u)_0},$$

where one takes the minimum over all functions that are L^2 -orthogonal to the constants. Higher eigenvalues can be obtained by successively applying the min-max principle to the orthogonal complements of the eigenspaces of lower eigenvalues.

The first non-trivial eigenvalue λ_1 tells a great deal about the geometry of the underlying Riemannian manifold. As an example, consider Cheeger's isoperimetric constant

$$\lambda_C := \inf_{N \neq \emptyset} \left\{ \frac{\text{vol}_{n-1}(N)}{\min(\text{vol}_n(M_1), \text{vol}_n(M_2))} \right\},$$

where N runs over all compact codimension-1 submanifolds that partition M into two disjoint open sets M_1 and M_2 with $N = \partial M_1 = \partial M_2$. Intuitively, the optimal N for which λ_C is attained partitions M into two sets that have maximal volume and minimal perimeter. As an example, suppose that M has the shape of the surface of a smooth dumbbell. Then N is a curve going around the axis of the dumbbell at the location where the dumbbell is thinnest.

A relation of Cheeger's constant to the first non-trivial eigenvalue of the Laplacian is provided by the Cheeger inequalities

$$\frac{\lambda_C^2}{4} \leq \lambda_1 \leq c(K\lambda_C + \lambda_C^2),$$

where the constant c only depends on dimension and $K \geq 0$ provides a lower bound on the Ricci curvature of M in the sense that $Ric(M, g) \geq -K^2(n-1)$; see [10, 13].

Recall that for surfaces, Ricci curvature and Gauß curvature coincide. The first non-trivial eigenvalue of the Laplacian is thus related to the metric problem of minimal cuts—thus providing a relation between an analytical quantity (the first eigenvalue) and a purely geometric quantity (the Cheeger constant). Intuitively, if λ_1 is small, then M must have a small bottleneck; vice-versa, if λ_1 is large, then M is somewhat thick.

Equipped with the full set of eigenfunctions $\{\varphi_i\}$ of the Laplace–Beltrami operator, one can perform Fourier analysis on manifolds by decomposing any square-integrable function u into its Fourier-modes,

$$u = \sum_i (u, \varphi_i)_0 \varphi_i,$$

provided that one chooses the eigenfunctions such that $(\varphi_i, \varphi_i) = \delta_{ij}$. (Notice that $(\varphi_i, \varphi_j)_0 = 0$ is automatic for eigenfunctions belonging to different eigenvalues.) The Fourier perspective is of great relevance in signal and geometry processing.

Maintaining a spectral eye on geometry, it is natural to ask the inverse question: How much *geometric* information can be reconstructed from information about the Laplacian? If the entire Laplacian is known on a smooth manifold, then one can reconstruct the metric, for example, by using the expression of Δ in local coordinates. If, however, “only” the spectrum is known, then less can be said in general. For example, Kac’s famous question *Can one hear the shape of a drum?* [36], that is, whether the entire geometry can be inferred from the spectrum alone, has a negative answer: There exist isospectral but non-isometric manifolds [30, 47].

2.3 Discrete Laplacians

Discrete Laplacians can be defined on simplicial manifolds or, more generally, on graphs. We treat the case of graphs first and discuss simplicial manifolds further below. We let our discussion of discrete Laplacians be guided by drawing upon the smooth setup above.

2.3.1 Laplacians on graphs

Consider an undirected graph $\Gamma = (V, E)$ with vertex set V and edge set E . For simplicity we only consider finite graphs here. Suppose that every edge $e \in E$ between vertices $i \in V$ and $j \in V$ carries a real-valued weight $\omega_e = \omega_{ij} = \omega_{ji} \in \mathbb{R}$.

We discuss below how weights can be chosen; suppose for now that such a choice has been made. A discrete Laplacian acting on a function $u : V \rightarrow \mathbb{R}$ is defined as

$$(Lu)_i := \sum_{j \sim i} \omega_{ij}(u_i - u_j), \quad (1)$$

where the sum ranges over all vertices j that are connected by an edge with vertex i .² This allows for representing the linear operator L as a matrix by

$$L_{ij} := \begin{cases} -\omega_{ij} & \text{if there is an edge between } i \text{ and } j, \\ \sum_{k \sim i} \omega_{ik} & \text{if } i = j, \\ 0 & \text{otherwise.} \end{cases}$$

The matrix L is called the discrete Laplace matrix. This definition may seem to come a bit out of the blue. In order to see how it relates to smooth Laplacians, consider again the smooth case and the quantity

$$E_D[u] := \frac{1}{2} \int_{\Omega} \|\nabla u\|^2,$$

which is known as the *Dirichlet energy* of u . In the discrete setup, one may discretize the gradient ∇u along an edge $e = (i, j)$ as the finite difference $(u_i - u_j)$. Accordingly, one defines discrete Dirichlet energy as

$$E_D[u] := \frac{1}{2} \sum_{e \in E} \omega_{ij}(u_i - u_j)^2,$$

where the sum ranges over all edges. One then has

$$\text{(discrete)} \quad E_D[u] = \frac{1}{2} u^T L u \quad \text{vs.} \quad \text{(smooth)} \quad E_D[u] = \frac{1}{2} (u, \Delta u)_0,$$

which justifies calling L a Laplace matrix. Due to this representation (and using the language of partial differential equations [25]) we call discrete Laplacians of the form (1) *weakly defined* instead of *strongly defined*. We return to this distinction below.

Weakly defined discrete Laplacians of the form (1) are always symmetric—they satisfy SYM due to the assumption that $\omega_{ij} = \omega_{ji}$. However, whether or not a discrete Laplacian satisfies (at least some of) the other properties of the smooth setting heavily depends on the choice of weights.

The simplest choice of weights is to set $\omega_{ij} = 1$ whenever there is an edge between vertices i and j . This results in the so-called *graph Laplacian*. The diagonal

²Some authors include a division by vertex weights in the definition of Laplacians on graphs. Such a division arises naturally when considering strongly defined Laplacian, instead of weakly defined Laplacians. We come back to this distinction below.

entries of the graph Laplacian are equal to the degree of the respective vertex, that is, the number of edges adjacent to that vertex. The graph Laplacian is just a special case of what we call a *Laplacian on graphs* here.

Positive edge weights are a natural choice if weights resemble transition probabilities of a random walker. Discrete Laplacians with positive weights are always positive semi-definite PSD and, just like in the smooth setting, they only have the constant functions in their kernel provided that the graph is connected. As a word of caution we remark that positivity of weights is *not* necessary to guarantee PSD. Below we discuss Laplacians that allow for (some) negative edge weights but still satisfy PSD.

Laplacians with positive edge weights always satisfy the mean value property since every harmonic function u (a function for which $Lu = 0$) satisfies

$$u_i = \sum_{j \sim i} l_{ij} u_j \quad \text{with} \quad l_{ij} = \frac{\omega_{ij}}{L_{ii}} > 0.$$

Therefore, discrete Laplacians with positive weights also satisfy the maximum principle MAX since $\sum_{j \sim i} l_{ij} = 1$ and thus u_i is a convex combination of its neighbors u_j for discrete harmonic functions.

2.3.2 The spectrum

As in the smooth case, one cannot discuss discrete Laplacians without mentioning their spectrum and their eigenfunctions, which provide a fingerprint of the structure of the underlying graph.

As an example consider again Cheeger's isoperimetric constant. In order to define this constant in the discrete setting consider a partitioning of Γ into two disjoint subgraphs Γ_1 and $\bar{\Gamma}_1$ such that the vertex set V of Γ is the disjoint union of the vertex sets V_1 of Γ_1 and \bar{V}_1 of $\bar{\Gamma}_1$. Here a subgraph of Γ denotes a graph whose vertex set is a subset of the vertex set of Γ such that two vertices in the subgraph are connected by an edge if and only if they are connected by an edge in Γ . For positive edge weights, the discrete Cheeger constant (sometimes called *conductance* of a weighted graph) is defined as

$$\lambda_C := \min \left\{ \frac{\text{vol}(\Gamma_1, \bar{\Gamma}_1)}{\min(\text{vol}(\Gamma_1), \text{vol}(\bar{\Gamma}_1))} \right\},$$

where

$$\text{vol}(\Gamma_1, \bar{\Gamma}_1) := \sum_{i \in V_1, j \notin V_1} \omega_{ij} \quad \text{and} \quad \text{vol}(\Gamma_1) := \sum_{i \in V_1, j \in V_1} \omega_{ij},$$

and similarly for $\text{vol}(\bar{\Gamma}_1)$. Notice that for the case of the graph Laplacian $\text{vol}(\Gamma_1)$ equals twice the number of edges in Γ_1 and $\text{vol}(\Gamma_1, \bar{\Gamma}_1)$ equals the number of edges with one vertex in Γ_1 and another vertex in its complement.³

Similar to the smooth case, one then obtains the Cheeger inequalities

$$\frac{\lambda_C^2}{2} \leq \tilde{\lambda}_1 \leq 2\lambda_C,$$

where $\tilde{\lambda}_1$ is the first nontrivial eigenvalue of the rescaled Laplace matrix

$$\tilde{L} := SLS,$$

where S is a diagonal matrix with $S_{ii} = 1/\sqrt{\omega_{ii}}$. This rescaling is necessary since λ_C is invariant under a uniform rescaling of edge weights (and so is \tilde{L}), whereas L scales linearly with the edge weights. A proof of the discrete Cheeger inequalities for the case of the graph Laplacians ($\omega_{ij} = 1$) can be found in [15]; the proof for arbitrary positive edge weights is nearly identical.

The Cheeger constant—and alongside the corresponding partitioning of Γ into the two disjoint subgraphs Γ_1 and $\bar{\Gamma}_1$ —has applications in graph clustering, since the edges connecting Γ_1 and $\bar{\Gamma}_1$ tend to “cut” the graph along its bottleneck [37].

Any discrete Laplacian (having positive edge weights or not) that satisfies SYM and PSD can be used for Fourier analysis on graphs. Indeed, let $\{\varphi_i\}$ be the eigenfunctions of L , chosen such that $\varphi_i^T \varphi_j = \delta_{ij}$. Then one has

$$u = \sum_i (u^T \varphi_i) \varphi_i,$$

just like in the smooth setting. This decomposition of discrete functions on graphs into their Fourier modes has a plethora of applications in geometry processing; see [39] and references therein.

As in the smooth setting, it is natural to ask the inverse question of how much geometric information can be inferred from information about the Laplacian. Recall that in the smooth case, knowing the full Laplacian allows for recovering the Riemannian metric. Similarly, in the discrete case it can be shown that for simplicial surfaces the knowledge of the cotan weights (that are introduced below) for discrete Laplacian allows for reconstructing edge lengths (i.e., the discrete metric) of the underlying mesh up to a global scale factor [55]. If, however, only the spectrum of the Laplacian is known, then there exist isospectral but non-isomorphic graphs [9].

³Some authors use a different version of the respective volumes in the definition of the Cheeger constant, resulting in different versions of the Cheeger inequalities; see [48].

In fact, for the case of the cotan Laplacian (see below), the exact same isospectral domains considered in [30] that were originally proposed for showing that “One cannot hear the shape of a drum” for smooth Laplacians work in the discrete setup.

A curious fact concerning the connection between discrete Laplacians and the underlying geometry is *Rippa’s theorem* [43]: The Delaunay triangulation of a fixed point set in \mathbb{R}^n minimizes the Dirichlet energy of any piecewise linear function over this point set. In [14], this result is taken a step further, where the authors show that the spectrum of the cotan Laplacian obtains its minimum on a Delaunay triangulation in the sense that the i -th eigenvalue of the cotan Laplacian of any triangulation of a fixed point set in the plane is bounded below by the i -th eigenvalue resulting from the cotan Laplacian associated with the Delaunay triangulation of the given point set.

2.3.3 Laplacians on simplicial manifolds

Recall that in the smooth case, Laplacians acting on k -forms take the form

$$\Delta = dd^* + d^*d.$$

In order to mimic this construction in the discrete setting, one requires a bit more structure than just an arbitrary graph. To this end, consider a simplicial manifold, such as a triangulated surface. We keep referring to this manifold as M . As in the smooth case, for simplicity, suppose that M is orientable and has no boundary.

Simplicial manifolds allow for a natural definition of discrete k -forms as duals of k -cells. Indeed, every 0-form is a function defined on vertices, a 1-form α is dual to edges, that is, $\alpha(e)$ is a real number for any oriented 1-cell (oriented edge), a 2-form is dual to oriented 2-cells, and so forth. In the sequel, let the linear space of discrete k -forms (better known as simplicial cochains) be denoted by C^k .

As in the smooth case, the discrete differential δ (better known as the coboundary operator) maps discrete k -forms to discrete $(k+1)$ -forms, $\delta : C^k \rightarrow C^{k+1}$. Again, as in the smooth case, the discrete differential can be defined by *postulating Stokes’ formula*: Let α be a discrete k -form. Then one requires that

$$\delta\alpha(\sigma) = \alpha(\partial\sigma)$$

for all $(k+1)$ -cells σ , where ∂ denotes the simplicial boundary operator. The simplicial boundary operator, when applied to a vertex returns zero (since vertices do not have a boundary). When applied to an oriented edge, the boundary operator returns the difference between the edge’s vertices. Likewise, ∂ applied to an oriented

2-cell σ returns the sum of oriented edges of σ (with the orientation induced by that of σ). Since the boundary of a boundary is empty ($\partial \circ \partial = 0$) one has $\delta \circ \delta = 0$, just like in the smooth case. Notice that the definition of δ does not require the notion of inner products.

In order to define the discrete codifferential δ^* one additionally requires an inner product $(\cdot, \cdot)_k$ on the linear space of k -forms for each k . Below we discuss the construction of such inner products. Given a fixed choice of inner products on discrete k -forms, the codifferential is defined by requiring that

$$(\delta\alpha, \beta)_{k+1} = (\alpha, \delta^*\beta)_k$$

for all k -forms α and all $(k+1)$ -forms β , and the discrete *strongly defined* Laplacian acting on k -forms takes the form

$$\mathbb{L} := \delta\delta^* + \delta^*\delta. \quad (2)$$

This perspective is that of *discrete exterior calculus* (DEC) [16, 19], where—by slight abuse of notation—inner products are referred to as “discrete Hodge stars”.

Strongly defined Laplacians are self-adjoint with respect to the inner products $(\cdot, \cdot)_k$ on discrete k -forms, since

$$(\mathbb{L}\alpha, \beta)_k = (\delta\alpha, \delta\beta)_{k+1} + (\delta^*\alpha, \delta^*\beta)_{k-1} = (\alpha, \mathbb{L}\beta)_k.$$

Moreover, strongly defined Laplacians are always positive semi-definite PSD, since

$$(\mathbb{L}\alpha, \alpha)_k = (\delta\alpha, \delta\alpha)_{k+1} + (\delta^*\alpha, \delta^*\alpha)_{k-1} \geq 0.$$

In particular, a discrete k -form is harmonic ($\mathbb{L}\alpha = 0$) if and only if $\delta\alpha = \delta^*\alpha = 0$, just like in the smooth setting.

2.3.4 Strongly and weakly defined Laplacians

Every strongly defined Laplacian as given by (2) has a weakly defined cousin L acting on discrete functions u . The weak version is obtained by requiring that at every vertex i the resulting function Lu is equal to

$$(Lu)_i := (\mathbb{L}u, 1_i)_0 = (\delta^*\delta u, 1_i)_0 = (\delta u, \delta 1_i)_1,$$

where 1_i is the indicator function of vertex i . In particular, let \mathbb{M}_0 and \mathbb{M}_1 be the symmetric positive definite matrices that encode the inner products between 0-forms and 1-forms, respectively,

$$(u, v)_0 = u^T \mathbb{M}_0 v \quad \text{and} \quad (\alpha, \beta)_1 = \alpha^T \mathbb{M}_1 \beta.$$

Then the weakly and strongly defined Laplacians satisfy, respectively,

$$L = \delta^T \mathbb{M}_1 \delta \quad \text{and} \quad \mathbb{L} = \mathbb{M}_0^{-1} L.$$

As an example, consider diagonal inner products on 0-forms and 1-forms,

$$(u, v)_0 = \sum_{i \in V} m_i u_i v_i \quad \text{and} \quad (\alpha, \beta)_1 = \sum_{e \in E} \omega_e \alpha(e) \beta(e),$$

with positive vertex weights $m_i > 0$ and positive edge weights $\omega_e > 0$. The resulting strongly defined Laplacian acting on 0-forms (functions) takes the form

$$(\mathbb{L}u)_i = \frac{1}{m_i} \sum_{j \sim i} \omega_{ij} (u_i - u_j)$$

and its associated weakly defined cousin is the Laplacians on graphs defined in (1). In particular, if $\omega_e = 1$, one recovers the graph Laplacian as the weak version.

2.3.5 Hodge decomposition

Given a choice of inner products for k -forms on simplicial manifolds, one always obtains a discrete Hodge decomposition. Indeed, for every discrete k -form α one has

$$\alpha = \delta\mu + \delta^*\nu + h,$$

where μ is a $(k-1)$ -from, ν is a $(k+1)$ -form and h is a harmonic k -from ($\mathbb{L}h = 0$). As in the smooth case, this decomposition is unique and orthogonal with respect to the inner products on k -forms,

$$0 = (\delta\mu, \delta^*\nu)_k = (h, \delta\mu)_k = (h, \delta^*\nu)_k,$$

which immediately follows from $\delta \circ \delta = 0$ and the fact that harmonic forms satisfy $\delta h = \delta^*h = 0$.

Akin to the smooth case, the Hodge decomposition establishes relations to global properties of simplicial manifolds, since the linear space of harmonic k -forms is isomorphic to the k -th simplicial cohomology of the simplicial manifold M . Again, as an application of this fact, consider a compact simplicial surface without boundary. Then the dimension of the space of harmonic 1-forms is equal to twice the genus of the surface—*independent* of the concrete choice of inner products on k -forms.

2.3.6 The cotan Laplacian

We conclude the discussion of Laplacians on simplicial manifolds by providing an important example of inner products. In [53], Whitney constructs a map from simplicial k -forms (k -cochains) to piecewise linear differential k -forms. In a nutshell, the idea is to linearly interpolate simplicial k -forms across full-dimensional cells. As the simplest example, consider linear interpolation of 0-forms (functions) on vertices. This kind of interpolation can be extended to arbitrary k -forms. The resulting map

$$W : C^k \rightarrow L^2 \Lambda^k$$

takes simplicial k -forms to square-integrable k -forms on the simplicial manifold, where we assume each simplex to carry the standard Euclidean structure. The Whitney map is the right inverse of the so-called de Rham map,

$$\alpha(\sigma) = \int_{\sigma} W(\alpha)$$

for all discrete k -forms α and all k -cells σ . For details we refer to [53]. The Whitney map W is a chain map—it commutes with the differential ($dW = W\delta$) and thus factors to cohomology.

Dodziuk and Patodi [22] use the Whitney map in order to define an inner product on discrete k -forms (k -cochains) by

$$(\alpha, \beta)_k := \int_M g(W\alpha, W\beta) \text{vol}_g,$$

where (in our case) g denotes a piecewise Euclidean metric on the simplicial manifold. From the perspective of the *Finite Element Method* (FEM), Whitney's construction is a special case of constructing stable finite elements; see [2].

For triangle meshes the resulting strongly defined Laplacian acting on 0-forms (functions) takes the form

$$\mathbb{L} = \mathbb{M}_0^{-1} L,$$

where \mathbb{M}_0 is the *mass matrix* given by

$$(\mathbb{M}_0)_{ij} := \begin{cases} \frac{A_{ij}}{12} & \text{if } i \sim j, \\ \frac{A_i}{6} & \text{if } i = j, \\ 0 & \text{otherwise.} \end{cases}$$

Here A_{ij} denotes the combined area of the two triangles incident to edge (i, j) and A_i is the combined area of all triangles incident to vertex i . The corresponding weakly

defined Laplacian L is the so-called *cotan Laplace* matrix with entries

$$L_{ij} := \begin{cases} -\frac{1}{2} (\cot \alpha_{ij} + \cot \beta_{ij}) & \text{if } i \sim j, \\ -\sum_{j \sim i} L_{ij} & \text{if } i = j, \\ 0 & \text{otherwise,} \end{cases}$$

where α_{ij} and β_{ij} are the two angles opposite to edge (i, j) .

The cotan Laplacian has been rediscovered many times in different contexts [23, 24, 42]; the earliest explicit mention seems to go back to MacNeal [40], but perhaps it was already known at the time of Courant. The cotan Laplacian has been enjoying a wide range of applications in geometry processing (see [16, 39, 45] and references therein), including barycentric coordinates, mesh parameterization, mesh compression, fairing, denoising, spectral fingerprints, shape clustering, shape matching, physical simulation of thin structures, and geodesic distance computation.

The construction of discrete Laplacians based on inner products can be extended from simplicial surfaces to meshes with (not necessarily planar) polygonal faces [1, 7, 8]. The cotan Laplacian has furthermore been extended to semi-discrete surfaces [12] as well as to subdivision surfaces [18].

2.3.7 Desiderata for ‘perfect’ discrete Laplacians

Structural properties of discrete Laplacians play an important role in applications to geometry processing, e.g., when solving the ubiquitous Poisson problem

$$\mathbb{L}u = f$$

for a given right hand side f and an unknown function u with Dirichlet boundary conditions. For solving this problem, one often prefers to work with the weak formulation ($Lu = \mathbb{M}_0 f$) instead of the strong one ($\mathbb{L}u = f$) since the weakly defined cousins of strongly defined Laplacians satisfy properties **SYM** and **PSD**, which allows for efficient linear solvers.

Which properties are desirable for discrete Laplacians on top of **SYM** and **PSD**? Moreover, is it possible to maintain *all* properties of smooth Laplacians in the discrete case? To answer this question, we follow [52].

Smooth Laplacians are differential operators that act *locally*. Locality can be represented in the discrete case by working with (weakly defined) discrete Laplacians based on edge weights:

$$\text{vertices } i \text{ and } j \text{ do not share an edge} \Rightarrow \omega_{ij} = 0. \quad (\text{LOC})$$

This property reflects locality of action by ensuring that if vertices i and j are not connected by an edge, then changing the function value u_j at a vertex j does not alter the value $(Lu)_i$ at vertex i . Property LOC results in sparse matrices, which can be treated efficiently in computations.

In the smooth setting, linear functions on \mathbb{R}^2 are in the kernel of the standard Laplacian on Euclidean domains. For discrete Laplacians on a graph Γ , this property translates into requiring that $(Lu)_i = 0$ at each interior vertex whenever Γ is embedded into the plane with straight edges and u is a *linear* function on the plane, point-sampled at the vertices of Γ , i.e.,

$$\Gamma \subset \mathbb{R}^2 \text{ embedded and } u : \mathbb{R}^2 \rightarrow \mathbb{R} \text{ linear} \Rightarrow (Lu)_i = 0 \text{ at interior vertices. (LIN)}$$

In applications, this *linear precision* property is desirable for de-noising of surface meshes [20] (where one expects to remove normal noise only but not to introduce tangential vertex drift), mesh parameterization [27, 33] (where one expects planar regions to remain invariant under parameterization), and plate bending energies [45] (which must vanish for flat configurations).

Furthermore, it is often natural and desirable to require positive edge weights:

$$\text{vertices } i \text{ and } j \text{ share an edge} \Rightarrow \omega_{ij} > 0. \quad (\text{POS})$$

This requirement implies PSD and is a sufficient (but not a necessary) condition for a *discrete maximum principle* MAX. In diffusion problems corresponding to $u_t = -\Delta u$, POS ensures that flow travels from regions of higher potential to regions of lower potential.

The combination LOC+SYM+POS is related to Tutte's embedding theorem for planar graphs [31, 50]: Positive weights associated to edges yield a straight-line embedding of an abstract planar graph for a fixed convex boundary polygon. Tutte's embedding is unique for a given set of positive edge weights, and it satisfies LIN by construction since each interior vertex (and therefore its x - and y -coordinate) is a convex combination of its adjacent vertices with respect to the given edge weights.

2.3.8 No free lunch

Given an arbitrary simplicial mesh, does there exist a discrete Laplacian that satisfies *all* of the desirable properties LOC, SYM, POS, and LIN? Let us start by asking this question for the discrete Laplacians considered so far.

Perhaps the simplest case is to consider the graph Laplacian ($\omega_{ij} = 1$). This Laplacian clearly satisfies LOC+SYM+POS, but in general fails to satisfy LIN due its indifference to the geometry of a graph's embedding.

Next, consider the cotan Laplacian. The edge weights of the cotan Laplacian turn out to be a special case of weights arising from *orthogonal duals*. In particular, edge weights of the cotan Laplacian arise by considering the orthogonal dual obtained by connecting circumcenters of (primal) triangles of a planar triangulation by straight edges; see Figure 2 (left). More generally, consider a graph embedded into the plane with straight edges that do not cross. An orthogonal dual is a realization of the dual graph in the plane, with straight dual edges that are orthogonal to their corresponding primal ones. Different from primal edges, dual edges are allowed to cross each other. Together, a primal graph and its orthogonal dual determine edge weights (on primal edges) defined as the ratio between the *signed* lengths of dual edges and the unsigned lengths of primal edges,

$$\omega_e = \frac{|\star e|}{|e|}.$$

Here, $|e|$ denotes the usual Euclidean length, whereas $|\star e|$ denotes the *signed* Euclidean length of the dual edge. The sign is obtained as follows. The dual edge $\star e$ connects two dual vertices $\star f_1$ and $\star f_2$, corresponding to the primal faces f_1 and f_2 , respectively. The sign of $|\star e|$ is positive if along the direction of the ray from $\star f_1$ to $\star f_2$, the primal face f_1 lies before f_2 . The sign is negative otherwise. For the special case of duals that arise from connecting circumcenters of a triangulation of the plane, one obtains the cotan weights.

Edge weights obtained from orthogonal duals give rise to discrete Laplacians that satisfy LOC+SYM+LIN. Indeed, while LOC and SYM are immediate by construction, LIN is equivalent to dual edges forming a *closed* polygon (dual face) per primal vertex. To see this equivalence, consider the x - and y - Euclidean coordinates of primal vertices, considered as linear functions over the plane. These linear functions (and therefore all linear functions) are in the kernel of the discrete Laplacian arising from edge weights obtained from orthogonal duals if and only if dual edges form closed polygons around all inner primal vertices. In fact, this equivalence can be reformulated in terms of a century-old result by Maxwell and Cremona [17, 41]: Regard the primal graph as a stress framework with positive edge weights corresponding to contracting edges and negative edge weights regarded as expanding edges. Then the stress framework is in static equilibrium if and only if it satisfies LIN (which constitutes the Euler-Lagrange equations for the equilibrium) and thus if and only if there exists an orthogonal dual network that gives rise to the given primal edge weights.

While properties LOC+SYM+LIN are always satisfied by discrete Laplacians

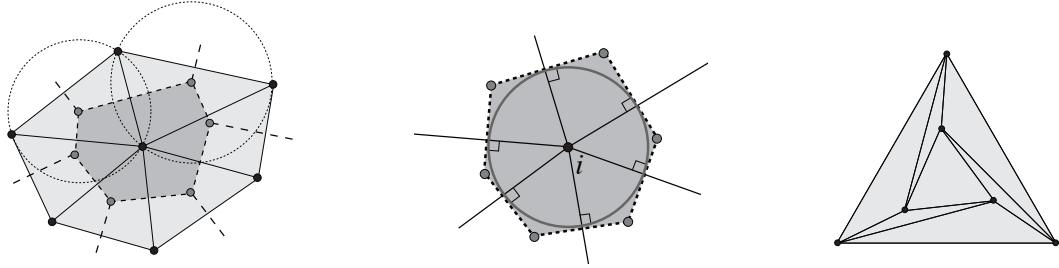


Figure 2: Left: Primal graph (solid lines) and orthogonal circumcentric dual graph (dashed lines) defining the cotan Laplacian. Middle: Mean value weights correspond to dual edges tangent to the unit circle around a primal vertex. Right: The projection of the Schönhardt polytope does not allow for a discrete Laplacian satisfying SYM+LOC+LIN+POS.

arising from orthogonal duals, these Laplacians fail to satisfy POS in general. In fact, so-called *weighted Delaunay triangulations* turn out to be the only triangulations that give rise to positive edge weights arising from orthogonal duals and thus admit discrete Laplacians that satisfy LOC+SYM+LIN+POS. For example, for the cotan Laplacian one has positive edge weights $(\cot \alpha_{ij} + \cot \beta_{ij}) > 0$ if and only if $(\alpha_{ij} + \beta_{ij}) < \pi$. This is the case if and only if the triangulation is Delaunay. As a consequence, if one starts with a triangulation of the plane that is not Delaunay, then the cotan Laplacian fails to satisfy POS. One may restore POS by successive edge flips (thereby changing the combinatorics of the triangulation that one started with) until one arrives at a Delaunay triangulation [6]. Unfortunately, the number of required edge flips to obtain a Delaunay triangulation from an arbitrary given triangulation cannot be bounded a priori. Therefore, while the approach of edge flips yields discrete Laplacians satisfying SYM+LIN+POS, it fails to yield Laplacian that satisfy LOC in general.

Like Rippa's theorem discussed above, the relation between discrete Laplacians and weighted Delaunay triangulations provides an instance of the intricate connection between properties of discrete differential operators and purely geometric properties.

For completeness, in order to illustrate that there indeed *are* discrete Laplacians that satisfy any choice of three but not all four of the desired properties LOC+SYM+LIN+POS, consider dropping the requirement of symmetry of edge weights. In this case, one enters the realm of barycentric coordinates [33], where one may still obtain an orthogonal *dual face per primal vertex*, but these dual faces no longer fit together to form a consistent dual graph; see Figure 2 (middle). In particular, for the case dual edges with positive lengths, one obtains edge weights satisfying LOC+LIN+POS but not SYM. Floater et al. [28] explored a subspace of this case: a one-parameter family of linear precision barycentric coordinates, including the

widely used mean value and Wachspress coordinates. Langer et al. [38] showed that each member of this family corresponds to a specific choice of orthogonal dual face per primal vertex.

Summing up, for general simplicial meshes there exists no discrete Laplace operator that satisfies all of the desired properties LOC+SYM+LIN+POS simultaneously; see 2 (right) for a simple example of a mesh that does not admit such a ‘perfect’ discrete Laplacian. This limitation provides a taxonomy on existing literature and explains the plethora of existing discrete Laplacians: Since not all desired properties can be fulfilled simultaneously, it depends on the application at hand to design discrete Laplacians that are tailored towards the specific needs of a concrete problem.

2.3.9 Convergence

Another important desideratum is *convergence*: In the limit of refinement of simplicial manifolds that approximate a smooth manifold, one seeks to approximate the smooth Laplacian by a sequence of discrete ones. For applications this is important in terms of obtaining discrete operators that are as mesh-independent as possible—re-meshing a given shape should not result in a drastically different Laplacian.

A closely related concept to convergence is *consistency*. A sequence of discrete Laplacians $(\Delta_n)_{n \in \mathbb{N}}$ is called consistent, if $\Delta_n u \rightarrow \Delta u$ for all appropriately chosen functions u . For example, it can be shown that Laplacians on point clouds, such as those considered in [4] are consistent; see [21].

Convergence is more difficult to show than consistency since it additionally requires that the solutions u_n to the Poisson problems $\Delta_n u_n = f$ converge (in an appropriate norm) to the solution u of $\Delta u = f$. Discussing convergence in detail is beyond the scope of this short survey. Roughly speaking, Laplacians on simplicial manifolds converge to their smooth counterparts (in an appropriate operator norm) if the inner products on discrete k -forms used for defining simplicial Laplacians converge to the inner products on smooth k -forms. In this case, one obtains convergence of solutions to the Poisson problem, convergence of the components of the Hodge decomposition, convergence of eigenvalues [22, 24, 32, 51, 54], and (using different techniques) convergence of Cheeger cuts [49].

REFERENCES

- [1] M. Alexa and M. Wardetzky. Discrete Laplacians on general polygonal meshes. *ACM Transactions on Graphics*, 30(4):102:1–102:10, 2011.
- [2] D. N. Arnold, R. S. Falk, and R. Winther. Finite element exterior calculus, homological techniques, and applications. *Acta Numerica*, 15:1–155, 2006.
- [3] V. Arnold and B. Khesin. *Topological Methods in Hydrodynamics*, volume 125 of *Applied Mathematical Sciences*. Springer, New York, 1998.
- [4] M. Belkin, J. Sun, and Y. Wang. Constructing Laplace operator from point clouds in \mathbb{R}^d . In *Proceedings of SODA*, pages 1031–1040, 2009.
- [5] M. Berger. *A Panoramic View of Riemannian Geometry*. Springer, Berlin-Heidelberg, 2003.
- [6] A. I. Bobenko and B. A. Springborn. A discrete Laplace–Beltrami operator for simplicial surfaces. *Discrete and Computational Geometry*, 38(4):740–756, 2007.
- [7] F. Brezzi, K. Lipnikov, and M. Shashkov. Convergence of mimetic finite difference methods for diffusion problems on polyhedral meshes. *SIAM J. Num. Anal.*, 43:1872–1896, 2005.
- [8] F. Brezzi, K. Lipnikov, and V. Simoncini. A family of mimetic finite difference methods on polygonal and polyhedral meshes. *Math. Models Methods Appl. Sci.*, 15:1533–1553, 2005.
- [9] R. Brooks. Isospectral graphs and isospectral surfaces. *Séminaire de théorie spectrale et géométrie*, 15:105–113, 1997.
- [10] P. Buser. A note on the isoperimetric constant. *Annales scientifiques de l’École Normale Supérieure*, 15(2):213–230, 1982.
- [11] Y. Canzani. Analysis on manifolds via the Laplacian, 2013. Lecture notes, Harvard University.
- [12] W. Carl. A Laplace operator on semi-discrete surfaces. *Foundations Comp. Math.*, 16:1115–1150, 2016.
- [13] I. Chavel. *Eigenvalues in Riemannian Geometry*. Academic Press, Orlando, San Diego, New York, London, Toronto, Montreal, Sydney, Tokyo, 1984.
- [14] R. Chen, Y. Xu, C. Gotsman, and L. Liu. A spectral characterization of the Delaunay triangulation. *Computer Aided Geometric Design*, 27(4):295–300, 2010.
- [15] F. Chung. Four proofs for the Cheeger inequality and graph partition algorithms. In *Proceedings of the ICCM*, 2007.
- [16] K. Crane, F. de Goes, M. Desbrun, and P. Schröder. Digital geometry processing with discrete exterior calculus. In *ACM SIGGRAPH 2013 Courses*, SIGGRAPH ’13. ACM, 2013.
- [17] L. Cremona. *Graphical statics (Transl. of Le figure reciproche nelle statica graphica, Milano, 1872)*. Oxford University Press, 1890.
- [18] F. de Goes, M. Desbrun, M. Meyer, and T. DeRose. Subdivision exterior calculus for geometry processing. *ACM Transactions on Graphics*, 35(4):133:1–133:11, 2016.
- [19] M. Desbrun, A. Hirani, M. Leok, and J. E. Marsden. Discrete Exterior Calculus. 2005. arXiv:math.DG/0508341.
- [20] M. Desbrun, M. Meyer, P. Schröder, and A. H. Barr. Implicit fairing of irregular meshes using diffusion and curvature flow. In *Proceedings of ACM SIGGRAPH*, pages 317–324, 1999.

- [21] T. Dey, P. Ranjan, and Y. Wang. Convergence, stability, and discrete approximation of Laplace spectra. In *Proceedings of SODA*, pages 650–663, 2010.
- [22] J. Dodziuk and V. K. Patodi. Riemannian structures and triangulations of manifolds. *Journal of Indian Math. Soc.*, 40:1–52, 1976.
- [23] R. Duffin. Distributed and Lumped Networks. *Journal of Mathematics and Mechanics*, 8:793–825, 1959.
- [24] G. Dziuk. Finite elements for the Beltrami operator on arbitrary surfaces. In S. Hildebrandt and R. Leis, editors, *Partial Differential Equations and Calculus of Variations*, volume 1357 of *Lec. Notes Math.*, pages 142–155. Springer, Berlin Heidelberg, 1988.
- [25] L. C. Evans. *Partial Differential Equations*, volume 19 of *Graduate Studies in Mathematics*. AMS, Providence, Rhode Island, 1998.
- [26] M. S. Floater. Mean value coordinates. *Comput. Aided Geom. Des.*, 20(1):19–27, 2003.
- [27] M. S. Floater and K. Hormann. Surface parameterization: A tutorial and survey. In N. A. Dodgson, M. S. Floater, and M. A. Sabin, editors, *Advances in Multiresolution for Geometric Modeling*, pages 157–186. Springer, Berlin, Heidelberg, 2005.
- [28] M. S. Floater, K. Hormann, and G. Kós. A general construction of barycentric coordinates over convex polygons. *Adv. Comp. Math.*, 24(1–4):311–331, 2006.
- [29] T. Frankel. *The Geometry of Physics: An Introduction*. Cambridge University Press, 2004.
- [30] C. Gordon, D. L. Webb, and S. Wolpert. One cannot hear the shape of a drum. *Bull. Amer. Math. Soc.*, 27:134–138, 1992.
- [31] S. J. Gortler, C. Gotsman, and D. Thurston. Discrete one-forms on meshes and applications to 3D mesh parameterization. *Computer Aided Geometric Design*, 23(2):83–112, 2006.
- [32] K. Hildebrandt, K. Polthier, and M. Wardetzky. On the convergence of metric and geometric properties of polyhedral surfaces. *Geometriae Dedicata*, 123:89–112, 2006.
- [33] K. Hormann and N. Sukumar, editors. *Generalized Barycentric Coordinates in Computer Graphics and Computational Mechanics*. Taylor & Francis, CRC Press, Boca Raton, 2017.
- [34] P. Joshi, M. Meyer, T. DeRose, B. Green, and T. Sanocki. Harmonic coordinates for character articulation. *ACM Trans. Graph.*, 26(3):71:1–71:10, 2007.
- [35] T. Ju, S. Schaefer, and J. Warren. Mean value coordinates for closed triangular meshes. *ACM Trans. Graph.*, 24(3):561–566, 2005.
- [36] M. Kac. Can one hear the shape of a drum? *The American Mathematical Monthly*, 73(4):1–23, 1966.
- [37] R. Kannan, S. Vempala, and A. Vetta. On clusterings: Good, bad and spectral. *Journal of the ACM*, 51(3):497–515, 2004.
- [38] T. Langer, A. Belyaev, and H.-P. Seidel. Spherical barycentric coordinates. In *Siggraph/Eurographics Sympos. Geom. Processing*, pages 81–88, 2006.
- [39] B. Lévy and H. R. Zhang. Spectral mesh processing. In *ACM SIGGRAPH 2010 Courses*, SIGGRAPH ’10. ACM, 2010.
- [40] R. MacNeal. The Solution of Partial Differential Equations by Means of Electrical Networks, 1949. PhD thesis, California Institute of Technology.
- [41] J. C. Maxwell. On reciprocal figures and diagrams of forces. *Phil. Mag.*, 27:250–261, 1864.
- [42] U. Pinkall and K. Polthier. Computing discrete minimal surfaces and their conjugates. *Experim. Math.*, 2:15–36, 1993.
- [43] S. Rippa. Minimal roughness property of the Delaunay triangulation. *Computer Aided Geometric Design*, 7(6):489–497, 1990.
- [44] S. Rosenberg. *The Laplacian on a Riemannian manifold*. Number 31 in Student Texts.

London Math. Soc., 1997.

- [45] M. Rumpf and M. Wardetzky. Geometry processing from an elastic perspective. *GAMM Mitteilungen*, 37(2):184–216, 2014.
- [46] G. Schwarz. *Hodge Decomposition - A Method for Solving Boundary Value Problems*, volume 1607 of *Lecture Notes in Mathematics*. Springer, Berlin Heidelberg, 1995.
- [47] T. Sunada. Riemannian coverings and isospectral manifolds. *Ann. of Math.*, 121(1):169–186, 1985.
- [48] T. Sunada. Discrete geometric analysis. In *Proc. Symposia in Pure Mathematics*, volume 77, pages 51–83, 2007.
- [49] N. G. Trillos, D. Slepčev, J. von Brecht, T. Laurent, and X. Bresson. Consistency of Cheeger and ratio graph cuts. *J. Mach. Learn. Res.*, 17(1):6268–6313, 2016.
- [50] W. T. Tutte. How to draw a graph. *Proc. London Math. Soc.*, 13(3):743–767, 1963.
- [51] M. Wardetzky. Discrete Differential Operators on Polyhedral Surfaces—Convergence and Approximation. Ph.D. Thesis, Freie Universität Berlin, 2006.
- [52] M. Wardetzky, S. Mathur, F. Kälberer, and E. Grinspun. Discrete Laplace operators: No free lunch. In *Siggraph/Eurographics Sympos. Geom. Processing*, pages 33–37, 2007.
- [53] H. Whitney. *Geometric Integration Theory*. Princeton Univ. Press, 1957.
- [54] S. O. Wilson. Cochain algebra on manifolds and convergence under refinement. *Topology and its Applications*, 154:1898–1920, 2007.
- [55] W. Zeng, R. Guo, F. Luo, and X. Gu. Discrete heat kernel determines discrete Riemannian metric. *Graphics Models*, 74(4):121–129, July 2012.

3 DISCRETE PARAMETRIC SURFACES

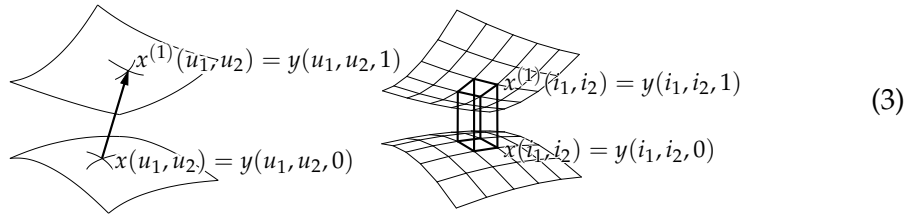
Johannes Wallner

3.1 Introduction

Discrete parametric surfaces are discrete analogues of smooth parametric surfaces. A discrete surface is not just an approximation of its smooth counterpart, but is the subject of a separate discrete theory. As it turns out, a systematic theory of parametric surfaces can be based on integrable systems, and the discrete case can be interpreted as a “master” case which contains smooth surfaces as a limit.

This section on discrete parametric surfaces is organized as follows: We first introduce notation. Two particular kinds of discrete surfaces are discussed next: circular nets in §3.2, and K-nets in §3.3 are examples of a 3-system and a 2-system, respectively. In the case of K-nets, we also discuss the relation to the sine-Gordon equation. We then show applications within mathematics in §3.4, cf. [4], and the connection with freeform architecture in §3.5, cf. [18].

Discrete, semidiscrete, and continuous surfaces. The simplest case of a continuous surface is a point $x(u_1, u_2)$ of space depending on two parameters u_1, u_2 . A discrete surface $x(i_1, i_2)$ is the same, only the parameters i_1, i_2 are integers. The notion of *transformation* of a surface usually refers to a pair $x(u_1, u_2)$ and $x^{(1)}(u_1, u_2)$ of surfaces which are in a certain relation (images taken from [7]):



The theory of transformations was fully developed in the 1920s [9]. Well known instances are Darboux transforms, Bäcklund transforms, or the Christoffel transform (which relates minimal surfaces with conformal mappings into sphere, and leads to the Weierstrass representation of minimal surfaces in terms of meromorphic functions). A sequence of surfaces created by iterated application of a transformation rule constitutes a *semidiscrete* object $y(u_1, u_2, i_3)$, where i_3 is an integer parameter:

$$y(u_1, u_2, 0) = x(u_1, u_2), \quad y(u_1, u_2, 1) = x^{(1)}(u_1, u_2), \quad y(u_1, u_2, 2) = x^{(11)}(u_1, u_2), \dots$$

Transformations of discrete surfaces can be treated in a similar way: With

$$y(i_1, i_2, 0) = x(i_1, i_2), \quad y(i_1, i_2, 1) = x^{(1)}(i_1, i_2), \quad y(i_1, i_2, 2) = x^{(11)}(i_1, i_2), \dots$$

we define a mapping y from \mathbb{Z}^3 to space. We see that a sequence of discrete k -dimensional surfaces is nothing but a discrete $(k+1)$ -dimensional surface, and the special role of the first two parameters disappears.

A particular feature of many transformations is that they enjoy *Bianchi permutability*: If x has transforms $x^{(1)}$ and $x^{(2)}$, then there exists $x^{(12)}$ which is a transform of both $x^{(1)}$ and $x^{(2)}$ simultaneously (image taken from [7]):

$$\begin{aligned} &x^{(12)}(u_1, u_2) = z(u_1, u_2, 1, 1) \\ &z(u_1, u_2, 1, 0) = x^{(1)}(u_1, u_2) \\ &z(u_1, u_2, 0, 1) = x^{(2)}(u_1, u_2) \end{aligned} \tag{4}$$

By iterating this procedure we create a two-dimensional lattice of surfaces, i.e., a mapping “ z ” from $\mathbb{R}^2 \times \mathbb{Z}^2$ to space. It can be seen as a semidiscrete 4-dimensional surface $z(u_1, u_2, i_3, i_4)$. It is very interesting that the 2D discrete surfaces $x(i_1, i_2) = z(u_1, u_2, i_3, i_4)$ contained in this 4-dimensional semidiscrete object typically exhibit geometric properties similar to discrete surfaces: *The transformations which apply to a class of smooth surfaces provide guidelines on how to find a class of analogous discrete surfaces.*

However if x is a discrete surface to begin with, a 2-dimensional lattice of surfaces is nothing but a 4-dimensional discrete surface $z(i_1, i_2, i_3, i_4)$. The special role of the first two parameters disappears.

It is a key principle of discrete differential geometry that the smooth theory can be obtained by a limit process from the discrete one. We can let a 2D discrete surface converge to a smooth surface, a 3D discrete surface to a sequence of smooth surfaces, and various further limits are possible.

History. Integrable equations. An important feature of parametric surfaces is the relation to integrable equations. This connection has a long tradition. The best known example concerns surfaces whose Gauss curvature equals the constant -1 , and a special “asymptotic” parametrization of these surfaces. It turns out that the angle $\phi(u_1, u_2)$ between parameter lines obeys the sine-Gordon equation

$$\partial_{12}\phi = \sin\phi. \tag{5}$$

It is a fact that for any solution $\phi(u_1, u_2)$, another solution $\phi^{(1)}$, called the *Bäcklund transform* of ϕ , can be defined by

$$\partial_1 \phi^{(1)} = \partial_1 \phi + 2a \sin \frac{\phi + \phi^{(1)}}{2}, \quad \partial_2 \phi^{(1)} = -\partial_2 \phi + \frac{2}{a} \sin \frac{\phi^{(1)} - \phi}{2}.$$

This Bäcklund transformation of functions corresponds directly to the Bäcklund transformation of surfaces: ϕ and $\phi^{(1)}$ are angle functions associated with a Bäcklund pair of surfaces x and $x^{(1)}$. There is even a Bianchi permutability theorem analogous to the surface case: With the arrow symbolizing the Bäcklund relation, we have

$$\begin{array}{ccc} \phi & \xrightarrow{\hspace{1cm}} & \phi^{(1)} \\ \phi \searrow & \Rightarrow \exists \phi^{(12)} \text{ such that } & \phi \nearrow \phi^{(1)} \\ & & \phi^{(2)} \end{array} \quad \begin{array}{c} \phi^{(1)} \\ \swarrow \quad \searrow \\ \phi^{(12)} \\ \nearrow \quad \nwarrow \\ \phi^{(2)} \end{array} \quad (6)$$

Surfaces of constant Gaussian curvature have been instrumental in the development of the systematic “integrability” theory of discrete surfaces. At the beginning, the original Bäcklund transform of smooth surfaces [1] and its permutability properties [3, Vol. II, §383] were found. Discrete surfaces were constructed in the 1950’s [19, 24]. The connection of discrete surfaces to the discrete Hirota equation, which is a discrete analogue of the sine-Gordon equation, was revealed by [5]. We are coming back to this topic in §3.3.

Typically, for any particular class of surfaces (e.g. the circular nets of §3.2 or the K-nets of §3.3) one needs some “elementary” geometric construction in order to establish multidimensional discrete surfaces. Since the discrete case serves as a *master theory* from which the continuous one is obtained by a limit process, that elementary geometric theorem can be seen as the discrete analogue of the various kinds of integrability needed to construct surfaces and their transformations.

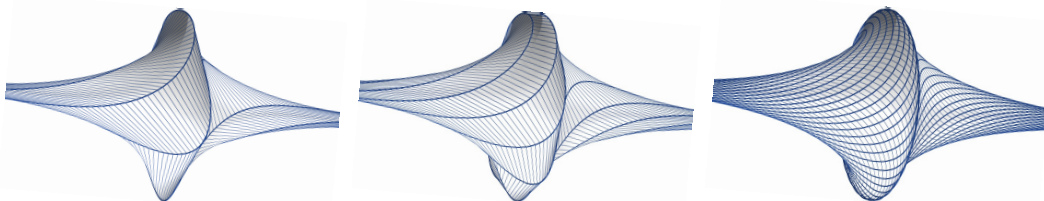


Figure 3: Discrete K-surfaces. Their defining property is that in each face, opposite edges have equal length, and in each vertex, all four incident edges are co-planar. Discrete surfaces can converge to semidiscrete or continuous surfaces.

Curvatures.. Surfaces classes can be equivalently characterized by different properties. E.g., a surface is minimal \iff it is locally area-minimizing \iff its mean curvature vanishes \iff it has a parametrization in terms of meromorphic functions $f(z)$ and $g(z)$ such that fg^2 is holomorphic, with $x(u, v) = \frac{1}{2} \operatorname{Re} \int_0^{u+iv} (f(z)(1-g(z)^2), if(z)(1+g(z)^2), 2f(z)g(z)) dz$.

It is this Weierstrass representation which leads to a discretization in the context of *parametric* surfaces (see §3.4). Area minimization is the basis of a different discretization, which is not parametric [14].

It is a curious fact that many classes of surfaces which are originally defined via *curvature* (K-surfaces, minimal surfaces, cmc surfaces) had well-established discrete counterparts which were defined by an equivalent characterization not involving curvatures. However, meanwhile curvatures for discrete surfaces have been studied in a systematic way, and there are general concepts of curvatures [6, 11] which apply to the discrete surface classes mentioned above.

Discretization principles. The difficulty of assigning curvatures illustrates an important issue: It is not clear a priori which of the various equivalent properties of a class of smooth surfaces should be the one which guides the discretization. However, a discretization is good, or worthy of further investigation, if not just one property carries over from the smooth to the discrete setting, but more than one. For example, the variational definition of discrete minimal surfaces by [14] leads to simplicial minimal surfaces which not only minimize area, but which also exhibit an associated family of minimal surfaces. The guiding principle of discretization in the case of *parametric* surfaces often is integrability, or (in the discrete case), so-called multidimensional consistency.

Notation for continuous and discrete nets. A smooth parametric surface maps a parameter value $u \in \mathbb{R}^d$ to a point $x(u) \in \mathbb{R}^n$. Derivatives are described by the symbols

$$\partial_k x, \partial_{kl} x, \dots$$

A discrete parametric surface maps an *integer* parameter value $u = (u_1, \dots, u_d) \in \mathbb{Z}^d$ to a point $x(u) \in \mathbb{R}^n$. The role of derivatives is played by differences, e.g.

$$\begin{aligned}\Delta_1 x(u_1, u_2, \dots, u_d) &= x(u_1 + 1, u_2, \dots, u_d) - x(u_1, u_2, \dots, u_d), \\ \Delta_2 x(u_1, u_2, \dots, u_d) &= x(u_1, u_2 + 1, \dots, u_d) - x(u_1, u_2, \dots, u_d).\end{aligned}$$

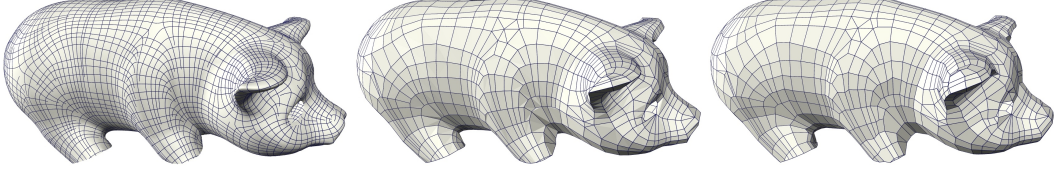
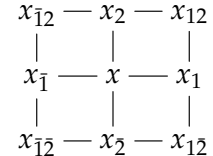


Figure 4: Left: A conjugate parametric surface $x : U \subset \mathbb{R}^2 \rightarrow \mathbb{R}^3$ covers most of this geometric shape. Center: discrete parametric surfaces extracted by sampling have elementary quadrilaterals which are almost planar. Right: Global optimization makes all faces planar. This optimization problem is feasible because we are already very close to a solution.

In general, we use a lower index i to indicate a forward shift in the i -th parameter, and the index \bar{i} to indicate a backward shift.

$$x_k(\dots, x_k, \dots) = x(\dots, u_k + 1, \dots) \quad x_{\bar{k}}(\dots, x_k, \dots) = x(\dots, u_k - 1, \dots)$$

We use the notation $x_{kk}, x_{kl}, x_{\bar{k}l}$, and so on for iterated shifts. E.g. in a 2-dimensional net $x(u_1, u_2)$ we use a diagram like the one shown in the inset figure to indicate the immediate neighborhood of a general point $x(u_1, u_2)$. The forward difference operator is expressed as $\Delta_k x = x_k - x$.



Examples. Conjugate surfaces. A *conjugate* parametrization is one where infinitesimal parameter quads are co-planar. For 2-surfaces, this means that we require

$$\begin{aligned} & 3 \text{ vol} (\text{c.h.}(x(u), x(u_1 + \varepsilon, u_2), x(u_1, u_2 + \varepsilon), x(u_1 + \varepsilon, u_2 + \varepsilon))) / \varepsilon^4 \\ &= \det(x(u_1 + \varepsilon, u_2) - x(u), x(u_1, u_2 + \varepsilon) - x(u), x(u_1 + \varepsilon, u_2 + \varepsilon) - x(u)) / 2\varepsilon^4 \\ &\approx \det(\varepsilon \partial_1 x, \varepsilon \partial_2 x, \varepsilon \partial_1 x + \varepsilon \partial_2 x + 2\varepsilon^2 \partial_{12} x) / 2\varepsilon^4 \\ &= \det(\partial_1 x, \partial_2 x, \partial_{12} x) = 0 \end{aligned}$$

The “ \approx ” sign means equality up to remainder terms in the Taylor expansion as $\varepsilon \rightarrow 0$. We say that all infinitesimal elementary quadrilaterals of the net are co-planar. It is obvious how to translate the defining property

$$\det(\partial_k x, \partial_l x, \partial_{kl} x) = 0$$

to the discrete case: a discrete conjugate net is defined by

$$\det(\Delta_k x, \Delta_l x, \Delta_{kl} x) = 0.$$



Figure 5: Left: 2D circular net. Right: An elementary cell of a 3D circular net.

Generically this is equivalent to

$$\begin{array}{c} x_l — x_{kl} \\ | \qquad | \\ x — x_k \end{array} \quad \text{co-planar,} \quad (7)$$

or to existence of coefficients c^{lk}, c^{kl} associated with the elementary quadrilateral $xx_kx_lx_{kl}$, such that

$$\Delta_k \Delta_l x = c^{lk} \Delta_k x + c^{kl} \Delta_l x.$$

For reasons which become apparent later, we use this property as definition of a discrete conjugate surface (a synonym is *conjugate net*).

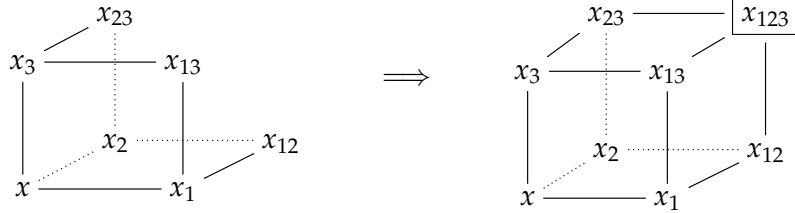
3.2 Circular nets: a 3-system

Definition 3.1. A circular net is a discrete parametric surface where all elementary quadrilaterals are co-circular, i.e., for every vertex x and neighbors x_k, x_l , there is a circle which contains the four vertices x, x_k, x_l, x_{kl} .

Obviously, a circular net is also conjugate. The following result concerning existence of conjugate nets and circular nets implicitly contains the definition of a 3-system:

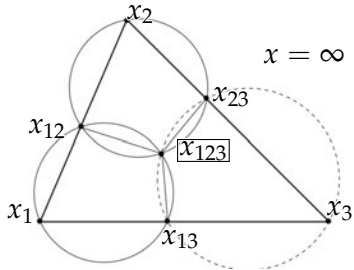
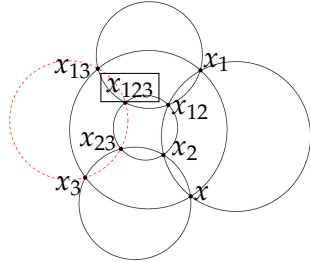
Theorem 3.2. Conjugacy of nets is a 3-system: Generically, a conjugate net $x(u_1, u_2, u_3)$ is uniquely determined by arbitrary initial values $x(0, u_2, u_3)$ and $x(u_1, 0, u_3)$ and $x(u_1, u_2, 0)$. The same applies to circularity.

Proof. Consider a combinatorial cube with diagonal $x—x_{123}$, see the figure below. Assume that the quadrilaterals $xx_1x_2x_{12}$, $xx_1x_3x_{13}$, $xx_2x_3x_{23}$ adjacent to x are plane. Does there exist x_{123} such that the three quads adjacent to x_{123} are planar?



The answer is trivially yes for a conjugate net in \mathbb{RP}^n , $n \geq 3$, since the planes carrying the three missing faces are given by three vertices each, and x_{123} is the intersection of these planes.

For circular nets, this is not so obvious: The circumcircles of the three three quads incident to x_{123} are given by three points each, but do they intersect in a common point x_{123} ? The answer is yes: whenever the three quads $xx_kx_lx_{kl}$ have a circumcircle, then the three circumcircles of $x_1, x_{12}, x_{13}, x_2, x_{23}, x_{21}, x_3, x_{31}, x_{32}$ meet in a common point x_{123} .



For a proof we observe that the statement is not affected by Möbius transformations. We therefore apply an inversion to move x to infinity. Circles passing through x become straight lines, so x_{kl} becomes a point of the edge x_kx_l of the triangle $x_1x_2x_3$. The statement about circumcircles is now shown by using elementary geometry. \square

The proof makes it clear that the “right” geometric setting for conjugate nets is projective space, whereas circular nets should be treated in Möbius geometry.

Proposition 3.3. *Assume that $x(i_1, i_2, i_3)$ is a conjugate net, and that all elementary quadrilaterals which contain vertices with $i_1 = 0$ or $i_2 = 0$ or $i_3 = 0$ are circular. Then, generically, circularity propagates through the net: all elementary quads are circular. The same is true for n -dimensional nets with $n \geq 3$.*

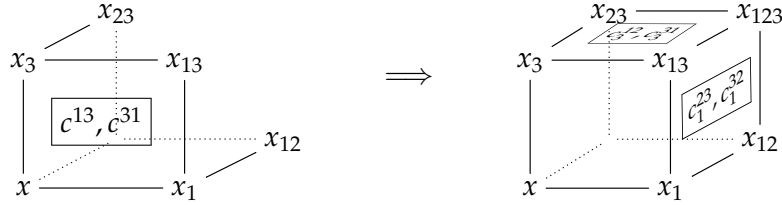
Proof. It is sufficient to show this statement for a 3-cell with diagonal $x—x_{123}$ where the three quads incident to x are circular. If we require circularity, then x_{123} is

uniquely determined as the intersection of circumcircles of the quads incident to it. But x_{123} is *already* uniquely determined by the intersection of the planes which carry those quads. It follows that x_{123} is the same regardless if it is computed via the 3-system “conjugacy” or via the 3-system “circularity”. \square

Lemma 3.4. *Consider the coefficient functions used in the definition of a conjugate net, see Eqn. 7, $\Delta_k \Delta_l x = c^{lk} \Delta_k x + c^{kl} \Delta_l x$. For a conjugate 3-net, there is a birational mapping*

$$(c^{12}, c^{21}, c^{23}, c^{32}, c^{31}, c^{13}) \xrightarrow{\phi} (c_3^{12}, c_3^{21}, c_1^{23}, c_1^{32}, c_2^{31}, c_2^{13})$$

of the coefficients in quads incident to x , to coefficients in quads incident to x_{123} .



Proof. We use the “product rule” $\Delta_j(a \cdot b) = a_j \cdot \Delta_j b + \Delta_j a \cdot b$ to expand

$$\begin{aligned} \Delta_i \Delta_j \Delta_k x &= \Delta_i(c^{kj} \Delta_j x + c^{jk} \Delta_k x) = c_i^{kj} \Delta_i \Delta_j x + \Delta_i c^{kj} \Delta_j x + \dots \\ &= (c_i^{kj} c^{ji} + c_i^{jk} c^{ki}) \Delta_i x + (c_i^{kj} c^{ij} + \Delta_i c^{kj}) \Delta_j x + (c_i^{jk} c^{ik} + \Delta_i c^{jk}) \Delta_k x. \end{aligned}$$

Permuting indices yields

$$\begin{aligned} \Delta_j \Delta_k \Delta_i x &= (c_j^{ik} c^{kj} + c_j^{ki} c^{ij}) \Delta_j x + (c_j^{ik} c^{jk} + \Delta_j c^{ik}) \Delta_k x + (c_j^{ki} c^{ji} + \Delta_j c^{ki}) \Delta_i x. \\ \Delta_k \Delta_i \Delta_j x &= (c_k^{ji} c^{ik} + c_k^{ij} c^{jk}) \Delta_k x + (c_k^{ji} c^{ki} + \Delta_k c^{ji}) \Delta_i x + (c_k^{ij} c^{kj} + \Delta_k c^{ij}) \Delta_j x. \end{aligned}$$

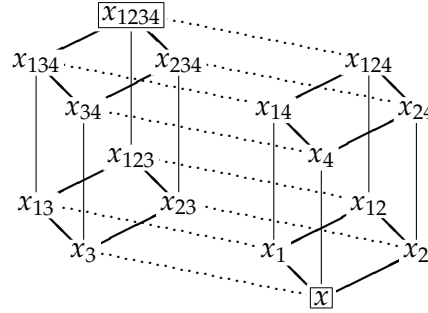
Since $\Delta_i \Delta_j \Delta_k$ is invariant w.r.t. permutations of indices, and generically the first derivatives are linearly independent, we get

$$\Delta_i c^{jk} = c_k^{ij} c^{jk} + c_k^{ji} c^{ik} - c_i^{jk} c^{ik} \quad (i \neq j \neq k \neq i).$$

This is a linear system in the 6 variables $(c_3^{12}, \dots, c_1^{32})$. Its explicit solution by matrix inversion yields the desired rational mapping ϕ , and analogously for the inverse ϕ^{-1} . Even if ϕ was derived under the assumption of linearly independent first derivatives, it may be applied to all input data. \square

The following result implicitly defines an *integrable* discrete 3-system:

Theorem 3.5. *Conjugacy is a 4-consistent (i.e., integrable) 3-system: If in the combinatorial 4-cube with diagonal $x \dots x_{1234}$, conjugacy is imposed on the faces incident to x (and by the 3-system property , on the the four 3-cubes incident to x), then there is a generically unique choice of x_{1234} such that also the remaining quads of the hypercube enjoy the property. Analogously, circularity is 4-consistent.*



Proof. The hypercube with diagonal $x—x_{1234}$ contains four 3-cubes incident with x_{1234} . Within each of these cubes, x_{1234} is found as the intersection of 3 quads. E.g. from the cube with diagonal $x—x_{123}$ we get

$$x_{1234} \in \text{span}(x_{12}x_{123}x_{124}) \cap \text{span}(x_{13}x_{132}x_{134}) \cap \text{span}(x_{14}x_{142}x_{143}). \quad (8)$$

The cubes with diagonals $x—x_{124}$, $x—x_{134}$, and $x—x_{224}$ yield three more ways to express x_{1234} as intersection of three planes. We must show that all these are equal.

(1) Each of the quads mentioned above is the intersection of two adjacent 3-cubes. Counting shows that these six cubes are actually all four 3-cubes incident with x_{1234} .

(2) Thus, in case of dimension ≥ 4 and general position, Eqn. 8 is transformed into an intersection of four 3-spaces (each is the span of a 3-cube). Since all 3-cubes incident to x_{1234} occur in this expression, the transformed expression is invariant w.r.t. permutation of indices \Rightarrow all ways of computing x_{1234} yield the same result.

(3) x_{1234} can also be found in an alternative way, namely by using the coefficients c^{ij} defined by Eqn. 7. We can compute them in the quads incident to x , apply ϕ , and compute vertices $x_{123}, x_{124}, x_{134}, x_{234}$. Repetition of this procedure for the quads incident with x_{1234} yields four different expressions for x_{1234} , within each of the four cubes incident to x_{1234} , i.e., there are four rational functions of the arguments x, x_i, x_{ij} which in the general position case and dimension ≥ 4 evaluate to the same point x_{1234} , by (2).

(4) Since almost all arguments have the general position property, the rational

functions constructed above are equal. They are independent of the dimension, so they can be applied also in 3-space, proving 4-consistency.

Consistency of *circularity* follows as a corollary, since circularity propagates by Prop. 3.3. \square

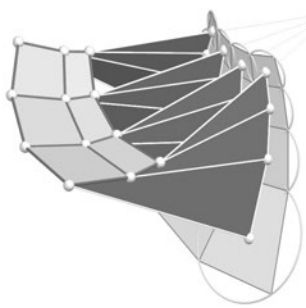
Theorem 3.6. *4-consistency of 3-systems implies n-consistency for all $n \geq 4$.*

Proof. Let $n = 5$. Suppose a property is imposed on the 4-cubes with diagonals

$$x-x_{1234}, \quad x-x_{1235}, \quad \dots \quad x-x_{2345}.$$

By 4-consistency, it can also be imposed on each of the 4-cubes incident to x_{12345} , but with a possible conflict regarding the location on the common vertex x_{12345} . An arbitrary pair of such 4-cubes share a common 3-cube incident with x_{12345} , so there is actually no conflict (because that 3-cube already determines the location of x_{12345}). The case $n \geq 6$ is analogous. \square

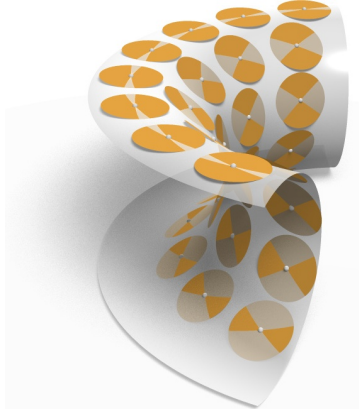
Principal curvature lines. We have not yet mentioned the smooth class of surfaces which corresponds to the circular nets: It is the parametrization of surfaces along principal curvature lines. There are several reasons for that: Circularity of quads is a discrete version of *orthogonality*, but a more compelling reason is the behavior of the surface normals. A curve $c(t)$ on a surface is a principal curvature line, if progress in that direction causes the unit normal vector to change in the same direction ($\frac{d}{dt}n(c(t)) = \lambda(t)\frac{d}{dt}c(t)$, the tangent vectors of these curves are eigenvectors of the Weingarten map $-dn$), so the surface traced out by the surface normals is developable.



- Developability means that a surface normal $N(c(t))$ and its infinitesimal neighbor $N(c(t + dt))$ “intersect” each other (in the same way an infinitesimal quad of a conjugate net is planar). It is this surface of normals which has a proper discrete analogue: As we progress along a sequence of adjacent faces, the successive axes of circles intersect, which yields a discrete developable surface. Further, convergence of circular nets to principal parametrizations can be shown [7].

3.3 K-nets: a 2-system

Asymptotic nets. Asymptotic parametrizations have elementary quads which are as non-planar as possible. For a negatively curved 2-surface in \mathbb{R}^3 , the asymptotic tangents in a point are found by intersecting the surface with its own tangent plane; the parameter lines of the asymptotic tangents are the integral curves of these tangents. The “asymptotic” condition reads



$$\partial_{11}x, \partial_{22}x \in \text{span}\{\partial_1x, \partial_2x\}. \quad (9)$$

A discrete version of this condition would be: All symmetric 2nd differences around a vertex are contained in the plane spanned by the first differences. This can be formulated in a symmetric way:

$$x, x_1, x_{\bar{1}}, x_2, x_{\bar{2}} \in \text{plane } P(u) \quad \begin{array}{c} x_2 \\ | \\ x_{\bar{1}} — x — x_1 \\ | \\ x_{\bar{2}} \end{array} \quad (10)$$

A-nets are defined by the requirement that all edges emanating from a vertex $x(u)$ must lie in a common plane $P(u)$.

Surfaces of constant Gaussian curvature. Surfaces of constant negative Gaussian curvature (*K-surfaces*) are interesting for a variety of reasons, e.g. because the geometry of their geodesics locally coincides with classical hyperbolic geometry. They are important for the development of discrete differential geometry, since they were among the first where a meaningful discretization has been obtained [19, 24], and because of the integrable equations associated with K-surfaces.

Like any other negatively curved surface in Euclidean 3-dimensional space, a K-surface has an asymptotic parametrization. It is not difficult to show that for a smooth asymptotic surface, the additional *Chebyshev condition*

$$\partial_2\|\partial_1x\| = \partial_1\|\partial_2x\| = 0 \quad (11)$$

characterizes $K = \text{const}$. Since the length of the derivative vectors w.r.t. one variable does not depend on the other variable, we can re-parametrize and achieve

$$\|\partial_1x\| = \|\partial_2x\| = 1. \quad (12)$$

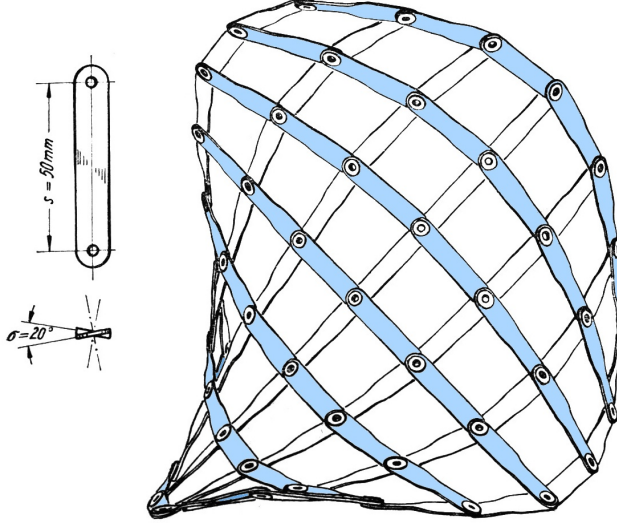


Figure 6: A discrete K-net built from edges of constant length and constant twist by W. Wunderlich (this drawing is published in [24]). It is a flexible mechanism. Different shapes of K-nets correspond to different embeddings of (part of) the hyperbolic plane into Euclidean space.

It turns out that in this case, when traversing a parameter line with velocity 1, the surface's normal vector is rotating with velocity $\sqrt{-K}$. An obvious discretization of the Chebyshev property is

$$\Delta_2 \|\Delta_1 x\| = \Delta_1 \|\Delta_2 x\| = 0. \quad (13)$$

The construction of discrete K-surfaces depends on the properties of a so-called Chebyshev quad, where opposite edges have equal lengths

$$\|x - x_1\| = \|x_2 - x_{12}\| \quad \text{and} \quad \|x - x_2\| = \|x_1 - x_{12}\| \quad (14)$$

and which does not lie in a plane (*skew parallelogram*). The following statement is elementary spatial geometry:

Lemma 3.7. *A non-planar quadrilateral $x-x_1-x_{12}-x_2$ with the Chebyshev property given by Eqn. 14 (opposite edges have equal lengths) is symmetric w.r.t. a 180° rotation about the axis spanned by the two midpoints of diagonals.*

In each vertex, the edges incident with that vertex span a plane, and we also consider unit normal vectors n, n_1, n_{12}, n_2 whose orientation is determined by the cycle of vertices. The twist angle along an edge which is enclosed by the planes at either end (resp. by their normal vectors) is the same for opposite edges,

$$\langle n, n_1 \rangle = \langle n_2, n_{12} \rangle, \quad \langle n, n_2 \rangle = \langle n_1, n_{12} \rangle$$

(the unit normal vectors constitute a Chebyshev quad). Further, we can reconstruct, up to scaling, the edges of the quadrilateral from these normal vectors by

$$x_1 - x = n \times n_1, \quad x_2 - x = -n \times n_2.$$

Also the converse is true: Every net of unit normal vectors which fulfills these conditions determines a K-net.

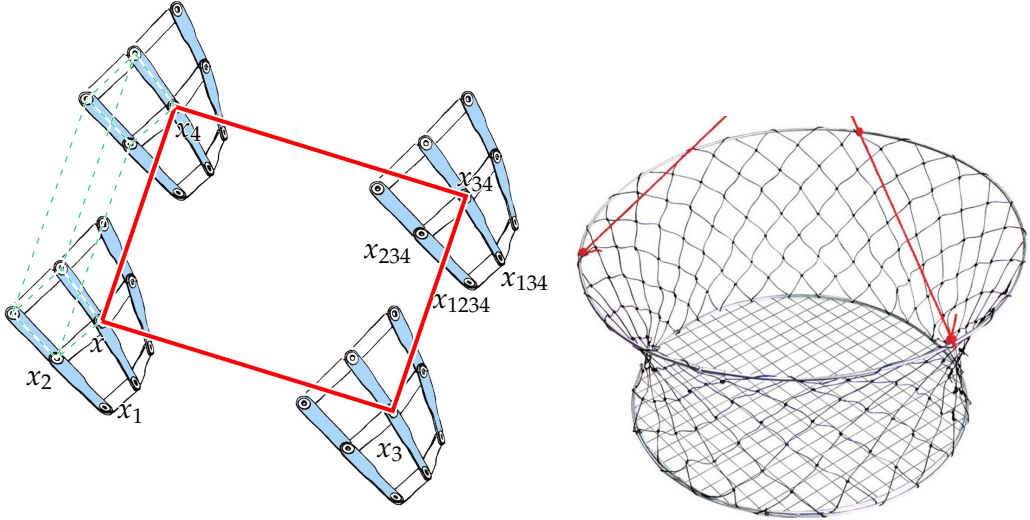


Figure 7: Left: A 4-dimensional discrete K-net, which at the same time is a 2D lattice of 2-dimensional K-nets, where each is in the Bäcklund transform relation with its neighbors. The thin dashed lines constitute a Bennet 12-bar linkage. Right: A K-net with rotational symmetry made from string (crab net).

For a proof we refer to [7, §4.2.1]. The equal angles property is an immediate corollary of the symmetry. Figure 6 shows a K-net which has actually been built, and where both the Chebyshev property and the angle property can be observed.

The systematic treatment of A-nets and K-nets $x(u)$ relies on the construction of the so-called Lelievre normal vector field $m(u)$, which has the property $x_k - x = m_k \times m$. It is a so-called T-net, the T-nets being an integrable 3-system. In this way the geometric considerations of [19, 24] concerning skew-parallelogram lattices can be treated in a more high-level manner. We summarize, without proof:

Theorem 3.8. *A discrete K-net $x(i_1, \dots, i_d)$ (an asymptotic net with the Chebyshev property) has unit normal vectors $n(i_1, \dots, i_d)$ which form a Chebyshev net themselves: The rotation angle of the normal vector along an edge xx_k depends only on the k -th parameter, and not on the others.*

The K-net property is a 2-system in the following sense: If unit normal vectors $n(i_1, 0)$ and $n(0, i_2)$ are given, then these data can be uniquely extended to a Chebyshev net $n(i_1, i_2)$ in the unit sphere, and a K-net x is derived from n by the formulae above.

The K-net property is d -dimensional consistent for $d \geq 3$ (i.e., integrable): Any choice of unit normal vectors

$$n(i_1, 0, \dots, 0), \quad n(0, i_1, \dots, 0), \quad \dots, \quad n(0, 0, \dots, i_d) \quad (d \geq 2)$$

can be extended to a Chebyshev net in the unit sphere, and define a K-net via the formulas given above.

Bäcklund transformation. Two smooth K-surfaces $x, x^{(1)}$, both parametrized such that parameter lines have unit speed, are Bäcklund transformations of each other, if the distance $\|x(u) - x^{(1)}(u)\|$ of corresponding points is constant, and if the line segment $x(u), x^{(1)}(u)$ is tangent to both surfaces in its endpoints. For a discrete surface $x(i_1, i_2)$ and its transform $x^{(1)}(i_1, i_2)$, the definition is literally the same, since even discrete K-nets possess tangent planes. However, it is clear from the definition that a K-net and its transform together constitute a 3-dimensional K-net.

Existence of 4D K-nets and the fact that they are determined by initial values (Theorem 3.8) shows Bianchi permutability of Bäcklund transforms, see Fig. 7.

Mechanisms based on skew parallelograms. The results on K-nets have as an immediate consequence the following remarkable fact which was first observed, at least in part, more than 100 years ago by G. T. Bennet [2]:

A K-net built with twisted metal bars as shown by Figure 6 is a flexible mechanism. Think of the K-net defined by normal vector data $n(i_1, 0)$ and $n(0, i_2)$. Deforming these initial values such that the angle between successive normal vectors remains constant yields a net $n(i_1, i_2)$ of normal vectors where the angle between neighbors remains constant. Computing the K-net from normal vector data yields a deformation of $x(i_1, i_2)$ such that both edge lengths and the twist along an edge remains constant.

Already a single quadrilateral is a nontrivial mechanism, called Bennet's four-bar mechanism or Bennet's isogram [2]. An elementary cube in a 3-dimensional K-net is Bennet's 12-bar mechanism, see also Figure 7.

It is worth noting that certain K-nets can be manufactured rather easily, namely as equilibrium positions of fishing nets with rotational symmetry, see the crab net shown by Figure 7.

The sine-Gordon equation. By Gauss' *theorema egregium*, the Gaussian curvature K of a surface $x(u_1, u_2)$ can be computed from the coefficient functions $E = \langle \partial_1 x, \partial_1 x \rangle$, $F = \langle \partial_1 x, \partial_2 x \rangle$ and $G = \langle \partial_2 x, \partial_2 x \rangle$ of the first fundamental form. Francesco

Brioschi's formula for Gaussian curvature says that

$$\begin{vmatrix} -\partial_{22}E + 2\partial_{12}F - \partial_{11}G & \partial_1 E & 2\partial_1 F - \partial_2 E \\ 2\partial_2 F - \partial_1 G & 2E & 2F \\ \partial_2 G & 2F & 2G \end{vmatrix} - \begin{vmatrix} 0 & \partial_2 E & \partial_1 G \\ \partial_2 E & 2E & 2F \\ \partial_1 G & 2F & 2G \end{vmatrix} = 8(EG - F^2)^2 K.$$

The unit speed (Chebyshev) property is expressed as $E = G = 1$, and with the angle $\phi(u_1, u_2)$ between parameter lines we have $F = \cos \phi$. Brioschi's formula yields $\partial_{12}\phi(u_1, u_2) = -K(u_1, u_2) \cdot \sin \phi(u_1, u_2)$. In the case of K-surfaces, it is no loss of generality to assume $K = -1$, so

$$\partial_{12}\phi = \sin \phi. \quad (15)$$

The meaning of this *sine-Gordon equation* in terms of the intrinsic geometry of a surface is this: If a surface is parametrized such that parameter lines are traversed with unit speed, and the angle between parameter lines evolves according to the sine-Gordon equation, then the surface has constant Gaussian curvature -1 .

Note that Eqns. 12+15 constitute a purely intrinsic characterization of surfaces with $K = -1$, while Eqns. 12+9 provide an extrinsic characterization.

Discrete sine-Gordon equation. Integrable equations. A discrete K-surface where all edge lengths are equal to ε is the most direct analogue of a smooth surface parametrized by unit speed with Gaussian curvature -1 . The evolution of the angle ϕ enclosed by edges xx_1 and xx_2 can be shown to obey the Hirota equation

$$\sin \frac{\phi_{12} - \phi_1 - \phi_2 + \phi}{4} = \frac{\varepsilon^2}{4} \sin \frac{\phi_{12} + \phi_1 + \phi_2 + \phi}{4}. \quad (16)$$

In these lecture notes we are not able to discuss the term *integrability* in a systematic manner, we refer to [7, §6] instead. We only mention some salient facts: • integrable equations turn out to be closely related with multidimensionally consistent geometric properties of nets • discrete nets are easier to treat than continuous ones, in particular the special role of transformations disappears. The smooth case is obtained from the discrete case by a limit process. • typical properties of integrable systems (Bäcklund transforms, zero curvature representations,...) are a consequence of multidimensional consistency.

3.4 Applications: computing minimal surfaces

There is a nice version of discrete minimal surfaces which connects an analytic approach with discrete geometry and circle patterns. It is also capable of solving a significant problem, namely computing the shape of a minimal surface from the combinatorics of its principal curve network [4].

Isothermic surfaces and their duals. Isothermic surfaces represent a classical topic of differential geometry. Informally they are defined by the condition that their infinitesimal quadrilaterals are flat squares. Certain surface classes, including the minimal surfaces, admit an isothermic parametrization. It is a bit of a mystery why certain classes of surfaces have this property, for a good overview see [8].

Theorem 3.9. *An isothermic surface $x : U \subseteq \mathbb{R}^2 \rightarrow \mathbb{R}^3$, characterized by the condition that it is a conformal curvature-line parametrization, i.e.,*

$$\|\partial_1 x\| = \|\partial_2 x\| = s, \quad \langle \partial_1 x, \partial_2 x \rangle = 0, \quad \partial_{12} x \in \text{span}(\partial_1 x, \partial_2 x),$$

with $s : U \rightarrow \mathbb{R}_+$, has a Christoffel-dual surface x^* defined by

$$\partial_1 x^* = \frac{1}{s^2} \partial_1 x \quad \partial_2 x^* = -\frac{1}{s^2} \partial_2 x. \quad (17)$$

x^* is again isothermic, with $\|\partial_j x^*\| = 1/s$.

Proof. We have $\partial_{12} x = a\partial_1 x + b\partial_2 x$, for certain coefficient functions a, b . Further, $\partial_2(s^2) = 2 \langle \partial_1 x, \partial_{12} x \rangle = 2 \langle \partial_1 x, a\partial_1 x + b\partial_2 x \rangle = 2as^2$. Differentiating $\partial_1 x^*$ yields

$$\partial_2(\partial_1 x^*) = -\frac{\partial_2(s^2)}{s^4} \partial_1 x + \frac{1}{s^2} \partial_{12} x = -\frac{2a}{s^2} \partial_1 + \frac{1}{s^2} (a\partial_1 x + b\partial_2 x) = \frac{1}{s^2} (b\partial_2 x - a\partial_1 x).$$

For $\partial_1(\partial_2 x^*)$ an analogous computation yields the same result, so x^* exists. Obviously, x^* fulfills the isothermicity conditions. \square

The Christoffel transformation is particularly interesting for *minimal surfaces*, since they admit isothermic parameters, and they are Christoffel-dual to their own unit normal vector field (which is then a conformal parametrization of the unit sphere). Conversely, any conformal parametrization of the unit sphere by Christoffel duality is converted into a minimal surface. If the unit sphere is identified with $\mathbb{C} \cup \{\infty\}$ by stereographic projection, and the definition of the Christoffel dual is written as an integral, this yields the Weierstrass representation of minimal surfaces.

Some parts of this relationship are easy to show. E.g. if x is a conformal parametrization of the unit sphere, then x is isothermic. The common unit normal vector field of x and the Christoffel dual x^* is furnished by x itself. Compute the principal curvatures of x^* :

$$\kappa_1 = \frac{\partial_1 x}{\partial_1 x^*} = s^2, \quad \kappa_2 = \frac{\partial_2 x}{\partial_2 x^*} = -s^2.$$

i.e., x^* is a minimal surface. We also see how the speed of parametrization (which is s) is related to the values of the principal curvatures.

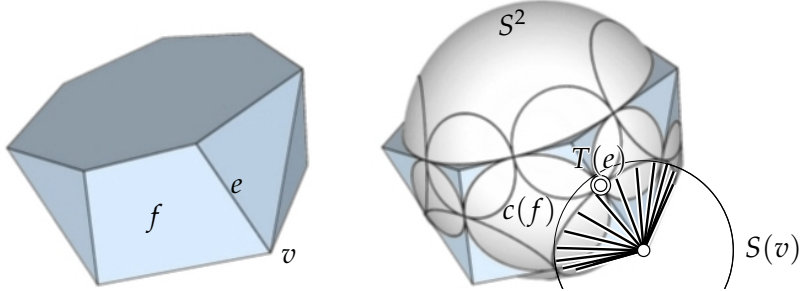


Figure 8: A Koebe polyhedron has edges tangent to a sphere. The orthogonal circle pattern defined by this polyhedron consists of the incircles of faces, and the circles of tangency of cones whose vertex is a vertex of the polyhedron. The vertex-centered sphere used in the definition of an s -isothermic surface is also shown.

Discrete s -isothermic surfaces. We start this discussion with a remarkable result on polyhedra. It can be seen as a discrete version of the Koebe uniformization theorem in the genus 0 case, and it can be made computationally efficient [21].

Theorem 3.10. *For each convex polyhedron there is a combinatorially equivalent convex polyhedron whose edges are tangent to the unit sphere (Koebe polyhedron).*

It becomes unique if we require that its center of mass equals 0, otherwise it is unique only up to Möbius transforms, i.e., up to projective automorphisms of the unit sphere.

Each Koebe polyhedron has two associated circle packings, see Fig. 8. System (i) arises by intersecting the faces' planes with the sphere; System (ii) arises in a dual way as the circles of tangency of cones whose vertex is a vertex of the polyhedron. System (ii) can also be replaced by vertex-centered spheres, showing that a Koebe polyhedron fulfills the definition of n discrete s -isothermic surface, see Fig. 9.

Definition 3.11. *A polyhedral surface (in particular a discrete conjugate net) is s -isothermic, if the following conditions are fulfilled.*

- Every face f contains an incircle $c(f)$, every vertex v is the center of a sphere $S(v)$.
- Every edge e contains a point $T(e)$, such that:
 - (*) $v \in e \implies S(v)$ intersects e orthogonally in $T(e)$
 - (*) $e \subset f \implies c(f)$ touches e in $T(e)$
- Vertices have degree four, and faces have even degree.

If in addition the surface is part of a Koebe polyhedron, i.e., its edges are tangent to S^2 , then we regard it as a discrete-conformal parametrization of S^2 .

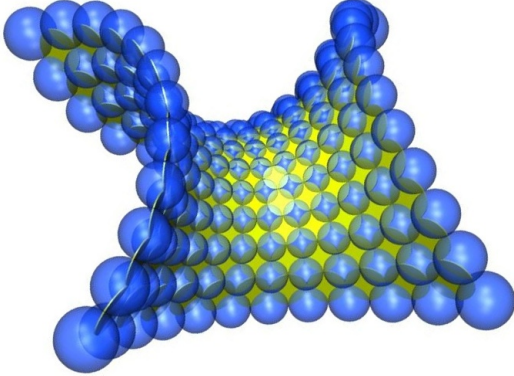
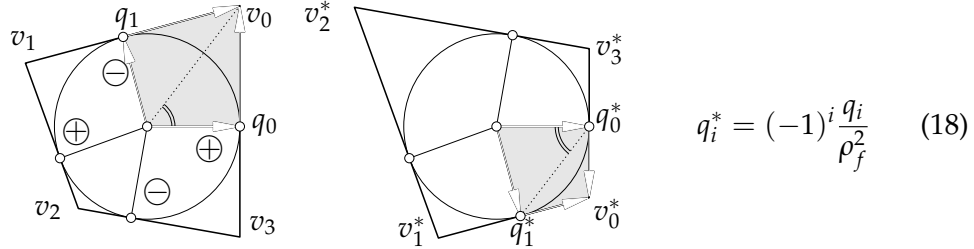


Figure 9: An s-isothermic surface is defined as a circle/sphere arrangement where circles (green) touch circles, spheres (blue) touch spheres, and circles orthogonally intersect spheres. This example is a discrete Enneper surface (image courtesy T. Hoffmann).

Dualizing s-isothermic surfaces. Consider a face $f = (v_0, \dots, v_{n-1})$ with n even, and incircle of radius ρ_f . The edge $v_i v_{i+1}$ touches the incircle in the point q_i . Then the dual face f^* likewise has an incircle of radius $\rho_{f^*} = 1/\rho_f$, and the new contact points q_i^* are defined by



It follows that the edges of the dual and primal polygon are related by

$$p_j^* - p_{j+1}^* = (-1)^j \frac{1}{r_j r_{j+1}} (p_i - p_{i+1}), \text{ where } r_j = \|v_j - q_j\| = \|v_j - q_{j+1}\|. \quad (19)$$

The values r_j are the radii of the vertex-centered spheres which occur in the definition of an s-isothermic surface. The proof is an exercise in complex numbers. Similarly, one can show that the subdivision of the faces into quads as in Eqn. 18 yields corresponding discrete surfaces $x(i_1, i_2)$ and $x^*(i_1, i_2)$ where

$$\Delta x_1^* = \frac{1}{\|\Delta x_1\|^2} \Delta x_1, \quad \Delta x_2^* = -\frac{1}{\|\Delta x_2\|^2} \Delta x_2. \quad (20)$$

This is completely analogous to the smooth case of Eqn. 17.

For any given s-isothermic surface, we now assign labels \oplus and \ominus to all edges, such that for each face, the cycle of edges is assigned labels $\oplus, \ominus, \oplus, \ominus, \dots$ in an alternating way, indicating if the factor $+1$ or -1 is to be used in Eqn. 18. By Eqn. 19,



Figure 10: Attempting to dualize a piece of Koebe polyhedron where one face has odd valence. The dual of the triangle does not close up (we cannot even assign labels \oplus, \ominus to edges in a consistent manner). However, if the given discrete surface is seen as a discrete branched covering, with the triangle actually being a hexagon, the dual surface will close after the original one is traversed twice (images courtesy B. Springborn).

the edge lengths of dual edges are independent of the face they are contained in. An interior angle $\alpha_{v,f}$ at the vertex v in the face f corresponds to the $\alpha_{v^*,f^*}^* = \pi - \alpha_{v,f}$ in the dual face, so the angle sum around the vertex v^* is

$$\sum_{f^* \ni v^*} \alpha_{v^*,f^*}^* = \sum_{f \ni v} (\pi - \alpha_{v,f}) = (\deg(v) - 2)\pi = 2\pi.$$

This shows that a discrete s-isothermic surface can be dualized.

Definition 3.12. A discrete s-isothermic surface is minimal, if its dual is spherical, i.e., is part of a Koebe polyhedron.

[4] discusses how to compute the shape of a minimal surface from the combinatorics of its network of principal curvatures lines. One starts by computing a Koebe polyhedron with the desired combinatorics, and dualizes, see Fig. 10. One can even show convergence to smooth minimal surface, by using the fact that correspondences between combinatorially equivalent circle packings can be shown to converge to conformal mappings [10].

Curvatures of discrete surfaces. Discrete surfaces have been assigned curvatures in different ways. E.g. the variational definition of the mean curvature vector field \bar{H} as the gradient of the area functional leads to *cotangent formula* for mean curvature of simplicial surfaces. Another approach uses the *Steiner formula*: A surface in \mathbb{R}^3 , with unit normal vector n , has constant-distance offset surfaces where a point p of the original surface moves to $p + tn(p)$. Surface area changes according to

$$A^t = \int (1 - 2Ht + Kt^2) dA, \quad (21)$$

where dA refers to the canonical surface area measure, and H, K are mean curvature and Gaussian curvature, respectively.

[16, 6] proposed to use the same principle for a polyhedral surface (V, E, F) equipped with a polyhedral Gauss image $(\sigma(V), \sigma(E), \sigma(F))$ (i.e., normal vector field), such that corresponding faces of surface and Gauss image are parallel. An example is furnished by the s-isothermic minimal surfaces and the corresponding Koebe polyhedron. We define a constant-distance offset (V^t, E^t, F^t) by vertices

$$v^t = v + t\sigma(v).$$

The oriented area of closed polygon $f = (v_0, \dots, v_{n-1})$ in \mathbb{R}^2 is a quadratic form with associated symmetric bilinear form ("mixed area"),

$$A(f) = \frac{1}{2} \sum_{i=0}^{n-1} \det(v_i, v_{i+1}), \quad A(f, g) = \frac{1}{2}(A(f+g) - A(f) - A(g))$$

(Leibniz' sector formula). Then the area of a face $f^t \in F^t$ is given by

$$A(f^t) = A(f) + 2tA(f, \sigma(f)) + t^2A(\sigma(f)). \quad (22)$$

Comparing Eqn. 21 with Eqn. 22 leads to the definition of a mean curvature H and a Gaussian curvature K of a face f :

$$H(f) = -\frac{A(f, \sigma(f))}{A(f)}, \quad K(f) = -\frac{A(\sigma(f))}{A(f)}. \quad (23)$$

With this definition it is not difficult to compute the mean curvature of s-isothermic surfaces, it turns out to be zero. The considerations above have been extended to more general surface classes by [11]. E.g the discrete K-surface indeed enjoy the property that the Gaussian curvature equals -1 .

3.5 Applications: freeform architecture

With computer-aided design, it has become rather easy for professionals to design free forms in architecture, but building them is another matter. The geometric questions which arise in this context have a rich connection to discrete differential geometry. Unfortunately, in practice, geometric forms and even the manner of their realization is determined early in the design phase, where geometric knowledge is not widespread. Recent surveys are [18, 15]. Examples of specific geometric issues in the context of freeform architecture are the following.



Figure 11: This torsion-free support structure (image courtesy Evolute) guides members and nodes in the outer hull of the Yas Marina hotel in Abu Dhabi, so that members have a nice intersection in each node (at right, image courtesy Waagner-Biro Stahlbau). Note that the faces of this mesh are not planar.

- Steel-glass constructions often are discrete surfaces with flat faces, because of the glass panels that are put there. For surfaces with quadrilateral faces, this is a nontrivial side-condition. Another issue with steel constructions is the manner of intersection of the beams in nodes. We discuss this topic below, see also [12, 16].
- Freeform skins might be required to be at constant distance from each other, or a steel-glass construction might be required to be of constant thickness. This topic leads to circular nets, conical nets, and even nets which are edgewise parallel to a Koebe polyhedron, depending on the question how distances are measures (between vertices, or faces, or edges), see [16].
- Developable surfaces occur in bent glass and in curved beams (whose sides are made by bending). A sequence of developables is a semidiscrete conjugate net, a viewpoint which has been exploited by [12, 17].
- The differential geometry of manifolds in line space, and discrete submanifolds of line space has been used by [23] to study lighting and shading.
- Circle packings and discrete uniformization turn up in the question of regular patterns, in particular hexagonal patterns [20].
- Self-supporting surfaces like brick vaults and their polyhedral Airy potential surface are related to isotropic geometry and curvatures [22]. A discrete stress state and corresponding polyhedral Airy potential is also relevant for material-minimizing structures [13].

Meshes. Torsion-free support structures. Here we discuss briefly some topics from the list which have to do with discrete *parametric* surfaces.

In order to describe structures from straight or curved beams, with or without panels covering the faces, we start with the combinatorics. Consider a graph (V, E)

which is embedded into a surface of genus g (usually $g = 0$), this embedding defining *faces*. Individual non-adjacent faces may be deleted, which leaves us with interior edges (incident with two remaining faces) and boundary edges (incident with one face). This defines the connectivity of a mesh (V, E, F) . We assign a position in space to each vertex, and a curve passing through the vertices to each edge. If faces are to be filled in, we also assign a surface passing through the boundary curves to each face; see Figure 11 for a mesh where faces are not filled in.

An alternative definition of a mesh connectivity starts with a graph (V, E) and a declaration of certain edge cycles as faces, such that the 1-ring neighborhood of each vertex is represented either as a cycle of faces (for interior vertices) or as a chain of faces (boundary vertex). A *triangle mesh* is nothing but a simplicial surface. Established terminology is also *quad mesh* and *hex mesh* for meshes whose faces, or at least, most of whose faces, are quadrilaterals and hexagons. The discrete parametric surfaces mapping from \mathbb{Z}^2 to \mathbb{R}^3 are quad meshes in a natural way.

Definition 3.13. *A torsion-free support structure associated to a mesh (V, E, F) with straight edges is an assignment of a line $\ell(v)$ to each vertex $v \in V$ and a plane $\pi(e)$ to each edge $e \in E$, such that $v \in e \implies \ell(v) \subset \pi(e)$ (plus certain nondegeneracy conditions).*

If the edges of the mesh are curves, $\pi(e)$ is a developable surface containing the edge.

The relevance of a torsion-free support structure is that straight beams in a steel construction can be aligned with the planes $\pi(e)$, and the symmetry planes of beams nicely intersect in the line $\ell(v)$, whenever beams come together in a node, see Fig. 11. Such an intersection of beams is called torsion-free. If the intersection is not torsion-free, and beams intersect anyhow, the intersection is complicated to manufacture, see Fig. 12. However, if the intersection is torsion-free, one can simply use a cylindrical node element and connect the beams to it.

Proposition 3.14. *A triangle mesh has only trivial support structures, where all elements pass through a single center z : for all $v \in V, e \in E$ we have $\ell(v) = v \vee z$ and $\pi(e) = e \vee z$.*

Proof. In projective space, and ignoring degeneracies, we argue as follows. In a face $f = v_i v_j v_k$, we have $\ell(v_i) = \pi(v_i v_j) \cap \pi(v_i v_k)$, and similar for $\ell(v_j), \ell(v_k)$. Thus, the point $z(f) = \pi(v_i v_j) \cap \pi(v_i v_k) \cap \pi(v_j v_k)$ lies on all lines $\ell(v_i), \ell(v_j), \ell(v_k)$. If $f' = (v_i v_j v_l)$ is a neighbor face, then $z(f) = \ell(v_i) \cap \ell(v_j) = z(f')$. By connectedness, $z(f)$ is the same point for all faces $f \in F$. \square

This result is one reason why quad meshes are attractive for steel-glass constructions. Unfortunately, imposing planarity of faces on quad meshes is nontrivial.

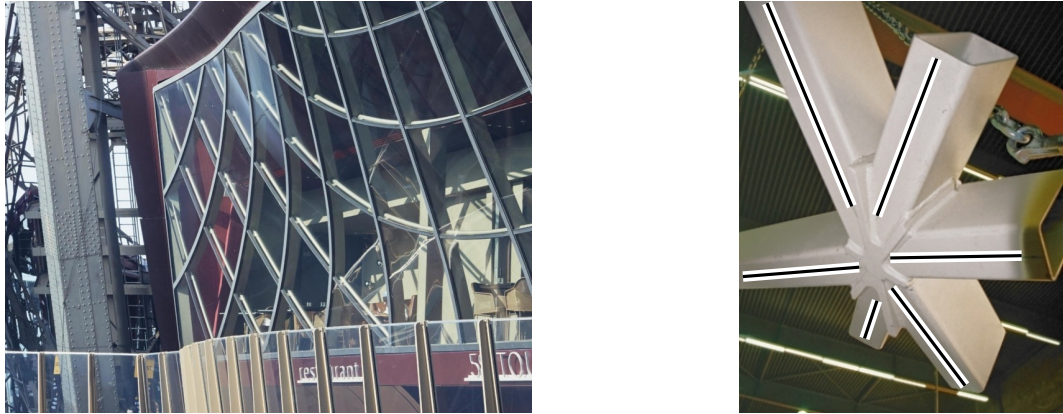


Figure 12: Left: A curved support structure (Eiffel tower pavilions, Paris. Image courtesy RFR). Right: An intersection of beams which does not follow a torsion-free support structure (courtesy Waagner Biro Stahlbau).

The design dilemma. When using mathematical methods in an artistic context, one faces a problem which is not known from applications in the natural sciences: It is usually not desirable that Mathematics yields a definite answer to a certain question. We illustrate this by means of torsion-free support structures: Such a structure either consists of developable surfaces, or of discrete developables following the edges of the mesh. If they are to be *orthogonal* to the reference surface, like in the case of Figure 12, left, then they must follow the surface's principal curvature lines, cf. the discussion at the end of §3.2. Since the principal curvature lines are determined by the reference surface, there is no longer any design freedom for the beams except perhaps their spacing. Such a situation, which amounts to a restriction of the artist's freedom of expression, is unacceptable to the designer. In such a situation an alternative usually must be found. In the case of the Eiffel tower pavilions, design freedom was restored by the fact that small changes to the design surface can cause big changes in the network of principal curvature lines. It was possible to achieve the desired layout of beams by only minimally changing the reference surface.

Meshes with planar faces – conjugate nets. The design of quadrilateral meshes with planar faces was among the first topics where a connection between freeform architecture and discrete differential geometry was established [12]. If the mesh under consideration has the visual appearance of a smooth network of curves on a smooth surface, then such a quad mesh has mostly regular combinatorics and is therefore a conjugate net which approximates a conjugate curve network, see Fig. 4. If in addition to conjugacy we add orthogonality of curves, we have the principal network. In fact, any conjugate network useful for deriving a quad mesh from it is

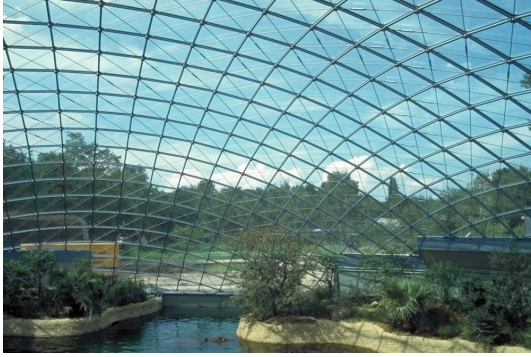


Figure 13: This quad mesh with parallelogram faces has been constructed by parallel-translating a polygon along another polygon (Hippo house, Berlin Zoo. Engineering by Schlaich Bergermann & Partners).

close to principal, which is another instance of the design dilemma mentioned above. Since the reference shape and a conjugate net on it cannot be designed separately, there are very few instances of such meshes which serve as basis of actual building skins, and most of those have been generated by a simple process like translating one polygon along another one, see Fig. 13.

Constant-distance offsets. With meshes with planar faces, the question of *meshes at constant distance* arises naturally. One can either look for a mesh which is combinatorially equivalent and whose faces are at a constant offset distances from the corresponding faces of the first mesh, or one can ask for edge-edge distances or vertex-vertex distances to be constant. The unifying notion is *parallelity of meshes*:

Definition 3.15. *Meshes (V, E, F) and (V', E', F') are parallel, if they have the same connectivity, and corresponding edges of E resp. E' lie in parallel lines, and corresponding faces of F resp. F' lie in parallel planes (details regarding nondegeneracy have been omitted).*

A conjugate net and its parallel net together constitute a 3D conjugate net. It is not difficult to show the following [16]:

- If (V', E', F') is parallel to (V, E, F) , then a torsion-free support structure is defined by $\ell(v) = v \vee v'$ and $\pi(e) = e \vee e'$, where v, v' and e, e' are pairs of corresponding vertices resp. edges. In the simply connected case, a torsion-free support structure also implies existence of parallel meshes

- Parallel meshes at constant vertex-vertex distance d are circular. This is because we can construct a third mesh by computing vertices according to $v'' = (v' - v)/d$, which is inscribed to the unit sphere and has planar faces, so it is circular. For a quadrilateral, circularity is expressed via the angles between edges only, so the two meshes we start with inherit the circular property.

These two statements show that conjugate nets and circular nets we studied in the beginning, have actual applications in a field which generally was not known for using much applied Mathematics at all, namely the design of freeform skins for architecture.

Acknowledgments. The author is supported by SFB-Transregio Program *Discretization in Geometry and Dynamics*, Austrian Science Fund grant no. I2978.

REFERENCES

- [1] A. Bäcklund. *Om ytor med konstant negativ kröknings*, volume 19 of *Lunds Univ. Årsskr.* 1883. 42 pages.
- [2] G. T. Bennet. The skew isogram mechanism. *Proc. London Math. Soc. (Ser. 2)*, 13:151–173, 1914.
- [3] L. Bianchi. *Lezioni di geometria differenziale*. Spoerri, Pisa, 2nd edition, 1902.
- [4] A. Bobenko, T. Hoffmann, and B. Springborn. Minimal surfaces from circle patterns: Geometry from combinatorics. *Ann. Math.*, 164:231–264, 2006.
- [5] A. Bobenko and U. Pinkall. Discrete surfaces with constant negative Gaussian curvature and the Hirota equation. *J. Diff. Geom.*, 43:527–611, 1996.
- [6] A. Bobenko, H. Pottmann, and J. Wallner. A curvature theory for discrete surfaces based on mesh parallelity. *Math. Annalen*, 348:1–24, 2010.
- [7] A. Bobenko and Yu. Suris. *Discrete differential geometry: Integrable Structure*. American Math. Soc., 2009.
- [8] F. E. Burstall. Isothermic surfaces: conformal geometry, Clifford algebras and integrable systems. In *Integrable systems, geometry, and topology*, pages 1–82. Amer. Math. Soc., 2006.
- [9] L. Eisenhart. *Transformations of Surfaces*. Princeton University Press, 1923.
- [10] Z. X. He and O. Schramm. Fixed points, Koebe uniformization and circle packings. *Annals Math.*, 137:369–406, 1993.
- [11] T. Hoffmann, A. O. Sageman-Furnas, and M. Wardetzky. A discrete parametrized surface theory in \mathbb{R}^3 . *Int. Mat. Res. Not.*, pages 4217–4258, 2017.
- [12] Y. Liu, H. Pottmann, J. Wallner, Y.-L. Yang, and W. Wang. Geometric modeling with conical meshes and developable surfaces. *ACM Trans. Graph.*, 25(3):681–689, 2006.
- [13] D. Pellis, M. Kilian, J. Wallner, and H. Pottmann. Material-minimizing forms and structures. *ACM Trans. Graphics*, 36(6):article 173, 2017.
- [14] U. Pinkall and K. Polthier. Computing discrete minimal surfaces and their conjugates. *Experiment. Math.*, 2(1):15–36, 1993.
- [15] H. Pottmann, M. Eigensatz, A. Vaxman, and J. Wallner. Architectural geometry. *Computers and Graphics*, 47:145–164, 2015.
- [16] H. Pottmann, Y. Liu, J. Wallner, A. Bobenko, and W. Wang. Geometry of multi-layer freeform structures for architecture. *ACM Trans. Graph.*, 26:article 65, 2007.
- [17] H. Pottmann, A. Schiftner, P. Bo, H. Schmiedhofer, W. Wang, N. Baldassini, and J. Wallner. Freeform surfaces from single curved panels. *ACM Trans. Graph.*, 27(3):article 76, 2008.
- [18] H. Pottmann and J. Wallner. Geometry and freeform architecture. In W. König, editor, *Mathematics and Society*, pages 131–151. European Math. Soc., 2016.
- [19] R. Sauer. Parallelogrammgitter als Modelle pseudosphärischer Flächen. *Math. Zeitschr.*, 52:611–622, 1950.
- [20] A. Schiftner, M. Höbinger, J. Wallner, and H. Pottmann. Packing circles and spheres on surfaces. *ACM Trans. Graph.*, 28(5):article 139, 2009.

- [21] S. Sechelmann. Discrete minimal surfaces, Koebe polyhedra, and Alexandrov's theorem. variational principles, algorithms and implementation. Master's thesis, TU Berlin, 2007.
- [22] E. Vouga, M. Höbinger, J. Wallner, and H. Pottmann. Design of self-supporting surfaces. *ACM Trans. Graph.*, 31(4):article 87, 2012.
- [23] J. Wang, C. Jiang, P. Bompas, J. Wallner, and H. Pottmann. Discrete line congruences for shading and lighting. *Comput. Graph. Forum*, 32(5):53–62, 2013.
- [24] W. Wunderlich. Zur Differenzengeometrie der Flächen konstanter negativer Krümmung. *Sitz. Öst. Akad. Wiss. Math.-Nat. Kl.*, 160:39–77, 1951.

4 DISCRETE MAPPINGS

Yaron Lipman

4.1 Overview

Piecewise-linear triangle meshes are widely popular for surface representation in the digital computer; mappings of meshes are therefore central for applications such as computing good coordinate systems on surfaces (parameterization), finding correspondence between shapes, and physical simulation. However, representation and calculation of mappings in a computer pose several challenges: (i) how to define faithful discrete analogs of properties of smooth mappings (e.g., angle or area preservation), (ii) how to guarantee properties such as injectivity and/or surjectivity, and (iii) how to construct mappings between non-Euclidean (curved) domains. One particularly interesting sub-class of simplicial mappings is the collection of convex combination mappings, in which the image of each vertex of the triangulation is restricted to the convex-hull of its immediate neighbors images. Convex combination mappings can guarantee injectivity, are simple to compute algorithmically, offer a discrete analog to harmonic mappings, and can be used to approximate conformal mappings. This lecture provides an introduction to convex combination mappings and their generalizations, as well as their algorithmic aspects and practical applications.

4.2 Triangulations and discrete mappings.

Surfaces in computer graphics are often represented or approximated by triangulations $M = (V, E, F)$, where $V = \{v_i\} \subset \mathbb{R}^d$ (typically $d = 2, 3$) is the vertex set, $E = \{e_{ij}\}$ the edge set, and $F = \{f_{ijk}\}$ the face set. Edges are convex-hulls of pairs of points, $e_{ij} = \text{hull}\{v_i, v_j\}$, and faces are convex-hulls of triplets of points $f_{ijk} = \text{hull}\{v_i, v_j, v_k\}$. M is a simplicial complex, meaning that:

- (i) The intersection of any two faces is either an edge, a vertex or an empty set; the intersection of any two edges is either a vertex or empty.
- (ii) All edges of a triangle are in E ; all vertices of an edge are in V .

Note that a triangulation M is not necessarily a topological surface (*i.e.*, each point has a neighborhood homeomorphic to a disk), as shown for example in Figure 14(a).

To assure a triangulation is indeed a topological surface we add the requirement that

- (iii) The link of each vertex is a simple closed polygon.

The link of a vertex v_i is the union of all edges e_{jk} that do not contain v_i but share a triangle f_{ijk} with it, namely

$$\text{link}(v_i) = \bigcup_{\{e_{jk} \mid f_{ijk} \in F\}} e_{jk}.$$

Definition 1. A surface triangulation is a triangulation $M = (V, E, F)$ satisfying (i)-(iii).

For example, Figure 14(a)-left is not a surface triangulation since the link of the middle vertex consists of two closed polygonal loops; the right example is not a surface since the link of a vertex at any of the two ends of the center edge contains a subset of edges homeomorphic to the symbol \cap .

To allow for surface triangulations with boundary we relax Condition (iii):

- (iii') The link of each vertex is a simple closed polygon or a simple polygonal arc.

Definition 2. A surface triangulation with a boundary is a triangulation $M = (V, E, F)$ satisfying (i)-(ii) and (iii').

The boundary of a surface triangulation M is a one-dimensional simplicial complex, that is a polygonal curve. It consists of all edges with only one adjacent face and all vertices whose link is a polygonal arc. We denote it by $M_B = (V_B, E_B)$. The interior vertex set is denoted $V_I = V \setminus V_B$. Note that in general, in contrast to our intuition from the continuous case, not every boundary vertex has an interior vertex as a neighbor; *e.g.*, stitch a triangle to the boundary of disk-type mesh and consider its dangling vertex.

A surface triangulation $M = (V, E, F)$ is connected if its underlying graph $V = (V, E)$ is connected. It is 3-connected if it cannot be disconnected by removing any two vertices. If M is 3-connected the relation of boundary vertices V_B to interior vertices V_I is similar to the continuous case: every boundary vertex has an interior vertex neighbor (if interior vertices exist). In fact, a stronger claim holds in the

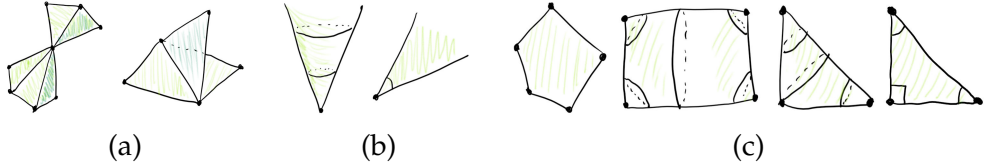


Figure 14: (a) Non manifold triangulations; (b) a cone (left) and a sector (right); (c) Euclidean cone surfaces: convex polygonal region (left), Euclidean orbifolds (middle, right).

3-connected case [9]: any interior vertex v_i can be connected to any other vertex v by a path $P = [v_i, v_1, v_2, \dots, v_k, v]$ of interior vertices $v_j \in V_I$, $1 \leq j \leq k$.

We want to discuss mappings of surface triangulations. The most natural class of mappings of a triangulation consists of simplicial maps:

Definition 3. A simplicial map $f : M \rightarrow \mathbb{R}^d$ is a continuous piecewise-linear mapping defined as the unique piecewise-linear extension of a vertex map taking vertices $v_i \in V$ to $u_i \in \mathbb{R}^d$. By linear extension we mean that every point in the interior of some simplex σ (edge or face) $x = \sum_i \lambda_i v_i$, where $\lambda_i \geq 0$, $\sum_i \lambda_i = 1$, and v_i are the vertices of σ , is mapped to $f(x) = \sum_i \lambda_i u_i$.

A guiding problem for us is:

Problem 1. Given two topologically equivalent surface triangulations M_1 , M_2 , compute a simplicial homeomorphism $f : M_1 \rightarrow M_2$. We would like this homeomorphism to have some minimal distortion property and potentially interpolate given point data $\{(x_i, y_i)\}_{i \in I} \subset M_1 \times M_2$.

Unfortunately, directly computing a homeomorphic simplicial map $M_1 \rightarrow M_2$ is in general a non-convex difficult problem. We will tackle this problem by considering a canonical (topologically equivalent) domain \mathcal{N} and show how to compute a simplicial homeomorphisms $f_1 : M_1 \rightarrow \mathcal{N}$ and $f_2 : M_2 \rightarrow \mathcal{N}$. We then define $f = f_2^{-1} \circ f_1 : M_1 \rightarrow M_2$. The canonical surface \mathcal{N} will be chosen from a particular family of special surfaces $\mathcal{F} = \{\mathcal{N}\}$ we will consider in this note.

4.3 Convex combination mappings.

Our goal is to build a homeomorphic simplicial map $M \rightarrow \mathcal{N}$ onto a member surface of a special family of surfaces $\mathcal{F} = \{\mathcal{N}\}$. Building the homeomorphism $M \rightarrow \mathcal{N}$ will be accomplished by solving a sparse linear system of equations. The method of constructing this simplicial map is called convex combination mapping. It is

originated in [23] and was generalized and given this name in [10, 9, 19]. Both these works allowed homeomorphic simplicial mappings of topological disks into convex polygonal regions. In [16, 21, 13] the embedding was generalized to the topological torus. In [13] sufficient conditions to non-convex, as-well as multiply connected domains were formulated. In [2], the construction was generalized to the collection of Euclidean orbifolds (which contains the torus as a particular case). The following is based mostly on the above papers.

\mathcal{F} will soon be defined as a certain collection of Euclidean cone surfaces.

Definition 4. A compact oriented surface \mathcal{N} is a Euclidean cone surface if it is a metric space locally isometric to an open disk, a cone, or a sector, and the number of cone points is finite.

A cone and a sector are shown in Figure 14(b). For each point $x \in \mathcal{N}$ we define the angle $\theta(x)$ to be the angle sum at point x . Interior points have $\theta(x) = 2\pi$ and boundary points $\theta(x) = \pi$. An interior point is a cone if $\theta(x) \neq 2\pi$. A boundary point is a cone if $\theta(x) \neq \pi$. We will consider a specific family of Euclidean cone surfaces:

$$\mathcal{F} = \{\mathcal{N} \mid \mathcal{N} \text{ is a convex polygonal domain or a Euclidean (parabolic) orbifold}\}.$$

A convex polygonal domain is shown in, *e.g.*, Figure 14(c), left. Figure 14(c), right, shows three examples of Euclidean orbifolds: two topological spheres and a topological disk. The Euclidean orbifolds is a specific family of Euclidean cone surfaces defined by taking the quotient of the plane \mathbb{R}^2 w.r.t. a wallpaper symmetry group of the plane, G , *i.e.*, \mathbb{R}^2/G . Put differently, a symmetry group G defines an equivalence relation $u \sim w$ iff $u = g(w)$ for some $g \in G$. Taking the quotient topology w.r.t. such an equivalence relation leads to a surface \mathcal{N} where the orbits of G , namely $[u] = \{g(u) \mid g \in G\}$, are identified as points. The orbifolds are in one-to-one correspondence with the 17 wallpaper groups. Euclidean orbifolds are characterized by their topological type, and number, order and types of cones. There are two types of cones: reflective (where the surface is locally isometric to a sector, see Figure 14(b), right), and rotational (where the surface is locally isometric to a cone, see Figure 14(b), left). The order of a cone point x is $2\pi/\theta(x)$ for rotational and $\pi/\theta(x)$ for reflectional cones. Figure 16 lists all Euclidean orbifolds using the so-called orbifold notation [5]. Figure 14(c) shows (2222), (244), and (*244) orbifolds, respectively.

Each Euclidean orbifold has a fundamental domain, namely a domain that represent a connected choice of a representative per orbit. As fundamental domains we use (closed) disk-type polygonal domains Ω defined by a closed convex polygonal curve $[p_1, p_2, \dots, p_m]$ together with a list of identifications of pairs of edges $[p_i, p_{i+1}] \leftrightarrow [p_j, p_{j+1}]$ by rigid motions $g \in G$, *i.e.*, $g([p_i, p_{i+1}]) = [p_j, p_{j+1}]$. Note that

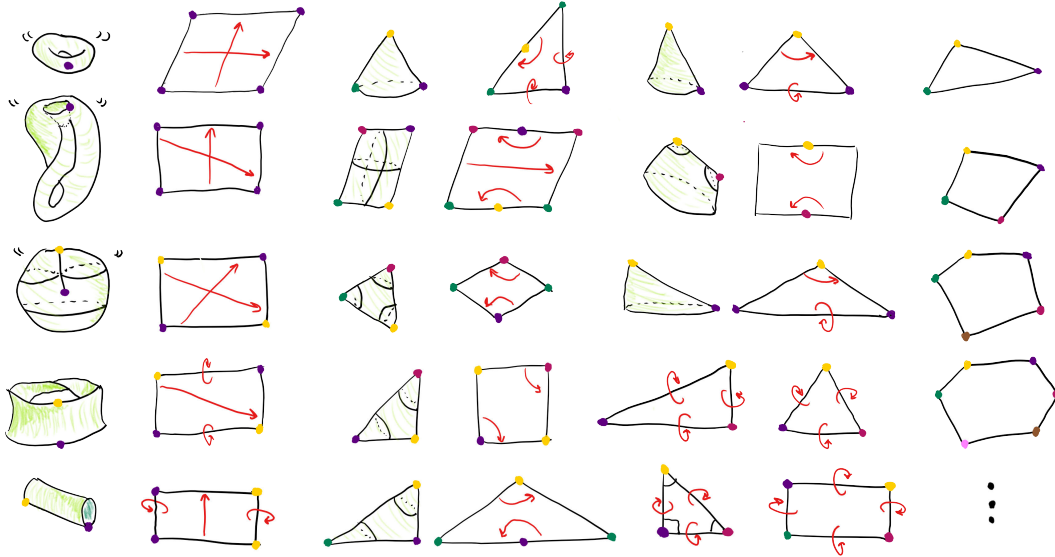


Figure 15: All types of fundamental domains; rigid motion identifications of edges are depicted with arrows.

these rigid identifications g also generate G . Pairs of different edges are identified with rotations, translations, or glides (a composition of a reflection and translation along a line), while self identified edges are identified with reflections. Figure 15 that shows all fundamental domains where the identification are visualized by arrows. Arrows between different edges include rotations, translations, and glides (slanted arrows); self arrows indicate reflection across the infinite line supporting the edge. The edge identification implies an equivalence relation in $\Omega \times \Omega$ where identified points are in the same equivalence class. Once we quotient Ω by this relation (*i.e.*, the edges of Ω are stitched together) we achieve the orbifold \mathcal{N} . For convex polygonal domains we denote $\Omega = \mathcal{N}$ with all edges self-identified (right column in Figure 15).

We will build a simplicial mapping $f : M \rightarrow \mathcal{N}$ called a convex combination mapping. This is done by assigning a positive weight, $\omega_{ij} > 0$, to each edge $e_{ij} \in E$.

Definition 5. A convex combination mapping $f : M \rightarrow \mathbb{R}^2$ is a simplicial map mapping each interior vertex $v_i \in V_I$ to a planar point $u_i \in \mathbb{R}^2$ so that

$$\sum_{j \in \mathfrak{N}_i} \omega_{ij} (u_j - u_i) = 0, \quad (24)$$

where $\mathfrak{N}_i = \{j \mid e_{ij} \in E\}$ is the neighbor index set of v_i . Geometrically, u_i is strictly inside the convex-hull defined by its immediate neighbors.

An important property of convex combination mappings is the discrete maxi-

topology	cones
sphere	(236), (244), (333), (2222)
disk	(*236), (*244), (*333), (*2222), (2 * 22), (3 * 3), (4 * 2), (22*)
projective plane	(22x)
torus	(o)
Klein bottle	(xx)
annulus	(**)
Möbius band	(*x)

Figure 16: The types of Euclidean orbifolds. On left to * (or without any *) are rotational cone orders; on the right to * reflective cone orders.

mum principle. It is useful to formulate it in the functional setting: Let $h : M \rightarrow \mathbb{R}$ satisfy the convex combination property (24) at each interior vertex V_I . That is, to each vertex $v_i \in M$ one associates a scalar $h_i \in \mathbb{R}$ and these scalars satisfy (24) for all $v_i \in V_I$. For example, one can consider the x - or y -coordinate of convex combination mapping. Then, as proved *e.g.*, in [9],

Proposition 1. (Discrete maximum principle.) Let $h : M \rightarrow \mathbb{R}$ be a convex combination function, and M a 3-connected surface triangulation. Let $v_i \in V_I$. If $h_i = \min_j h_j$ or $h_i = \max_j h_j$ then h is constant function. In particular this implies that the maximum and minimum is achieved on the boundary V_B . The last assertion is true also if M is not 3-connected.

Proof. Assume $h_i = \min h_j$. The convex combination property together with the fact that h_i achieves the minimum imply that its immediate neighbors also equal h_i . Using the 3-connectedness we can construct an interior path to any other vertex, therefore continuing in this manner the proposition is proved. \square

Convex combination mappings by themselves are not sufficient for building homeomorphisms. For example, the trivial (*i.e.*, constant) convex combination mapping $u_i = u, \forall i$ always exist. To achieve a homemorphism certain boundary conditions should be applied. These boundary conditions in essence force the image of the map, $f(M)$, to cover \mathcal{N} . Bijectivity follows from the particular properties of the family of surfaces \mathcal{F} and is not true in general for Euclidean cone surfaces.

We deal with M of one of the topological types that appear in \mathcal{F} (all possible topological types and fundamental domains are listed in Figure 16 and depicted in Figure 15). Given a choice of target cone surface $\mathcal{N} \in \mathcal{F}$ with m cones, let its fundamental disk domain be denoted Ω . Choose a connected polygonal path $\Gamma \subset V \cup E$ passing through at-least m vertices of M , denoted $C = \{v_{c_1}, v_{c_2}, \dots, v_{c_m}\} \subset V$,

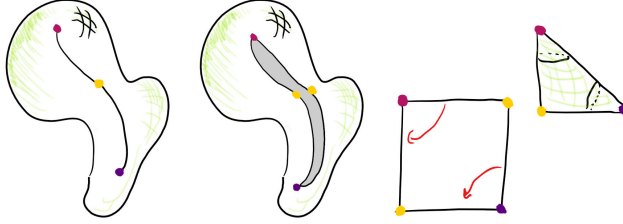


Figure 17: A surface triangulation M (left) is cut into M' (middle-left) to be homeomorphic to the fundamental domain Ω (middle-right) of a selected target \mathcal{N} (right).

so that $M \setminus \Gamma$ is homeomorphic to Ω° (i.e., the interior of Ω). Let $M' = \{V', E', F'\}$ be the (uniquely defined) triangulation so that $F' = F$ and M' is homeomorphic to Ω . Figure 17 shows an example of (from left to right) triangulations M , M' , Ω and a target orbifold \mathcal{N} . To compute the simplicial homeomorphism $f : M \rightarrow \mathcal{N}$ we consider M' and define a simplicial map $s : M' \rightarrow \mathbb{R}^2$ by solving a linear system of equations. The unknowns of the linear system are $u_i = s(v_i)$, $v_i \in V'$; the simplicial map s is the unique piecewise linear extension of this vertex map. The total degrees of freedom of s are therefore $u = \{u_1, u_2, \dots, u_{|V'|}\}$. The linear system consists of three sets of equations:

- (a) For interior vertices, V'_I , we set the convex combination equation (24), that is, every interior vertex is mapped strictly inside the convex hull of its immediate neighbors.
- (b) For boundary vertices, $V'_B \setminus C$ we formulate equations preserving the edge identification rigid motions (see Figure 15), and maintaining the convex combination condition across the boundary of M' .
- (c) For cone vertices C , we restrict their position to the vertices of the fundamental domain Ω ,

$$u_{c_i} = p_i, \quad i = 1, \dots, m. \quad (25)$$

Equations (b) are dependent on the choice of target surface $\mathcal{N} \in \mathcal{F}$ and realize the edge identification in the fundamental domain. The inclusion map $\iota : M' \hookrightarrow M$ induces an equivalence relation $x \sim y \iff \iota(x) = \iota(y)$. Taking the quotient of M' by this equivalence relation results in M . This in particular induces an equivalence relation in the vertex set, $v_i \sim v_j$ in V' . The equivalence classes $\langle v_i \rangle = \{v_{i'} \in V' \mid v_{i'} \sim v_i\}$ include interior vertices as singletons, and boundary vertices either as singletons, $V'_{BS} = \{\langle v_i \rangle \mid v_i \in V'_B, \langle v_i \rangle = \{v_i\}\}$ (in case of v_i is also boundary of M) or pairs $V'_{BP} = \{\langle v_i \rangle \mid v_i \in V'_B, \langle v_i \rangle = \{v_i, v_{i'}\}\}$ (v_i is not a boundary of M). Singleton boundary vertices V'_{BS} are aligned by reflections, namely, stay on

some infinite line,

$$a_i^T u_i + b_i = 0, \quad \forall \langle v_i \rangle \in V'_{BS}, \quad (26)$$

where $a_i \in \mathbb{R}^2$, $b_i \in \mathbb{R}$. Pairs of boundary vertices V'_{BP} are aligned by rotations, translations, or glide-reflections

$$u_i = r_{ii'} u_{i'} + t_{ii'}, \quad \forall \langle v_i \rangle \in V'_{BP}, \quad (27)$$

where $r_{ii'} \in O(2)$ and $t_{ii'} \in \mathbb{R}^2$. Note that (26) and (27) do not capture all the degrees of freedom for non-cone boundary vertices, $V'_B \setminus C$; there is still one degree of freedom for singleton boundary vertex and two degrees of freedom for a pair of boundary vertices. These degrees of freedom are used to assure the convex combination property is preserved across the boundary of M' :

$$\sum_{j \in \mathfrak{N}_i} \omega_{ij} (a_i^\perp)^T (u_j - u_i) = 0, \quad \forall \langle v_i \rangle \in V'_{BS}, \quad (28)$$

where $a_i^\perp \perp a_i$, and

$$\sum_{j \in \mathfrak{N}_i} \omega_{ij} (u_j - u_i) + \sum_{j \in \mathfrak{N}_{i'}} \omega_{i'j} r_{ii'} (u_j - u_{i'}) = 0, \quad \forall \langle v_i \rangle \in V'_{BP}. \quad (29)$$

We denote the linear system

$$\mathcal{L} = (a) + (b) + (c).$$

Proposition 2. The linear system \mathcal{L} is non-singular.

Proof. Assume a non-trivial solution u is in the kernel of the linear system \mathcal{L} . Let $h(u) = a^T u + b$ be an arbitrary linear functional in \mathbb{R}^2 . h defined by $h_i = a^T u_i + b$ is a convex combination function over the interior of M' . Since $h_{c_i} = 0$ we know that $\min_i h_i \leq 0$. Assume that $\min_i h_i < 0$, and let $h_j = \min_i h_i$. Consider a path P connecting v_j and its nearest cone v_c in M . If this path intersects the boundary of M' note that h can be extended through this boundary preserving the convex combination property and $h_{c_i} = 0$ for all duplicated cones. Note this path traverses only vertices satisfying the convex combination property and therefore, reusing the discrete maximum principle it means $h_c < 0$, in contradiction. Since h is arbitrary we get that $u_i = 0, \forall v_i \in V'$ contradicting our assumption of a non-trivial kernel. \square

The simplicial map $s : M' \rightarrow \Omega$ defines a unique map $f : M \rightarrow \mathcal{N}$ by

$$f(\langle x \rangle) = [s(x)], \quad \forall x \in M'.$$

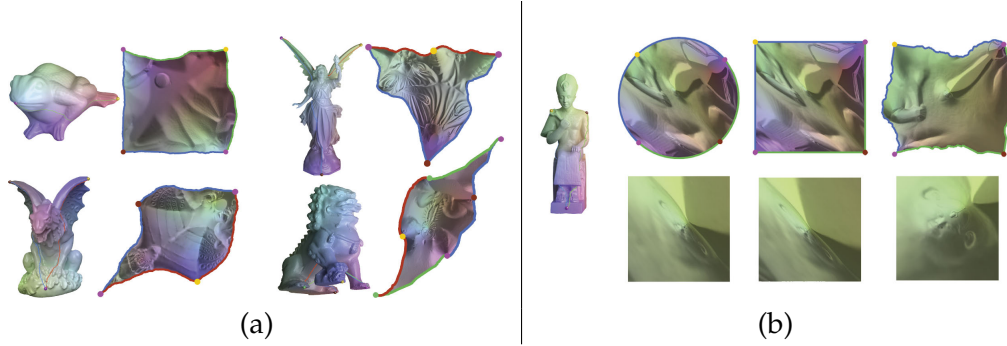


Figure 18: (a) shows convex combination homeomorphism of surface triangulations to different sphere-type orbifolds (from top-left): (244), (236), (333), and (2222). (b) shows convex homeomorphism to a convex polygonal domain (two left columns) and to a sphere-type (244) orbifold; bottom row shows blow-ups of the image. Note that the orbifold map is approximately conformal. Images taken from [2].

Remember that $\langle x \rangle$ represents points in \mathcal{M} . The map is well defined since pairs $y, z \in \langle x \rangle$ are in M'_B (*i.e.*, the boundary of M') and are mapped, due to the boundary conditions (26), (27), to points $f(y), f(z)$ in the same orbit of G , that is, $[f(y)] = [f(z)]$. Figure 18(a) shows some examples of convex combination homeomorphisms of topological spheres onto a sphere-type Euclidean orbifold; (b) shows a comparison of convex combination mappings of the same cut surface M' onto two convex polygonal domains (disk-like and square) and a sphere-type orbifold. Note how angles are better preserved in the latter mapping; this will be discussed later on. Note that in case that \mathcal{N} is a convex polygonal domain only equations (a) and (c) are used and there is no need for (b). That is, all boundary vertices of M are mapped to vertices of $\Omega = \mathcal{N}$.

Theorem 1. *Let M be a 3-connected surface triangulation and $\mathcal{N} \in \mathcal{F}$ a homeomorphic target domain. Then, the simplicial map f defined by \mathcal{L} is a homeomorphism.*

4.4 Proof of homeomorphism.

It is not a-priori clear that $f : M \rightarrow \mathcal{N}$ constructed above is a homeomorphism. Indeed, f constructed with \mathcal{N} taken to be a non-convex polygonal domain or a different Euclidean cone surface in general will not be a homeomorphism. Next we will prove the homeomorphism of f using arguments from different papers [3, 16, 15]. We will prove only the case of \mathcal{N} being a orbifold for two reasons: first, the proof for convex polygonal domains can be easily deduced from the proof below (it is almost a particular case), and second, the proof for convex polygonal domains has many excellent versions in the literature, *e.g.*, the concise proof in [8], and the

proof based on a discrete index theorem in [13]. We also note the proof in [16]. In the original orbifold paper [2] the proof of the embedding is done by reduction to the torus case, which is a particular instance of a Euclidean orbifold and is a sub-group of all other wallpaper groups. We provide here, hopefully, a clear, short and self-contained proof. The proof follows the steps:

- (i) The simplicial map $s : M' \rightarrow \mathbb{R}^2$ defined by the solution to \mathcal{L} does not degenerate and maintain the orientation at-least one triangle of M' .
- (ii) Given two triangles sharing an edge in M' . If s does not degenerate one of the triangles then it also does not degenerate the other triangle and the images of the two triangles under f will be on two different sides of the common edge.
- (iii) s does not degenerate and maintains the orientations of the triangles of M' and therefore defines a homeomorphism $f : M \rightarrow \mathcal{N}$.

An instrumental part of the proof is to use a (branched) cover mesh M'' constructed from M' as follows. Use the symmetry group action G and stitch $s(M')$ to itself along boundaries to create an infinite triangulation in the plane (with no boundary); call this triangulation M'' and the image of each vertex $v_i \in V''$ is $u_i \in \mathbb{R}^2$. We will keep denoting this simplicial map s . Note that $s : M'' \rightarrow \mathbb{R}^2$ satisfies the convex combination property at *all* vertices. Indeed, it is clearly so (*i.e.*, by construction) at vertices in M'' originated from interior and boundary non-cone vertices of M' . It is also true for vertices originated from cone vertices of M' since at these points a point sub-group of G was applied to the neighbors of the cone points and therefore they are at the centroid of its neighbors in M'' .

We start with (i). Consider a generic point $u \in \mathbb{R}^2$ (*i.e.*, a point not on any edge image of M'' , *i.e.*, $u \notin s(E'')$). We will show it is contained in some non-degenerate positively oriented triangle $s(f_{ijk})$. To find such a triangle we can compute the winding number $\omega(u, t)$ of u w.r.t. the oriented boundary curve of some oriented triangle $t = s(f_{ijk})$. If $u \in t$ then $\omega(u, t) = \pm 1$ otherwise $\omega(u, t) = 0$. Another property of the winding number is that

$$\sum_i \omega(u, t_i) = \omega(u, \cup_i t_i). \quad (30)$$

Let us denote the diameter of $s(M')$ by $d > 0$. To find a triangle containing u let us consider a tiling of enough copies of M' around u using group transformations G so that: (i) any copy of M' not considered is of distance greater than d to u ; and (ii) the boundary of the union of this tiling is a closed polygonal line of distance at-least d to u . From (i)+(ii) we get that the winding number of u w.r.t. the boundary of the tiling is 1. On the other hand by (30) the winding number equals the sum of

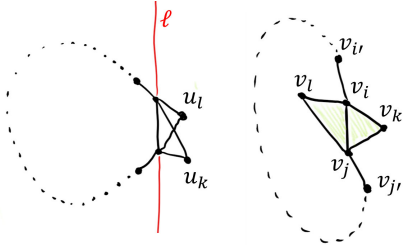


Figure 19: Diagram for proof of (ii) in homeomorphism proof.

windings of all triangles in the tiling. Therefore, there has to be at-least one triangle positively oriented and containing u .

To prove (ii) we will start with the following lemma for the infinite triangulation M'' :

Lemma 1. *Let M'' be a tiling generated from a convex combination map M' defined as the solution of \mathcal{L} . Consider an infinite line $\ell \subset \mathbb{R}^2$ and vertices u_i, u_j which are strictly on one side of ℓ . Then, there is a path $P \subset E''$ connecting u_i, u_j that is also strictly on the same side of ℓ .*

Before proving this Lemma let us use it to prove (ii). Let f_{ijk}, f_{ikl} two faces in M' sharing an edge and f_{ijk} is not degenerate. It is enough to show (ii) for a copy of these faces in M'' (since all these copies are rigid motions of the original triangles). For a bit of notational convenience we will treat $u \in \mathbb{C} \cong \mathbb{R}^2$, and $\text{Re}(u)$ will denote the real part of u . Without loosing generality assume that $\ell = \{u \mid \text{Re}(u) = 0\}$ and $\text{Re}(u_k) > 0$. Assume toward contradiction that $\text{Re}(u_l) \geq 0$, see Figure 19. By the convex combination property there are v_i, v_j neighbors of v_i, v_j (resp.) so that $\text{Re}(u_{i'}), \text{Re}(u_{j'}) < 0$. Use Lemma 1 to connect $v_{i'}$ and $v_{j'}$ by a path $P = [v_{i'} = v_{p_0}, v_{p_1}, v_{p_2}, \dots, v_{p_k}, v_{j'} = v_{p_{k+1}}]$ with $\text{Re}(u_{p_i}) < 0$, for $i = 1, \dots, k$. Now consider the simple closed path $Q = [v_j, v_i, P]$. The path Q divides M'' to two connected parts, one bounded and one unbounded. Consider the bounded part $U \subset V''$: it contains either v_k or v_l . Since $\text{Re}(u_q) \leq 0$ for all $u_q \in Q$, the (second part of the) discrete maximum principle (Proposition 1) implies that $\text{Re}(u_j) \leq 0$ for all $v_j \in U$. Since $\text{Re}(u_k) > 0$, U cannot contain v_k . So $v_l \in U$. Consider the maximal 3-connected sub-graph containing v_l in U . We claim it has to contain a boundary point $v_b \in Q$ other than v_i, v_j . Indeed otherwise we can disconnect the graph by removing v_i, v_j which contradicts the 3-connectedness. Since $\text{Re}(u_l) \geq 0$ and we already know that $\text{Re}(u_j) \leq 0$ for all $u_j \in U$, the (first part of) discrete maximum principle implies that $u_j = u_l = 0$ for all $v_j \in U$, however $v_b \in U$ and $\text{Re}(u_b) < 0$, a contradiction.

Proof. (Lemma 1)

Lets assume, as before, without loosing generality that $\ell = \{u \mid \text{Re}(u) = 0\}$. Let us first show that we can find an infinite path $P = [v_i, v_{i_1}, v_{i_2}, \dots]$ starting from v_i so that $\text{Re}(v_i) \leq \text{Re}(v_{i_k}) \nearrow \infty$. Assume that v_i has a neighbor v_{i_1} so that $\text{Re}(v_{i_1}) > \text{Re}(v_i)$. Then from the convex combination property we can construct a strictly monotone infinite series $P = [v_i, v_{i_1}, v_{i_2}, \dots]$. We need to show that $\text{Re}(v_{i_k}) \rightarrow \infty$. Since M'' is made out of finite number of types of edges there is a number $\delta > 0$ so that $\text{Re}(v_{i_{k+1}}) - \text{Re}(v_{i_k}) \geq \delta$ and the convergence to infinity is proven.

If v_i does not have such a neighbor, the convex combination property means all its neighbors are on the line $\ell + \text{Re}(v_i)$. Since M'' is not contained in $\ell + \text{Re}(v_i)$ there is some vertex $v_{i'}$ connected to v_i by a simple path so that $\text{Re}(v_{i'}) > \text{Re}(v_i)$. Now we can continue as above to construct P .

Let $P = [v_i, v_{i_1}, v_{i_2}, \dots]$ and $Q = [v_j, v_{j_1}, v_{j_2}, \dots]$ be two monotonic paths starting from v_i and v_j (resp.) and going to infinity. If P, Q intersect at some vertex we have a simple path connecting v_i, v_j . So lets assume they do not intersect. As before, let $d > 0$ denote the diameter of one copy of the image of M' in \mathbb{R}^2 . Therefore, any two cones v_{c_1}, v_{c_2} , or a vertex v_k and a cone v_{c_1} in the same copy of M' , can be connected by a shortest path that is contained in a disk of diameter d . Therefore given two arbitrary vertices v_k, v_l , such that $\text{Re}(v_k) \leq \text{Re}(v_l)$ they can be connected by a path R going from v_k to a nearest cone v_{c_1} , traveling on the two dimensional grid made of cones to a nearest cone v_{c_2} to v_l and then to v_l . Note that the cone grids of all Euclidean orbifolds are regular and made out of two generators, $n\eta + m\xi$. All the vertices of R satisfy $\text{Re}(v_r) > \text{Re}(v_k) - 2d$. Therefore continuing P, Q until their distance from ℓ is at-least $2d$, they can be connected by a path R also to the right of ℓ . Concatenating P, R, Q^{-1} , possibly eliminating cycles will provide the desired path. \square

To prove (iii) we note that we have by now that all triangles in M'' are non degenerate and positively oriented. We will repeat the winding number argument above to conclude that every generic point $u \in \mathbb{R}^2$ is covered by exactly one triangle $s(f_{ijk})$. Repeating the same argument we see the winding w.r.t. a sufficiently large tiling is 1. Also the triangles not participating in the tiling are too far to contain u . Since all the triangles in the tiling can contribute either 0 or 1, we conclude exactly one triangle contain u . Since s is an open map it means that every point u is covered exactly once. Therefore $s : M'' \rightarrow \mathbb{R}^2$ is a homeomorphism, and consequently $f : M \rightarrow \mathcal{N}$ is a homeomorphism on \mathcal{N} .

4.5 Variational principle.

When the weights are symmetric, $w_{ij} = w_{ji}$, convex combination maps have variational formulation. Denote the discrete Dirichlet energy by

$$E_D(u) = \frac{1}{2} \sum_{e_{ij} \in E} w_{ij}(u_i - u_j)^2. \quad (31)$$

The linear system of equations \mathcal{L} characterizes the solution of the following variational problem:

$$\min_u E_D(u) \quad (32a)$$

$$\text{s.t. } a_i^T u_i + b_i = 0, \quad \forall \langle v_i \rangle \in V'_{BS} \quad (32b)$$

$$u_i = r_{ii'} u_{i'} + t_{ii'}, \quad \forall \langle v_i \rangle \in V'_{BP} \quad (32c)$$

$$u_{c_i} = p_i, \quad i = 1, \dots, m \quad (32d)$$

One way [18, 9] to figure out a good choice of weights w_{ij} is to choose it so that (31) becomes the Dirichlet energy, $\int_M |\nabla f|^2$, when computed on the piecewise linear simplicial map f . A calculation shows that in this case

$$w_{ij} = \cot \alpha_{ij} + \cot \beta_{ij},$$

where α_{ij}, β_{ij} are the angles opposite to the edge e_{ij} in M . These weights are called the cotan weights for obvious reasons. The cotan weights are symmetric and since $w_{ij} = \frac{\sin(\alpha_{ij} + \beta_{ij})}{\sin \alpha_{ij} \sin \beta_{ij}}$ they are positive iff the sum of angles supporting e_{ij} is smaller than π ; such a triangulation M is this called Delaunay (without 4 co-circle points). Using non-positive weights will generically damage the homeomorphism property of the map f but approximation properties will not be affected (discussed later). Another interesting option of weights which are not symmetric but always positive are the mean-value weights [11]. Although they don't posses variational principle due to the non-symmetry these weights can be used in the linear system \mathcal{L} to produce homeomorphic convex combination mappings.

4.6 Approximation of conformal mappings.

The variational representation (32) leads to an interesting observation in case w_{ij} are the cotan weights [2]. The Dirichlet energy can be seen as an upper-bound to the area functional,

$$E_D(u) \geq E_A(u),$$

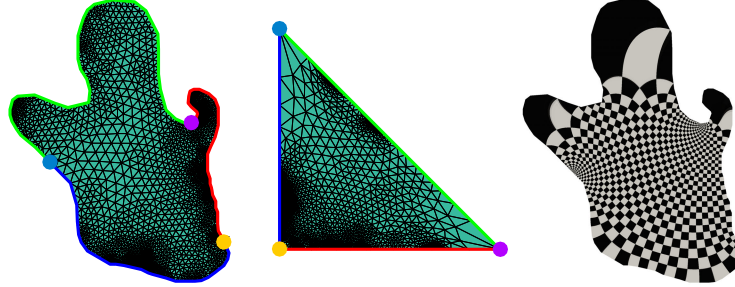


Figure 20: Convex combination homeomorphism, mapping a triangulation of a simply connected polygonal domain (left) onto a Euclidean orbifold triangle (middle). On the right, a pull-back checkerboard texture via the inverse of the mapping to visualize the conformality of the discrete mapping.

where E_A denotes the area functional, measuring the sum of (positive) triangle areas in $s(M')$. In case M is 3-connected and Delaunay, $w_{ij} > 0$, and Theorem 1 implies that $E_A(u) = \text{area}(\Omega) = \text{area}(\mathcal{N})$. The difference

$$E_C(u) = E_D(u) - E_A(u)$$

can be seen as the conformal distortion, and in the case u is a homeomorphism it equals the so-called least-squares conformal energy [14]. When using $\mathcal{N} \in \mathcal{F}$ with just three cones the number of constrained points is exactly right by the Riemann mapping theorem. Therefore, one can ask if $f : M \rightarrow \mathcal{N}$ actually converges under refinement to the unique conformal map, mapping three prescribed points in M to the cones of \mathcal{N} . This is proved recently in [7] for the case of a simply connected polygonal domain in the plane, and when $\mathcal{N} \in \mathcal{F}$ is a triangle. In fact it is shown that convergence in H^1 holds for any triangle (not just ones that can tile the plane) and any mesh (not necessarily Delaunay) however it is uniform when M is Delaunay and $\mathcal{N} \in \mathcal{F}$ (so f is a homeomorphism):

Theorem 2. Let $\mathcal{P} \subset \mathbb{R}^2$ be a simply-connected polygonal domain and \mathcal{N} a triangle. Let M_h be surface triangulations of \mathcal{P} with maximal edge length $h \rightarrow 0$ and all angles of the triangulations bounded below by some $\delta > 0$. Let $f_h : \mathcal{P} \rightarrow \mathcal{N}$ denote the simplicial maps defined by solving \mathcal{L} fixing three pre-images in $\partial\mathcal{P}$ to the cones of the triangle. Let $\Phi : \mathcal{P} \rightarrow \mathcal{N}$ be the Riemann map fixing the same pre-images. Then,

$$\|f_h - \Phi\|_{H^1} \rightarrow 0.$$

If M_h are Delaunay, the convergence is also uniform.

Figure 20 shows an example of an approximation of a Riemann mapping from a polygonal domain to an Euclidean orbifold. Note the texture on the right demonstrating the conformality of the discrete mapping.



Figure 21: A simplicial map between pairs of surface triangulations composed out of two convex combination mappings to a common orbifold (here (2222)); the colored spheres indicate the interpolated points $(x_i, y_i) \in M_1 \times M_2$ in the map. Images taken from [2].

4.7 Surface to surface mappings.

Another application of convex combination mappings is Problem 1, namely construction of a homeomorphism $f : M_1 \rightarrow M_2$ between two surface triangulations M_1, M_2 . Consider a cone surface $\mathcal{N} \in \mathcal{F}$ that is topologically equivalent to both M_1 and M_2 . Construct a simplicial homeomorphism $f_1 : M_1 \rightarrow \mathcal{N}$ and $f_2 : M_2 \rightarrow \mathcal{N}$ and consider $f = f_2^{-1} \circ f_1 : M_1 \rightarrow M_2$. The map f is also simplicial if one considers an isomorphic joint subdivision (a.k.a. meta-mesh) M of M_1 and M_2 . Using \mathcal{N} with three cones provides a simplicial homeomorphism approximating the conformal map interpolating arbitrary three vertices between M_1 and M_2 . (Note that M_1, M_2 are in particular Riemann surfaces.) Using $\mathcal{N} \in \mathcal{F}$ with four cones (i.e., orbifold of type (2222)) provides a quasiconformal map $f : M_1 \rightarrow M_2$ with approximately constant conformal distortion. Therefore the four cone \mathcal{N} provides a quasiconformal approximation to the Teichmüller map interpolating four points on the sphere [1]. Indeed, it is possible to write $f = f_2^{-1} \circ A \circ f_1$, where f_1, f_2 are homeomorphisms of finite surface triangulations, which makes them quasiconformal, and since f_1, f_2 approximate conformal mappings their dilatation is close to 0; A is an affine map. Figure 21 depicts examples of approximate quasiconformal mapping between pairs of surface triangulations interpolating four landmark points.

4.8 Other Euclidean cone surfaces.

Problem 2. When convex combination mappings onto Euclidean cone surfaces not in \mathcal{F} are homeomorphism?

This could be useful for discrete mappings for two reasons: (i) it will allow constraining more than three or four points; and (ii) it will potentially allow choosing

\mathcal{N} so to reduce isometric distortion exerted by the map. As far as the author knows there are no Euclidean cone surfaces outside the family \mathcal{F} that generically allow homeomorphic convex combination maps. Furthermore, an interesting (and not completely solved) problem is:

Problem 3. Find a characterization when a Euclidean cone surface provides homeomorphic convex combination map, even if it does not allow it generically.

Let us review several known results addressing this latter problem discussing other Euclidean cone surfaces $\mathcal{N} \notin \mathcal{F}$. In [13] a non-convex polygonal domains are discussed and a sufficient condition for a convex combination map to be bijective in this case is that every reflex cone (*i.e.*, a cone x with angle sum $\theta(x) > \pi$) is at the convex hull of its neighbors. (Notice that this latter condition can fail.) A similar generalization to multiply-connected domains also exists.

In [4] a Euclidean cone manifold with rational cone angles $k\frac{2\pi}{q}$, $k, q \in \mathbb{N}$ is considered and it is shown that if the triangles adjacent to the cones are positively oriented the convex combination map is locally a homeomorphism.

In [22, 3] convex combination mappings are considered into the hyperbolic plane by minimizing the discrete hyperbolic Dirichlet energy [20]:

$$E_D(u) = \frac{1}{2} \sum_{e_{ij} \in E} w_{ij} d(u_i, u_j)^2,$$

where $u_i \in \mathcal{H}$ are points in the hyperbolic plane and $d(\cdot, \cdot)$ denotes the hyperbolic distance. Boundary conditions can be added to form a variational problem generalizing (32) to the hyperbolic case, namely for defining and computing homeomorphic simplicial mappings of a surface triangulation onto one of the hyperbolic orbifolds $\{\mathcal{N}\}$. Hyperbolic orbifolds, are defined similarly to the Euclidean orbifolds as \mathcal{H}/G where G is a symmetry group of the hyperbolic plane. In contrast to Euclidean orbifolds, hyperbolic orbifolds are an infinite family of (hyperbolic) cone surfaces that can possess arbitrary genus surfaces and arbitrary number of cones ≥ 5 . The boundary conditions are similar to (32b)-(32d) forcing identified boundary vertices of M' to correspond via the relevant hyperbolic isometries, namely Möbius transformations. It is proved in [3], basically following the same proof as the Euclidean case above (this time in the Klein hyperbolic model), that critical points of this non-linear problem provide homeomorphisms onto the respective hyperbolic orbifold. Figure 22(a) shows a sphere-type hyperbolic orbifold with seven cones of angle π , *i.e.*, with symbol (2^7) ; (b) shows a homeomorphic hyperbolic convex combination mapping to this hyperbolic orbifold; (c) shows a homeomorphism $f = f_2^{-1} \circ f_1 : M_1 \rightarrow M_2$ between two human surface triangulations M_1, M_2 interpolating seven landmark

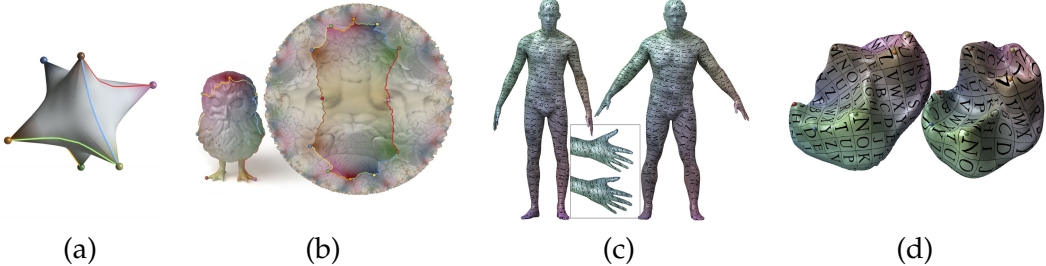


Figure 22: (a) shows a sphere-type hyperbolic orbifold with seven cones of angle π ; (b) hyperbolic convex combination mapping of a sphere-type triangulation (owl) to this target orbifold; (c)-(d) homeomorphisms of surface triangulation by composing hyperbolic convex combination mappings to a common orbifold. Images taken from [3, 17].

points, where $f_i : M_i \rightarrow \mathcal{N}$, $i = 1, 2$ are hyperbolic convex combination mapping to the same hyperbolic orbifolds. Note that allowing the interpolation of seven points produces a more faithful map than the one generated with four interpolated points in the Euclidean case, Figure 21, right. Figure 22(d) shows another application of mapping anatomical surfaces (teeth).

4.9 Convex combination in higher dimensions.

A natural question is the generalization of convex combination mapping to three dimensional simplicial complexes. Consider a tetrahedral mesh $M = (V, E, F, T)$, where $T = \{t_{ijkl}\}$ is the tetrahedra set, $t_{ijkl} = \text{hull } \{v_i, v_j, v_k, v_l\}$. Convex combination mappings can be defined as before using (24). Unfortunately, even in the most basic case of a convex polyhedron boundary conditions (assuming M is topologically a ball) the convex combination map is not guaranteed to be a homeomorphism, and counter examples were found [6, 12].

Acknowledgements. The author of this note would like to thank Noam Aigerman and Nadav Dym for good advice and proof reading. This work was funded by the Israel Science Foundation (grant No. 1830/17).

REFERENCES

- [1] L. V. Ahlfors, C. J. Earle, I. Kra, M. Shishikura, and J. H. Hubbard. *Lectures on quasiconformal mappings*, volume 3. van Nostrand Princeton, 1966.
- [2] N. Aigerman and Y. Lipman. Orbifold tutte embeddings. *ACM Trans. Graph.*, 34(6):190–1, 2015.
- [3] N. Aigerman and Y. Lipman. Hyperbolic orbifold tutte embeddings. *ACM Trans. Graph.*, 35(6):217–1, 2016.
- [4] A. Bright, E. Chien, and O. Weber. Harmonic global parametrization with rational holonomy. *ACM Transactions on Graphics (TOG)*, 36(4):89, 2017.
- [5] J. Conway, H. Burgiel, and C. Goodman-Strauss. *The symmetry of things*. Wellesley, MA, A K Peters, 2008.
- [6] É. C. De Verdière, M. Pocchiola, and G. Vegter. Tutte’s barycenter method applied to isotopies. *Computational Geometry*, 26(1):81–97, 2003.
- [7] N. Dym, Y. Lipman, and R. Slutsky. A linear variational principle for riemann mapping and discrete conformality. *arXiv preprint arXiv:1711.02221*, 2017.
- [8] H. Edelsbrunner and J. Harer. *Computational topology: an introduction*. American Mathematical Soc., 2010.
- [9] M. Floater. One-to-one piecewise linear mappings over triangulations. *Mathematics of Computation*, 72(242):685–696, 2003.
- [10] M. S. Floater. Parametrization and smooth approximation of surface triangulations. *Computer aided geometric design*, 14(3):231–250, 1997.
- [11] M. S. Floater. Mean value coordinates. *Computer aided geometric design*, 20(1):19–27, 2003.
- [12] M. S. Floater and V. Pham-Trong. Convex combination maps over triangulations, tilings, and tetrahedral meshes. *Advances in Computational Mathematics*, 25(4):347–356, 2006.
- [13] S. J. Gortler, C. Gotsman, and D. Thurston. Discrete one-forms on meshes and applications to 3d mesh parameterization. *Computer Aided Geometric Design*, 23(2):83–112, 2006.
- [14] B. Lévy, S. Petitjean, N. Ray, and J. Maillot. Least squares conformal maps for automatic texture atlas generation. In *ACM transactions on graphics (TOG)*, volume 21, pages 362–371. ACM, 2002.
- [15] Y. Lipman. Bijective mappings of meshes with boundary and the degree in mesh processing. *SIAM Journal on Imaging Sciences*, 7(2):1263–1283, 2014.
- [16] L. Lovász. Discrete analytic functions: an exposition. *Surveys in differential geometry*, 9:241–273, 2004.
- [17] H. Maron, M. Galun, N. Aigerman, M. Trope, N. Dym, E. Yumer, V. G. KIM, and Y. Lipman. Convolutional neural networks on surfaces via seamless toric covers. SIGGRAPH, 2017.
- [18] U. Pinkall and K. Polthier. Computing discrete minimal surfaces and their conjugates. *Experimental mathematics*, 2(1):15–36, 1993.
- [19] J. Richter-Gebert. *Realization spaces of polytopes*. Springer, 2006.
- [20] R. Shi, W. Zeng, Z. Su, H. Damasio, Z. Lu, Y. Wang, S.-T. Yau, and X. Gu. Hyperbolic harmonic mapping for constrained brain surface registration. In *Proceedings of the IEEE Conference on Computer Vision and Pattern Recognition*, pages 2531–2538, 2013.

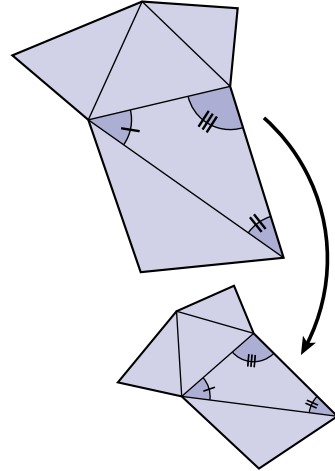
- [21] D. Steiner and A. Fischer. Planar parameterization for closed 2-manifold genus-1 meshes. In *Proceedings of the ninth ACM symposium on Solid modeling and applications*, pages 83–91. Eurographics Association, 2004.
- [22] A. Tsui, D. Fenton, P. Vuong, J. Hass, P. Koehl, N. Amenta, D. Coeurjolly, C. DeCarli, and O. Carmichael. Globally optimal cortical surface matching with exact landmark correspondence. In *Information processing in medical imaging: proceedings of the... conference*, volume 23, page 487. NIH Public Access, 2013.
- [23] W. T. Tutte. How to draw a graph. *Proceedings of the London Mathematical Society*, 3(1):743–767, 1963.

5 DISCRETE CONFORMAL GEOMETRY

Keenan Crane

5.1 Overview

What can be understood about a surface by taking measurements only with a protractor, but not a ruler? In other words, what information about a surface is encoded by *angles*, but not *lengths*? This question encapsulates the basic viewpoint of *conformal geometry*, which studies *holomorphic* or (loosely speaking) *angle-preserving* maps between manifolds. In the discrete setting, however, the idea of directly preserving angles leads to an interpretation of conformal geometry that is far too *rigid*, *i.e.*, the space of discrete solutions looks far more restricted than the space of smooth solutions it hopes to capture. Instead, one must consider how several equivalent points of view in the smooth setting lead to a number of *inequivalent* treatments of conformal geometry in the discrete setting.



Why study discrete conformal geometry? From an analytic point of view, *smooth* conformal maps provide a strong notion of regularity, since they are locally complex analytic and hence have derivatives of all orders. In the discrete setting one therefore obtains a strong notion of what it means for a discrete (*e.g.*, simplicial) map to be “regular,” even in situations where no derivatives are available in the classical sense. From a topological point of view, conformal maps help one define canonical mappings between spaces—for instance, the *uniformization theorem* effectively provides a (near-)canonical map between any two surfaces via conformal maps to a canonical surface of constant curvature. Likewise, discrete conformal geometry can be used to obtain (near-)canonical maps between discrete surfaces, even when (for instance) two surfaces do not have compatible triangulations. In applications, discrete conformal geometry has become a powerful starting point for digital geometry processing algorithms, since many problems ultimately boil down to sparse linear algebra problems or easy convex optimization. Conformal geometry can also be used to provide a common, canonical reference domain where many problems can be more easily solved, and over which different pieces of geometry can be compared and analyzed.

Discretization of conformal maps is an excellent example of “The Game” played in discrete differential geometry, since there are a huge number of different (yet equivalent) characterizations of conformal maps in the smooth setting, each of which leads to a distinct analogue in the discrete setting. Consider a smooth, orientation-preserving map f from a disk-like surface M with Riemannian metric g to the flat complex plane \mathbb{C} . A fairly comprehensive list of ways to characterize smooth conformal maps then includes:

1. **(ANGLES)** Preservation of angles—at every point $p \in M$ the angle between any two tangent vectors $X, Y \in T_p M$ is the same as the angle between their images $df_p(X), df_p(Y)$ in the plane.
2. **(CIRCLES)** Preservation of circles—the image of any geodesic circle of radius ε approaches a Euclidean circle as ε goes to zero.
3. **(ANALYTIC)** The map f satisfies the *Cauchy-Riemann equation*— $df(\mathcal{J}X) = i df(X)$ for all vector fields X , where i is the complex unit and $\mathcal{J}_p : T_p M \rightarrow T_p M$ is the *linear complex structure* expressing a rotation by $\pi/2$ in each tangent space ($\mathcal{J}_p^2 = -\text{id}$).
4. **(METRIC)** Rescaling of the metric—the metric g on M is related to the induced metric $\tilde{g} := df \otimes df$ by a pointwise rescaling $\tilde{g} = e^{2u} g$ for some function $u : M \rightarrow \mathbb{R}$ called the *log conformal factor*.
5. **(CONJUGATE)** Conjugate harmonic functions—the map f can be expressed as $f = a + bi$, where a, b are real harmonic functions with orthogonal gradients of equal magnitude ($\nabla b = \mathcal{J}\nabla a$).
6. **(DIRICHLET)** Critical points of Dirichlet energy—among all homeomorphisms from M to a fixed disk-like region $\Omega \subset \mathbb{C}$, the map f is a critical point of the *Dirichlet energy* $E_D(f) := \int_M |df|^2 dA$, where dA is the area measure on M .
7. **(HODGE)** Hodge duality—the Hodge star on differential 1-forms induced by f is the same as the pushforward under this map of the Hodge star on the original domain.

To someone familiar with smooth conformal maps this list may sound rather redundant, since in many cases cases the conceptual leap between one characterization and another is very small. Yet these minor shifts in perspective often lead to substantially different interpretations in the discrete setting. In almost all such discretizations, the domain M itself is treated as either

1. a simplicial surface (*i.e.*, a “triangle mesh”), or
2. a quadrilateral net (*i.e.*, a “quad mesh”).

These notes focus primarily on the former. For each of these two choices, one smooth characterization tends to stick out: for discretizations based on quad nets, one is naturally led toward the analytic picture of Riemann surfaces and discrete complex analysis; we defer to [2] and references therein for a discussion of this point of view. For discretizations based on simplicial surfaces, the perspective of *conformally equivalent discrete metrics* leads to a theory equivalence that captures much of the structure found in the smooth setting (Sec. 5.6). In fact, the purpose of these notes is to (briefly) explain *why* conformal equivalence of discrete metrics is in some sense the “only” complete theory of discrete conformal equivalence for general simplicial surfaces⁴. Perhaps the next closest candidate is the *circle packing* viewpoint originally promoted by Thurston—this approach has some close connections to the metric viewpoint, but in general does not provide a complete picture for irregular triangulations of curved surfaces.

Other discretizations of conformal maps capture isolated aspects of the smooth theory, but are generally too *rigid* to provide a complete discrete theory (a situation akin to the phenomenon of “locking” in finite element theory). This statement should not be confused with a value judgement on *utility*: discretizations that do not exactly capture structures found in the smooth theory are often perfectly suitable for obtaining an accurate numerical approximation (especially on finely tessellated domains), and in practice tend to be less computationally demanding than those that furnish a precise discrete theory. The same trade off can in fact be found throughout discrete differential geometry: exact structure preservation often comes at significant computational cost. A conclusion that might be drawn here is that, from a practical point of view, “exact” discretizations are not worth the trouble since results of similar quality can often be obtained via more efficient numerical methods. A more mature point of view is that one can achieve the best of both worlds by using the two in conjunction: approximate numerical methods provide cheap initialization for more expensive exact methods, which in turn provide valuable guarantees about the behavior of the output. More broadly, discrete conformal maps help to bridge several areas of mathematics, including some rather remarkable connections between geometry, analysis, and pure combinatorics, as discussed below.

⁴We consider the case of general curved surfaces; a brief summary of discrete conformal maps from $\mathbb{C} \rightarrow \mathbb{C}$ can be found in [30].

5.2 Preliminaries

To simplify exposition we will mainly consider a smooth map f from a disk-like surface M with Riemannian metric g to the Euclidean complex plane \mathbb{C} . Restricting our attention to disk-like domains allows us to focus on “local” properties, and avoid issues of global topology. The differential $df_p f : T_p \rightarrow T_{f(p)}\mathbb{C}$ expresses how tangent vectors on M are pushed forward to \mathbb{C} . We will generally require f to be an *immersion*, meaning that its differential df is nondegenerate, *i.e.*, at each point $p \in M$, $df_p(X) = 0$ if and only if $X = 0$. Conformal maps are globally injective, whereas *holomorphic* maps can have isolated *branch points* where the differential fails to be injective. As discussed in Sec. 5.1, there are many equivalent ways to express that f is *conformal*; below we consider each of these characterizations and their discrete analogues. Finally, a *linear complex structure* associated with a surface (M, g) is a tangent space automorphism $\mathcal{J} : TM \rightarrow TM$ such that in each tangent space $T_p M$, (i) $\mathcal{J}_p^2 = -\text{id}$, and (ii) $g_p(X, \mathcal{J}_p X) = 0$; intuitively, \mathcal{J} defines a quarter-rotation in each tangent space compatible with the metric g (in analogy with the imaginary unit i in the complex plane), and is hence unique up to a global choice of orientation.

In the discrete setting, we will replace the smooth surface M with an abstract simplicial 2-manifold \widehat{M} with vertices V , edges E , and triangles F . Sequences of vertex indices are used to denote simplices, *e.g.*, $ij \in E$ denotes an edge with endpoints $i, j \in V$, and $ijk \in F$ denotes a triangle with vertices $i, j, k \in V$. The *simplicial star* $\text{St}(i)$ of a vertex $i \in V$ is the subcomplex of \widehat{M} consisting of simplices that contain i . A *discrete Riemannian metric* on \widehat{M} is an assignment of positive edge lengths $\ell : E \rightarrow \mathbb{R}_{>0}$ that satisfy the triangle inequality in each 2-simplex, *i.e.*, for each triangle $ijk \in F$, $\ell_{ij} + \ell_{jk} \geq \ell_{ik}$. Geometrically, then, a simplicial surface \widehat{M} with discrete metric ℓ can be viewed as a disjoint union of Euclidean triangles (with given edge lengths), identified along shared edges. The resulting space (\widehat{M}, ℓ) is a Riemannian manifold with a globally flat Euclidean metric, away from an isolated collection of *cone points* at vertices. Any map $\hat{f} : V \rightarrow \mathbb{C}$ can hence be naturally extended to a simplicial map over all of (\widehat{M}, ℓ) via simplexwise affine interpolation of values at vertices; we adopt this convention throughout. A map \hat{f} is a *discrete immersion* if it is locally injective, or equivalently, if for each vertex $i \in V$ the restriction of \hat{f} to $\text{St}(i)$ is injective. As in the smooth setting, the condition that \hat{f} is a (discrete) immersion not only precludes things like vanishing angles, zero-length edges, and zero-area triangles, but also avoids discrete branch points (see Fig. 23). We will use θ_i^{jk} to denote the interior angle of triangle ijk at vertex i .

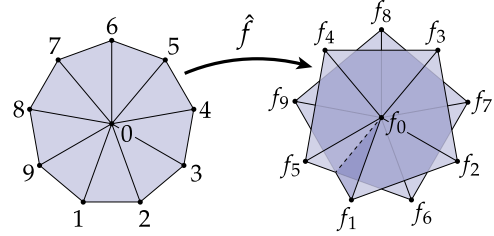


Figure 23: A discrete branch point, where a simplicial map fails to be a discrete immersion.

5.3 Angle Preservation

In the smooth setting, an immersion $f : M \rightarrow \mathbb{C}$ is conformal if at every point $p \in M$ the angle between any two tangent vectors $X, Y \in T_p M$ is the same as the angle between their images $df_p(X), df_p(Y)$ in the plane. A seemingly natural discrete analogue is to ask that for a discrete immersion $\hat{f} : \hat{M} \rightarrow \mathbb{C}$, the interior angles θ_i^{jk} at each corner i of each triangle $ijk \in F$ are preserved. However, it quickly becomes clear that a notion of discrete conformal equivalence based on exact preservation of angles is far too rigid: interior angles are preserved if and only if each triangle $ijk \in F$ experiences a similarity transformation, or equivalently, if the new and old edge lengths in each triangle ijk are related by a scale factor $\lambda_{ijk} > 0$, i.e., $\tilde{\ell}_{ab} = \lambda_{ijk} \ell_{ab}$ for $ab \in ijk$. At first glance this situation appears reminiscent of the characterization of (smooth) conformal maps in terms of a pointwise rescaling of the metric. However, since each interior edge is shared by two triangles, the scale factors λ_{ijk} must all be identical, i.e., any simplicial map that preserves interior angles is necessarily a global isometry, up to a global rescaling. In other words, an angle-based theory of conformal equivalence is entirely rigid: there is only one discrete metric in each such equivalence class. This elementary observation instigates a search for other notions of discrete conformal equivalence.

Alternatively, one can use a variational point of view to obtain a sort of weaker notion of discrete conformal map: roughly speaking, a discrete conformal map in this sense will be one that minimizes the deviation of angles from their original values [24]. More precisely, suppose we parameterize planar embeddings of a given simplicial disk by positive interior angles $\tilde{\theta}_i^{jk}$. In order to describe a discrete immersion, these angles must satisfy a collection of discrete integrability conditions that ensure they correspond to a planar discrete metric:

1. For each triangle $ijk \in F$, $\tilde{\theta}_i^{jk} + \tilde{\theta}_j^{ki} + \tilde{\theta}_k^{ij} = \pi$.
2. For each interior vertex $i \in V$, $\sum_{ijk \in \text{St}(i)} \tilde{\theta}_i^{jk} = 2\pi$.
3. For each interior vertex $i \in V$, $\prod_{ijk \in \text{St}(i)} \frac{\sin \tilde{\theta}_i^{jk}}{\sin \tilde{\theta}_k^{ij}} = 1$.

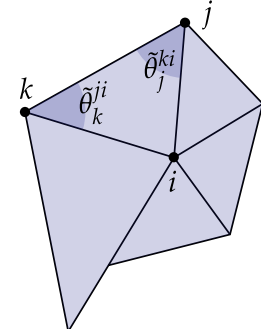


Figure 24: Collections of angles that exhibit Euclidean sums around triangles and vertices may still fail to characterize a valid triangulation.

The first condition is the usual Euclidean triangle postulate; the second is simply the requirement that every vertex have a Euclidean angle sum. As suggested in Fig. 24, the third condition is effectively a closure condition on edge lengths around each

vertex, obtained by applying the law of sines to the relationship

$$\prod_{ij \in \text{St}(i)} \frac{\tilde{\ell}_{i,j}}{\tilde{\ell}_{i,j+1}} = 1,$$

where $\tilde{\ell}_{i,j}$ and $\tilde{\ell}_{i,j+1}$ denote the lengths of consecutive edges in $\text{St}(i)$ (with respect to, say, counter-clockwise ordering). A discrete conformal map (in the sense of best angle preservation) is then any minimizer of the energy

$$E_{\text{ang}}(\tilde{\theta}) := \sum_{ijk \in F} (\tilde{\theta}_i^{jk} - \theta_i^{jk})^2,$$

subject to the condition that the new angles $\tilde{\theta}$ satisfy the discrete integrability conditions outlined above. From these angles one can trivially recover a unique discrete metric, and in turn a discrete immersion in the plane (up to Euclidean motions). Here again we observe too much rigidity in the sense that E_{ang} typically has only a single unique minimizer (up to Euclidean motions), whereas in the smooth setting there is a large family of conformal maps from any disk into the plane. However, this minimizer will at least exhibit a variable scaling of length across the domain, rather than a single global scale factor. Properties of such maps are not well-understood: empirically, they appear to approximate conformal maps of least area distortion under refinement, though this observation has never been carefully analyzed. A variety of numerical algorithms for computing such maps have been developed [24, 23, 31].

5.4 Circle Preservation

A linear map preserves angles if and only if it is the composition of a rotation and a dilation (no shear); hence, it also preserves circles. Since at each point $p \in M$ the differential df_p of a conformal map f is an angle-preserving linear map, it must also preserve infinitesimal circles. This point of view is the starting point for several distinct but closely-related approaches to discrete conformal maps, namely:

- circle packing,
- circle patterns, and
- inversive distance.

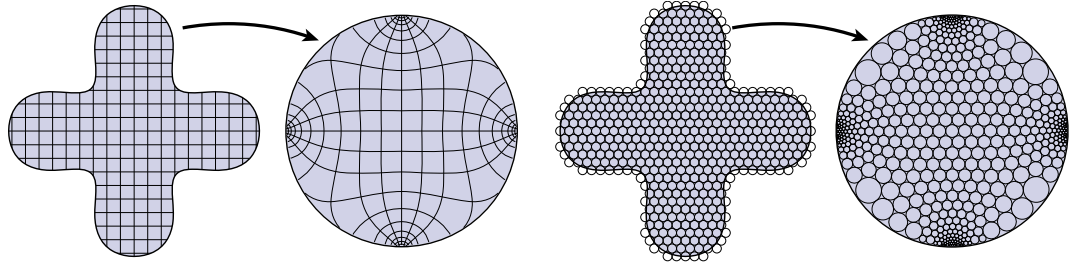


Figure 25: Left: a smooth Riemann mapping from a simply connected region in the plane to the unit circular disk. Right: a discrete Riemann mapping, expressed as a circle packing.

5.4.1 Circle Packing

A *circle packing* is a collection of closed circular disks in the plane (or other surface) that intersect only at points of tangency. (See [26] for an excellent overview.) To any such collection one can associate a graph $G = (V, E)$ where each vertex corresponds to a disk, and two vertices are connected by an edge if and only if their corresponding disks are tangent. A natural question to ask is: which graphs admit circle packings?

Theorem (Circle Packing). *Every planar graph $G = (V, E)$ can be realized as a circle packing.*

(For graphs that are not planar, one can consider circle packings on surfaces of higher genus.) A first hint that circle packings are connected to discrete conformal maps comes via the following theorem:

Theorem (Koebe). *If G is a connected maximal planar graph, then it has a unique circle packing up to Möbius transformations and reflections.*

Equivalently, since a maximal planar graph describes a triangulation of a disk (or the sphere, if one includes the outer face), Koebe's theorem says that any simplicial disk (or sphere) can be realized as a planar circle packing, and that applying a subsequent Möbius transformation gives another such realization. Likewise, if a smooth disk (M, g) is realized in the plane as the image of a conformal map $f : M \rightarrow \mathbb{C}$, post-composition with a conformal automorphism $\eta : \mathbb{C} \rightarrow \mathbb{C}$ (*i.e.*, a Möbius transformation) will give another conformal map $\tilde{f} := \eta \circ f$. However, this observation does not (yet) provide a complete picture of discrete conformal maps, since in the smooth setting the space of possible conformal flattenings of a disk is much larger than simply the Möbius transformations. One way to describe this space is via the *Riemann mapping theorem*:

Theorem. Any nonempty simply connected open set $\Omega \subsetneq \mathbb{C}$ can be mapped to the interior of the unit circular disk $D^2 := \{z \in \mathbb{C} \mid |z| < 1\}$ by a bijective map $\phi : \Omega \rightarrow D^2$ that is holomorphic (hence conformal) in both directions.

As a result, a disk (M, g) can be conformally mapped to any disk-like region Ω in the plane: let $f : M \rightarrow \mathbb{C}$ be a conformal flattening of M , let $\phi_\Omega : \Omega \rightarrow D^2$ be a Riemann map for Ω , and let $\phi_f : \text{im}(f) \rightarrow D^2$ be a Riemann map for the image of f . Then $\phi_\Omega^{-1} \circ \phi_f \circ f$ will be a conformal map from M onto Ω .

A more complete picture of circle packings as discrete conformal maps is likewise provided by a discrete analogue of uniformization, originally conjectured by Thurston, and later proved by Rodin and Sullivan [21]. Roughly speaking, the idea is to start with a regular hexagonal circle packing C of a simply connected region Ω by disks of radius $\varepsilon > 0$, i.e., for any hexagonal tiling of the plane, take only those disks that intersect Ω . Now find a circle packing C' that maintains the same incidence relationships, but where all disks along the boundary are now tangent to the unit circular disk D^2 (this idea is illustrated in Fig. 25, right). The relationship between these two packings defines an *approximate mapping* of Ω to D^2 : for sufficiently small ε any point $z \in \Omega$ will be contained in a circle c from C , and can be mapped to the center of the corresponding circle c' from C' . Rodin and Sullivan

show that the approximate mapping converges to a conformal homeomorphism as $\varepsilon \rightarrow 0$. As in the smooth setting, Möbius transformations of the unit disk provide the symmetry group for such mappings. Unlike the smooth setting, however, one cannot directly use circle packings to define discrete conformal maps between any two disk-like regions, since regular hexagonal packings of these regions will not in general have the same combinatorics. Moreover, this theory does not immediately account for curvature, or irregular triangulations of a domain. Consider for instance two simplicial disks with identical combinatorics but different discrete metrics (i.e., different edge lengths), as depicted in Fig. 26. Since circle packing depends only on combinatorics, both disks necessarily have identical realizations as circle packings in the unit disk—implying that all discrete metrics on a given simplicial disk are, effectively, conformally equivalent. In this sense, the standard theory of circle

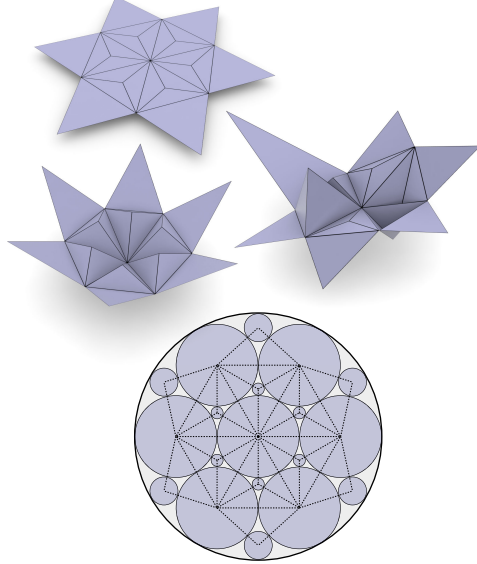


Figure 26: Discrete surfaces with identical combinatorics but different edge lengths (top) yield the same circle packing into the unit disk (bottom).

packings is *not rigid enough*. Thurston was however aware of a deeper connection between geometry and combinatorics. For instance, he writes [27]

"There are procedures to refine and modify any triangulation of a surface until every vertex has either 5, 6 or 7 triangles around it, or with more effort, so that there are only 5 or 6 triangles if the surface has positive Euler characteristic, only 6 triangles if the surface has zero Euler characteristic, or only 6 or 7 triangles if the surface has negative Euler characteristic. These conditions on triangulations are combinatorial analogues of metrics of positive, zero or negative curvature. How systematically can they be understood?"

Here one can also take a more local view, and imagine that the distribution of vertices of irregular degree in a combinatorial surface roughly corresponds to the distribution of Gaussian curvature on a smooth surface. Indeed, if one could produce, starting with a given smooth surface, a triangulation where (i) all edge lengths approach equal geodesic length and (ii) in each region the total deviation of vertex index from 6 is proportional to the total Gaussian curvature, one would likely obtain a circle packing into the unit disk that closely resembles the uniformization map for the original smooth surface.

5.4.2 Circle Patterns

Distinct from circle packings, which are purely combinatorial, circle *patterns* are determined by additional geometric data, namely the angle of intersection between neighboring circles. More precisely, consider an assignment of angles $\Phi : E \rightarrow (0, \pi]$ to the edges of a simplicial disk $\hat{M} = (V, E, F)$, and let $B \subset E$ denote the collection of edges along the boundary of \hat{M} . The *circle packing problem* seeks a discrete metric $\ell : E \rightarrow \mathbb{R}_{>0}$ such that

$$\begin{aligned}\Phi_{ij} &= \theta_k^{ij} + \theta_l^{ji}, \quad ij \in E \setminus B \\ \Phi_{ij} &= \theta_k^{ij}, \quad \quad \quad ij \in B\end{aligned}$$

where k and l denote vertices opposite ij (see Fig. 27). The first condition is equivalent to saying that the discrete metric exhibits a prescribed intersection angle between adjacent circles (and the second effectively provides boundary conditions). This problem can be solved by minimizing a

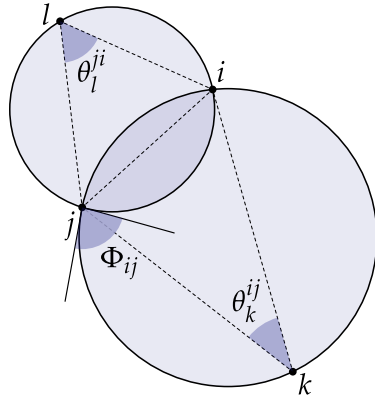


Figure 27: The circle pattern problem seeks a triangulation where circumcircles have prescribed intersection angles Φ .

convex functional [14] closely connected to variational principles for constructing ideal hyperbolic polyhedral with prescribed dihedral angles [20, 3]. Circle patterns naturally capture some features of the smooth theory: for instance, since both angles and finite circles are preserved by Möbius transformations, so too are intersection angles between circles. Like circle packings, however, the theory circle patterns does not furnish a completely satisfying notion of discrete conformality, since it does not exhibit many of the features found in the smooth setting. For instance, given a non-flat simplicial disk with intersection angles Φ , one will not in general find a flat metric that exhibits exactly the same intersection angles—even though, in the smooth setting, any disk can be conformally mapped to the Euclidean plane. On the other hand, circle patterns do have some close relationships to the theory of discrete conformal equivalence of discrete metrics, which we discuss in Sec. 5.6.

5.4.3 Inversive Distance

5.5 Cauchy-Riemann Equation

Perhaps the most traditional way to characterize smooth conformal maps is in terms of the *Cauchy-Riemann equations*, which say that a map $f : \mathbb{C} \rightarrow \mathbb{C}; (x, y) \mapsto u(x, y) + iv(x, y)$ is *holomorphic* if

$$\frac{\partial u}{\partial x} = \frac{\partial v}{\partial y} \quad \text{and} \quad \frac{\partial u}{\partial y} = -\frac{\partial v}{\partial x}. \quad (33)$$

If f is also an immersion (*i.e.*, the derivative df never vanishes), then it is *conformal*. On regular quadrilateral nets, where one has definite “x” and “y” directions, this traditional form of Cauchy-Riemann is a natural starting point for structure-preserving discretizations of holomorphic maps, which ultimately capture much of the rich structure found in complex analysis [2]. For general unstructured triangulations, one must take a different approach. A more suggestive way to write Eqn. 33 is

$$df(iX) = idf(X),$$

where i denotes the imaginary unit and X is any tangent vector field on \mathbb{C} . In other words, a complex map f is holomorphic if pushing forward vectors commutes with 90-degree rotation. A map f from a surface M with linear complex structure \mathcal{J} to the complex plane \mathbb{C} is likewise holomorphic if

$$df(\mathcal{J}X) = idf(X) \quad (34)$$

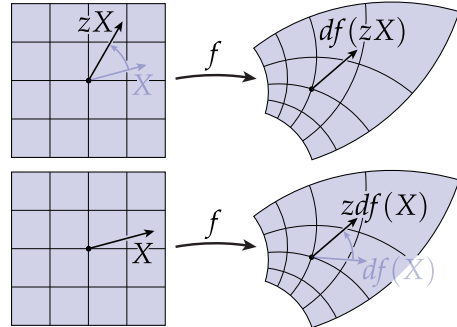


Figure 28: Geometrically, the Cauchy-Riemann equation asks that pushing forward vectors via given map f commutes with scaling and rotation.

for all tangent vector fields X on M . This characterization can be used as a starting point for discretizing Cauchy-Riemann on a simplicial surface $\hat{M} = (V, E, F)$ with discrete metric $\ell : E \rightarrow \mathbb{R}_{>0}$. In particular, consider a simplexwise affine map \hat{f} interpolating values $\hat{f}_i \in \mathbb{C}$ at vertices $i \in V$. Since each triangle has a well-defined Euclidean geometry, one can seek a map that satisfies Cauchy-Riemann in each triangle. Here, however, one encounters exactly the same kind of rigidity as when trying to preserve interior angles (Sec. 5.3): the only affine maps that satisfy Cauchy-Riemann are Euclidean motions and dilations. Since affine maps in individual triangles must agree across shared edges, the only piecewise affine maps \hat{f} that are globally holomorphic are isometries (up to a single global scale factor). Similar to “weak” angle preservation, one can define a discrete conformal map $\hat{f} : V \rightarrow \mathbb{C}$ (in the sense of Cauchy-Riemann) as a minimizer of the L^2 residual of Eqn. 34, *i.e.*, as the minimizer of the *conformal energy*

$$E_C(f) := \int_M |*df - idf|^2 dA, \quad (35)$$

where $*$ denotes the Hodge star on 1-forms. To minimize this energy in the discrete setting, one can apply the usual Galerkin finite element approach from numerical analysis (see [6, Chapter 7] for a detailed derivation). This approach was one of the earliest starting points for efficient algorithms in digital geometry processing [16]. As with the angle-based definition, the finite element approach yields a definition of discrete conformality that is again too rigid: generically, one obtains a unique minimizer, whose properties are not well-understood. One can however develop finite element methods that parameterize the full space of solutions, as discussed in Sec. 5.7.

5.6 Metric Scaling

In the smooth setting, two Riemannian metrics g, \tilde{g} on a surface M are *conformally equivalent* if they are related by a positive scaling, *i.e.*, if $\tilde{g} = \lambda g$ for some function $\lambda : M \rightarrow \mathbb{R}_{>0}$. A *conformal structure* on M is then an equivalence class of metrics. Since scaling is multiplicative, it is often useful to instead express the scale factor as $\lambda = e^{2u}$ for a function $u : M \rightarrow \mathbb{R}$ called the *log conformal factor*. Hence, e^u gives the length scaling, and e^{2u} is the area scaling. Superficially, this convention is useful since one does not need to worry about positivity. More importantly, since u is additive (whereas λ is multiplicative), one can often formulate easier linear equations, in both the smooth and discrete setting.

Recall that the metric of a discrete surface can be discretized as an assignment of edge lengths $\ell : E \rightarrow \mathbb{R}_{>0}$ that satisfy the triangle inequality in each face, *i.e.*, $\ell_{ij} + \ell_{jk} \geq \ell_{ki}$ for all $ijk \in F$. What does it mean for two discrete metrics $\ell, \tilde{\ell}$ to be

conformally equivalent? One idea is to simply ape the smooth definition and ask that $\tilde{\ell}_{ij} = \lambda_{ij}\ell_{ij}$ for some scale factor λ_{ij} on each edge $ij \in E$. This constraint is clearly “too flexible,” however, since then every pair of discrete metrics is conformally equivalent—simply let $\lambda_{ij} := \tilde{\ell}_{ij}/\ell_{ij}$. Also recall from Sec. 5.3 that a scale factor *per face* is “too rigid,” since one is then forced to make all scale factors equal. An approach taken by Luo [17] and others is to instead consider scale factors *per vertex*. Two discrete metrics are then considered discretely conformally equivalent if for each edge $ij \in E$,

$$\tilde{\ell}_{ij} = \lambda_i \lambda_j \ell_{ij},$$

for some collection of values $\lambda : V \rightarrow \mathbb{R}_{>0}$, or equivalently,

$$\tilde{\ell}_{ij} = e^{(u_i+u_j)/2} \ell_{ij},$$

for some collection of values $u : V \rightarrow \mathbb{R}$. These relationships again give the impression of merely mimicing the smooth relationship, and yet in this case the resulting theory is neither too rigid nor too flexible, but instead leads to a rich theory of discrete conformal equivalence that beautifully preserves much of the structure found in the smooth setting [3, 10], a perspective which has had a significant impact on (and has likewise been inspired by) algorithms from digital geometry processing [25, 1]. One elementary observation is that, locally, equivalence of discrete metrics is quite flexible:

Lemma 2. *Any two discrete metrics $\ell, \tilde{\ell}$ on a single triangle ijk are discretely conformally equivalent.*

Proof. The metrics are conformally equivalent if there exists an assignment of log scale factors u_i, u_j, u_k to the three vertices such that

$$e^{(u_a+u_b)/2} = \tilde{\ell}_{ab} / \ell_{ab}$$

for each edge $ab \in ijk$. Let $\lambda_{ij} := 2 \log(\ell_{ij})$ (and similarly for $\tilde{\ell}$). Then by taking the logarithm of the system above we obtain a linear system for the u values, namely

$$u_a + u_b = \tilde{\lambda}_{ab} - \lambda_{ab}, \quad \forall ab \in ijk.$$

This system has a unique solution, independent of the values of ℓ and $\tilde{\ell}$. In particular,

$$e^{u_i} = \frac{\tilde{\ell}_{ij} \ell_{jk} \tilde{\ell}_{ki}}{\ell_{ij} \tilde{\ell}_{jk} \ell_{ki}}, \tag{36}$$

and similarly for u_j, u_k . □

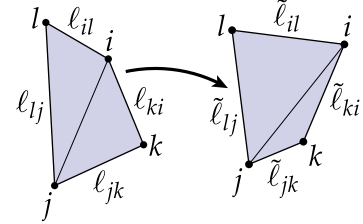


Figure 29: Two discrete metrics are considered conformally equivalent if for each pair of adjacent triangles the ratio of products of opposite edge lengths is equal.

At this point it might be tempting to believe that all discrete metrics are conformally equivalent, since they are equivalent on individual triangles. However, since scale factors (at vertices) are shared by several triangles, one still obtains an appropriate degree of rigidity. In particular, an important observation is that all metrics within the same discrete conformal equivalence class can be identified with a canonical collection of *length cross ratios* [25]:

Definition. Let $\ell : E \rightarrow \mathbb{R}_{>0}$ be a discrete metric on a simplicial surface $\hat{M} = (V, E, F)$. For any pair of triangles $ijk, jil \in F$ sharing a common edge $ij \in E$, the associated *length cross ratio* is the quantity

$$\mathfrak{c}_{ijkl} := \frac{\ell_{il}\ell_{jk}}{\ell_{ki}\ell_{lj}}.$$

Theorem. Two discrete metrics $\ell, \tilde{\ell}$ are discretely conformally equivalent if and only if they induce the same length cross ratios $\mathfrak{c}, \tilde{\mathfrak{c}}$.

Proof. First suppose that $\ell, \tilde{\ell}$ are discretely conformally equivalent, i.e., that $\tilde{\ell}_{ij} = e^{(u_i+u_j)/2} \ell_{ij}$ for some collection of log conformal factors $u_i : V \rightarrow \mathbb{R}$. Then

$$\tilde{\mathfrak{c}}_{ijkl} = \frac{\tilde{\ell}_{il}\tilde{\ell}_{jk}}{\tilde{\ell}_{ki}\tilde{\ell}_{lj}} = \frac{e^{(u_i+u_l)/2}e^{(u_j+u_k)/2}\ell_{il}\ell_{jk}}{e^{(u_k+u_i)/2}e^{(u_l+u_j)/2}\ell_{ki}\ell_{lj}} = \frac{\ell_{il}\ell_{jk}}{\ell_{ki}\ell_{lj}} = \mathfrak{c}_{ijkl}.$$

Now suppose that $\ell, \tilde{\ell}$ induce identical cross ratios, i.e., $\mathfrak{c} = \tilde{\mathfrak{c}}$. By Lemma 2, these metrics already satisfy the conformal equivalence relation on individual triangles. In particular, for any pair of adjacent triangles ijk, jil , we can find compatible log scale factors u_i, u_j, u_k and v_j, v_i, v_l . Moreover, these scale factors will agree on the shared edge ij if and only if $u_i = v_i$ and $u_j = v_j$. Applying Eqn. 36) we discover that this compatibility condition is equivalent to

$$\frac{\ell_{jk}}{\ell_{jk}} \frac{\tilde{\ell}_{ki}}{\ell_{ki}} = \frac{\tilde{\ell}_{il}}{\ell_{il}} \frac{\ell_{lj}}{\tilde{\ell}_{lj}},$$

i.e., equality of cross ratios. □

In particular, it is not hard to show that for a simplicial surface in \mathbb{R}^n , length cross ratios will be preserved by Möbius transformations of the vertices (assuming that the transformed vertices are connected by straight segments rather than circular arcs). As in the smooth setting, however, the space of discrete conformal maps is much larger than just the space of Möbius transformations. One characterization is that discrete conformal maps (in the sense of metric scaling) correspond to piecewise projective maps that preserve triangle circumcircles [25, Section 3.4]. Connections

between conformally equivalent discrete metrics and piecewise Möbius transformations have also been studied [28]. A more surprising connection is that the problem of finding a discrete metric with prescribed cross ratios is equivalent to finding an ideal hyperbolic polyhedron with prescribed edge lengths [3]. This observation provides a fascinating connection to the circle packing problem (Sec. 5.4.1), which is equivalent to finding a hyperbolic polyhedron with prescribed dihedral angles.

5.7 Conjugate Harmonic Pairs

Suppose we express a holomorphic map $f : M \rightarrow \mathbb{C}$ as $f = a + bi$ for a pair of real-valued functions a, b on a smooth surface (M, g) . A straightforward consequence of Cauchy-Riemann is that a and b are *conjugate harmonic functions*, i.e., they are real harmonic functions with orthogonal gradients:

$$\begin{aligned}\Delta a &= 0, \\ \Delta b &= 0, \\ \nabla b &= \mathcal{J} \nabla a,\end{aligned}$$

Here Δ is the Laplace-Beltrami operator on M , Δ is the gradient operator, and \mathcal{J} is the linear complex structure. Starting from the perspective of real harmonic functions is attractive from the perspective of discretization, since discrete harmonic functions are well-studied. In the simplicial setting, a discrete harmonic function is naturally defined as a simplexwise affine function in the kernel of a discrete Laplace-Beltrami operator, as discussed in Sec. 2. From this point of view, one need only define a discrete notion of conjugacy in order to obtain a definition of discrete conformal maps.

What does it mean for two discrete harmonic functions to be conjugate? One idea, studied by Mercat and others [18], is to consider functions on the combinatorial or *Poincaré dual* of a simplicial surface $\hat{M} = (V, E, F)$, which associates each vertex with a 2-cell, each edge with a 1-cell, and each triangle with a 0-cell. In this setting, two real-valued functions \hat{a}, \hat{b} on the primal and dual 0-cells (*resp.*) are discretely conjugate if for each edge e and corresponding dual edge e^* , the difference of \hat{a} values across e is equal to the difference of \hat{b} values across e^* , up to a scale factor $w_e \in \mathbb{R}$ that accounts for the geometry of the triangulation (as discussed in Sec. 5.9). In other words, if

$$\hat{b}_{j^*} - \hat{b}_{i^*} = w_{ij}(\hat{a}_j - \hat{a}_i)$$

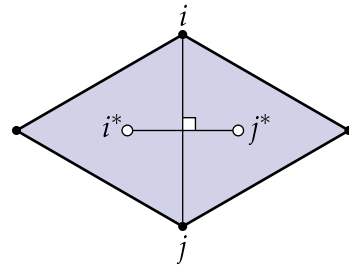


Figure 30: A function on primal (black) vertices is conjugate to a function on dual (white) vertices if the difference across each primal edge is equal to the difference across the corresponding dual edge, up to a constant factor that depends on the geometry of the triangulation.

for all edges $ij \in E$, where i^*, j^* are the associated dual vertices (see Fig. 30). Here one encounters two basic sources of difficulty. First, as detailed in Sec. 5.9, if one views the conformal structure of a simplicial surface as being determined by the edge weights w_{ij} (or *discrete Hodge star*), then one encounters severe rigidity: the weights uniquely determine a discrete metric. Moreover, pairs of functions \hat{a}, \hat{b} that are conjugate in this sense do not define a *simplicial* mapping from \widehat{M} to \mathbb{C} , since the coordinates \hat{b} are associated with 0-cells of the dual complex, rather than vertices of the original simplicial surface \widehat{M} .

Alternatively, one can take a variational approach: given a discrete harmonic function $\hat{a} : V \rightarrow \mathbb{R}$, its conjugate can be defined as the function $\hat{b} : V \rightarrow \mathbb{R}$ that minimizes the L^2 difference between $\mathcal{J}\nabla\hat{a}$ and $\nabla\hat{b}$, where \hat{a} and \hat{b} are interpreted as simplexwise affine functions interpolating values at vertices. The resulting map $\hat{f} := \hat{a} + \hat{b}i$ is then discrete conformal in the same sense as the finite element point of view discussed in Sec. 5.5 (see [22, Section 4.3.3]). Here, however, one obtains a more flexible point of view: whereas a “least squares” conformal map [16] is the unique (up to Euclidean motions) minimizer of the discrete conformal energy \hat{E}_C (Eqn. 35), one now has a whole family of discrete conformal maps \hat{f} parameterized by the given harmonic function \hat{a} . Since discrete harmonic functions are in turn parameterized by values at boundary vertices one ends up in precisely the same situation as in the smooth setting, where holomorphic maps $f : M \rightarrow \mathbb{C}$ can be parameterized by real functions on ∂M (see [22, Section 3.2] for a more detailed discussion). However, this notion of discrete conformal maps still does not preserve all the structure found in the smooth setting—for instance, there is no notion of composition of holomorphic functions, since the composition of two discrete harmonic functions is not necessarily discrete harmonic.

5.8 Critical Points of Dirichlet Energy

The *Dirichlet energy* of a differentiable map $f : \mathcal{M}_1 \rightarrow \mathcal{M}_2$ between Riemannian manifolds $\mathcal{M}_1, \mathcal{M}_2$ is the functional

$$E_D(f) := \int_{\mathcal{M}_1} |df|^2 dV,$$

where dV is the volume measure on \mathcal{M}_1 ; f is *harmonic* if it is a critical point of E_D . As discussed in Sec. 5.7, every conformal map from a disk-like surface M to the flat complex plane \mathbb{C} can be expressed as a pair of real harmonic functions. In some situations, however, one can instead simply ask that f itself is harmonic in the sense of being a critical point of E_D , leading once again to a different starting point for discretization. In particular, we have the following theorem in the smooth setting:

Theorem (Eells & Wood 1975). If $f : \mathcal{M}_1 \rightarrow \mathcal{M}_2$ is a harmonic map and $\chi(\mathcal{M}_1) + |\deg(f)\chi(\mathcal{M}_2)| > 0$, then f is either holomorphic or antiholomorphic (where χ denotes the Euler characteristic, and \deg is the topological degree).

(Antiholomorphic simply means angle-preserving and orientation *reversing*, rather than orientation preserving.) For instance, any harmonic map from the sphere to itself is automatically holomorphic (or antiholomorphic), since $\chi(S^2) = 2$. Likewise, any harmonic map f from a topological disk M to the unit disk $D^2 \subset \mathbb{C}$ will be (anti)holomorphic, since $\chi(M) = \chi(D^2) = 1$. Importantly, in this setting *harmonic* does not merely mean that each of the real components of $f = a + bi$ are harmonic (a condition which is necessary but not sufficient, as discussed in Sec. 5.7), but rather that f is a critical point of E_D among all continuous maps $f : M \rightarrow D^2$ that surjectively map ∂M to $\partial D^2 = S^1$.

For a simplicial surface $\hat{M} = (V, E, F)$ with discrete metric $\ell : E \rightarrow \mathbb{R}_{>0}$, one can define the discrete Dirichlet energy of a map $\hat{f} : V \rightarrow \mathbb{C}$ as

$$\hat{E}_D(\hat{f}) := \sum_{ij \in E} w_{ij} |f_j - f_i|^2 \quad (37)$$

for some collection of edge weights w_{ij} , such as the cotangent weights $w_{ij} := \frac{1}{2}(\cot \alpha_{ij} + \cot \beta_{ij})$ appearing in Eqn. 38. (Other definitions are also possible; see for instance [12].) A discrete conformal map to the disk is then a critical point of this energy, subject to the condition that boundary vertices are mapped to the unit circle, and the boundary polygon has a positive winding number relative to the origin (see Fig. 31 for two examples).

A closely related point of view is that, in the smooth setting, the conformal energy E_C (Eqn. 35) of any map $f : M \rightarrow \mathbb{C}$ can be expressed as the difference of its Dirichlet energy and the signed area $\mathcal{A}(f)$ of its image, *i.e.*,

$$E_C(f) = E_D(f) - \mathcal{A}(f)$$

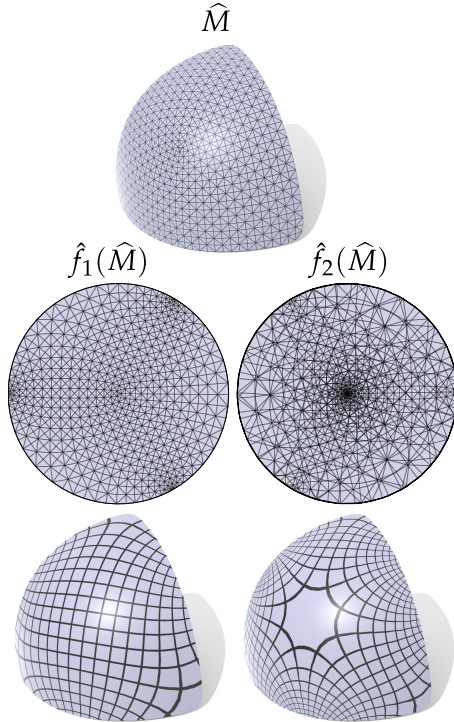


Figure 31: Top: two critical points \hat{f}_1, \hat{f}_2 of discrete Dirichlet energy among maps \hat{f} that take a simplicial disk \hat{M} to the unit circular disk in the plane. Bottom: maps visualized by pulling back coordinate lines under \hat{f}_1, \hat{f}_2 .

(see [6, Chapter 7]). In the case where the target is fixed (*e.g.*, if one considers only maps to the unit disk), the area term \mathcal{A} is constant, and hence E_D will have the same minimizers as E_C . More generally, one can define a discrete conformal map \hat{f} as a minimizer of the discrete Dirichlet energy \hat{E}_D (Eqn. 37) minus the signed area of the target polygon, which is another quadratic form in \hat{f} :

$$\hat{\mathcal{A}}(\hat{f}) := \frac{1}{2} \sum_{ij \in \partial \hat{M}} \hat{f}_i \times \hat{f}_j,$$

where $\partial \hat{M}$ denotes the collection of oriented edges in the boundary of \hat{M} . This point of view was considered by Hutchinson [13], and is used as the starting point for several algorithms in digital geometry processing [8, 19]. Note that this discrete conformal energy is identical to the energy considered in Sec. 5.5 [4]; its minimizers therefore exhibit the same degree of rigidity.

5.9 Hodge Duality

Consider the Hodge star $*$ on differential 1-forms α , which on a smooth surface with linear complex structure can be expressed via the relationship

$$*\alpha(X) = \alpha(JX)$$

for all tangent vector fields X ⁵. Since conformal maps preserve the linear complex structure, they therefore also preserve the 1-form Hodge star. In the discrete setting, one can reverse this relationship and try to *define* a discrete conformal map as one that preserves the (discrete) Hodge star [18]. In particular, differential forms can be discretized as cochains on a simplicial manifold and its polyhedral dual [29, 7]. A fairly common discretization of the Hodge star is then a “diagonal” linear map from primal k -cochains to dual $(n - k)$ -cochains determined by the ratio between primal and dual volumes. In the particular case of discrete 1-forms on a simplicial surface and its circumcentric dual, a discrete differential 1-form can be encoded via a value $\hat{\alpha}_{ij}$ per primal edge, and the corresponding (Hodge) dual 1-form can be expressed for each edge $ij \in E$ via the *cotangent formula*

$$*\alpha_{ij} := \frac{1}{2}(\cot \alpha_{ij} + \cot \beta_{ij})\alpha_{ij}, \quad (38)$$

where α_{ij}, β_{ij} are the angles opposite ij , as depicted in Fig. 32 (see [6, Section 6.3] for a calculation). A discrete conformal map in the sense of Hodge duality is then

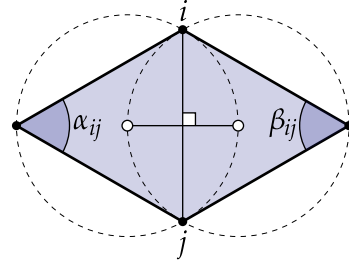


Figure 32: On a simplicial surface, the Hodge star on 1-forms is captured by the ratio of the length of each edge to the length of the orthogonal edge connecting triangle circumcenters.

⁵Note that some authors adopt an opposite orientation convention, *i.e.*, $*\alpha(X) = -\alpha(JX)$.

any simplicial map that preserves the sum $w_{ij} := \frac{1}{2}(\cot \alpha_{ij} + \cot \beta_{ij})$, or, from a more intrinsic point of view, any new assignment of edge lengths $\tilde{\ell}_{ij}$ that preserves this same quantity. Initially, one might be optimistic that a discretization based on the Hodge star yields less rigidity than one based on preservation of angles, since preservation of the edge weights w_{ij} effectively puts $|E| \approx 3|V|$ conditions on the map f , whereas exact preservation of interior angles θ_i^{jk} corresponds to $3|F| \approx 6|V|$ constraints. However, recent analysis [32, 9] extinguishes any such optimism:

Theorem. *The primal-dual length ratios $w_{ij} := \frac{1}{2}(\cot \alpha_{ij} + \cot \beta_{ij})$ on a given simplicial surface $\hat{M} = (V, E, F)$ uniquely determine the discrete metric $\ell : E \rightarrow \mathbb{R}$, up to global scaling.*

The proof relies on the fact that such ratios can be obtained as the minimizer of a convex object, where the Hessian at minimizers has a kernel consisting only of vectors corresponding to global scaling of ℓ . If one adopts an alternative notion of discrete metric based on the notion of *weighted triangulations*, then one obtains a closely related notion of discrete conformal equivalence based on *inversive distance* which is, finally, flexible [11, 9]. However, this notion of discrete conformal equivalence is not purely geometric in the sense that it requires auxiliary data: one cannot determine whether two simplicial surfaces are equivalent (in this sense) purely by reading off data from the triangulation itself. (See also Sec. 5.7 for discussion of a closely related point of view based on conjugate harmonic functions.)

5.10 Summary

The following table summarizes several different ways to discretize conformal maps from a disk-like surface M to the flat complex plane \mathbb{C} . To date, the approach based on conformal equivalence of discrete metrics appears to be the only one that exhibits the “right” amount of flexibility, *i.e.*, a space of discrete maps that is (loosely speaking) the same “size” as the one found in the smooth setting. Other definitions are typically too rigid (*e.g.*, no maps that exactly satisfy the definition, or only a single unique map) or too flexible (*e.g.*, providing no distinction between conformal equivalence and mere topological equivalence). However, as noted in Sec. 5.1 and discussed throughout, many of these discretizations nonetheless provide interesting connections to the smooth theory, and play an important role in practical algorithms. Moreover, while examining the simple “local” case of conformal flattening highlights many of the challenges of discretization, it is by no means a complete representation of contemporary work on discrete conformal geometry. Of particular interest are questions about *extrinsic* conformal geometry, *i.e.*, conformal surface immersions in \mathbb{R}^n , since a great deal of practical geometric

data processing involves transformations in three-dimensional space (rather than maps into two-dimensional surfaces like the plane or sphere). Some preliminary work has been done in this direction [5], including a recent theory compatible with the notion of conformally equivalent discrete metrics [15].

Approach	Data	Outcome	Comments
ANGLES (Sec. 5.3)	interior angles θ_i^{jk}	too rigid	similarity of triangles forces single global scale factor
CIRCLES (Sec. 5.4)	graph $G = (V, E)$	too flexible	only combinatorics are considered; no way to distinguish different metrics <i>e.g.</i> , cannot in general flatten while exactly preserving α
	intersection angles α_{ij}	too rigid	
METRIC (Sec. 5.6)	edge lengths ℓ_{ij}	just right	triangulation needs to be considered (Delaunay)
CONJUGATE (Sec. 5.7)	vertex coordinates f_i	too rigid	no composition; no Möbius transformations
DIRICHLET (Sec. 5.8)	vertex coordinates f_i	too rigid	(same as CONJUGATE)
HODGE (Sec. 5.9)	length ratio w_{ij}	too rigid	uniquely determines a discrete metric

Acknowledgements This work was supported by NSF Award #1717268.

REFERENCES

- [1] M. Ben-Chen, C. Gotsman, and G. Bunin. Conformal Flattening by Curvature Prescription and Metric Scaling. *CG Forum*, 2008.
- [2] A. Bobenko and F. Günther. Discrete Riemann Surfaces Based on Quadrilateral Cellular Decompositions. *Adv. Math.*, 311:885–932, 2017.
- [3] A. Bobenko, U. Pinkall, and B. Springborn. Discrete conformal maps and ideal hyperbolic polyhedra. *ArXiv e-prints*, May 2010.
- [4] D. Cohen-Steiner and M. Desbrun. Hindsight: LSCM and DNCP are One and the Same, 2002.
- [5] K. Crane. *Conformal Geometry Processing*. PhD thesis, Caltech, June 2013.
- [6] K. Crane, F. de Goes, M. Desbrun, and P. Schröder. Digital geometry processing with discrete exterior calculus. In *ACM SIGGRAPH 2013 Courses*, SIGGRAPH ’13. ACM, 2013.
- [7] M. Desbrun, A. N. Hirani, M. Leok, and J. E. Marsden. Discrete Exterior Calculus. *ArXiv Mathematics e-prints*, Aug. 2005.
- [8] M. Desbrun, M. Meyer, and P. Alliez. Intrinsic parameterizations of surface meshes. *Computer Graphics Forum*, 21(3):209–218, 2002.
- [9] F. d. Goes, P. Memari, P. Mullen, and M. Desbrun. Weighted triangulations for geometry processing. *ACM Trans. Graph.*, 33(3):28:1–28:13, June 2014.
- [10] X. Gu, F. Luo, J. Sun, and T. Wu. A discrete uniformization theorem for polyhedral surfaces. *ArXiv e-prints*, Sept. 2013.
- [11] R. Guo. Local rigidity of inversive distance circle packing. *ArXiv e-prints*, Mar. 2009.
- [12] J. Hass and P. Scott. Simplicial energy and simplicial harmonic maps. *ArXiv e-prints*, June 2012.
- [13] J. E. Hutchinson. Computing conformal maps and minimal surfaces. In *Theoretical and Numerical Aspects of Geometric Variational Problems*, pages 140–161, Canberra AUS, 1991. Centre for Mathematics and its Applications, Mathematical Sciences Institute, The Australian National University.
- [14] L. Kharevych, B. Springborn, and P. Schröder. Discrete conformal mappings via circle patterns. *ACM Trans. Graph.*, 25(2):412–438, Apr. 2006.
- [15] W. Y. Lam and U. Pinkall. Infinitesimal conformal deformations of triangulated surfaces in space. *ArXiv e-prints*, Feb. 2017.
- [16] B. Lévy, S. Petitjean, N. Ray, and J. Maillot. Least Squares Conformal Maps. *ACM Transactions on Graphics*, 21(3), 2002.
- [17] F. Luo. Combinatorial Yamabe Flow on Surfaces. *ArXiv Mathematics e-prints*, June 2003.
- [18] C. Mercat. Discrete Riemann Surfaces and the Ising Model. *Communications in Mathematical Physics*, 218:177–216, 2001.
- [19] P. Mullen, Y. Tong, P. Alliez, and M. Desbrun. Spectral conformal parameterization. In *Proceedings of the Symposium on Geometry Processing*, SGP ’08, pages 1487–1494, Aire-la-Ville, Switzerland, Switzerland, 2008. Eurographics Association.
- [20] I. Rivin. Euclidean structures on simplicial surfaces and hyperbolic volume. *Annals of Mathematics*, 139(3):553–580, 1994.
- [21] B. Rodin and D. Sullivan. The Convergence of Circle Packings to the Riemann Mapping. *J. Differential Geom.*, 26(2):349–360, 1987.
- [22] R. Sawhney and K. Crane. Boundary First Flattening. *ACM Trans. Graph.*, 36(5), 2017.

- [23] A. Sheffer, B. Lévy, M. Mogilnitsky, and A. Bogomyakov. ABF++ : Fast and Robust Angle Based Flattening. *ACM Trans. Graph.*, 24(2), 2005.
- [24] A. Sheffer and E. D. Sturler. Surface parameterization for meshing by triangulation flattening. In *Proc. 9th International Meshing Roundtable*, pages 161–172, 2000.
- [25] B. Springborn, P. Schröder, and U. Pinkall. Conformal Equivalence of Triangle Meshes. *ACM Trans. Graph.*, 27(3), 2008.
- [26] K. Stephenson. Circle packing: A mathematical tale. *Notices of the American Mathematical Society*, December 2003.
- [27] W. P. Thurston. Shapes of polyhedra and triangulations of the sphere. *ArXiv Mathematics e-prints*, Jan. 1998.
- [28] A. Vaxman, C. Müller, and O. Weber. Conformal mesh deformations with Möbius transformations. *ACM Trans. Graph.*, 34(4):55:1–55:11, July 2015.
- [29] S. O. Wilson. Geometric Structures on the Cochains of a Manifold. *ArXiv Mathematics e-prints*, May 2005.
- [30] W. Wood. Models of discrete conformal geometry. In *Proceedings of the Fifth Annual Conference for the Exchange of Mathematical Ideas*, Cedar Falls, IA, 2017.
- [31] R. Zayer, B. Lévy, and H.-P. Seidel. Linear Angle Based Parameterization. In *Proc. Symp. Geom. Proc.*, pages 135–141, 2007.
- [32] W. Zeng, R. Guo, F. Luo, and X. Gu. Discrete heat kernel determines discrete riemannian metric. *Graph. Models*, 74(4):121–129, July 2012.

6 OPTIMAL TRANSPORT ON DISCRETE DOMAINS

Justin Solomon

NOTE: This chapter is not yet complete.

6.1 Introduction

Many tools from discrete differential geometry (DDG) were inspired by practical considerations in areas like computer graphics and vision. Disciplines like these require fine-grained understanding of geometric structure and the relationships between different shapes—problems for which the toolbox from smooth geometry can provide substantial insight. Indeed, a triumph of discrete differential geometry is its incorporation into a wide array of computational pipelines, affecting the way artists, engineers, and scientists approach problem-solving across geometry-adjacent disciplines.

A key but neglected consideration hampering adoption of ideas in DDG in fields like computer vision and machine learning, however, is *resilience* to noise and uncertainty. The view of the world provided by video cameras, depth sensors, and other equipment is extremely unreliable. Shapes do not necessarily come to a computer as complete, manifold meshes but rather may be scattered clouds of points that represent e.g. only those features visible from a single position. Similarly, it may be impossible to pinpoint a feature on a shape exactly; rather, we may receive only a fuzzy signal indicating where a point or feature of interest *may* be located. Such uncertainty only increases in high-dimensional statistical contexts, where the presence of geometric structure in a given dataset is itself not a given. Rather than regarding this messiness as an “implementation issue” to be coped with by engineers adapting DDG to imperfect data, however, the challenge of developing principled yet noise-resilient discrete theories of shape motivates new frontiers in mathematical research.

Probabilistic language provides a natural means of formalizing notions of uncertainty in the geometry processing pipeline. In place of representing a feature or shape directly, we might instead use a probability distribution to encode a rougher notion of shape. Unfortunately, this proposal throws both smooth and discrete constructions off their foundations: We must return to the basics and redefine notions like distance, distortion, and curvature in a fashion that does not rely on knowing shape with infinite precision and confidence. At the same time, we must prove that the classical case is recovered as uncertainty diminishes to zero.

The mathematical discipline of *optimal transport* (OT) shows promise for making geometry work in the probabilistic regime. In its most basic form, optimal transport provides a means of lifting distances between points on a domain to distances between probability distributions *over* the domain. The basic construction of OT is to interpret probability distributions as piles of sand; the distance between two such piles of sand is defined as the amount of work it takes to transform one pile into the other. This intuitive construction gave rise to an alternative name for OT in the computational world: The “earth mover’s distance” (EMD) [10]. Indeed, the basic approach in OT is so natural that it has been proposed and re-proposed in many forms and with many names, from OT to EMD, the Mallows distance [7], the Monge–Kantorovich problem [13], the Hitchcock–Koopmans transportation problem [3, 6], the Wasserstein/Vaserštejn distance [12, 2], and undoubtedly many others.

Many credit Gaspard Monge with first formalizing the optimal transportation problem in 1781 [9]. Beyond its early history, modern understanding of optimal transport dates back only to the World War II era, through the Nobel Prize-winning work of Leonid Kantorovich [4]. Jumping forward several decades, while many branches of DDG are dedicated to making centuries-old constructions on smooth manifolds work in the discrete case, optimal transport has the distinction of continuing to be an active area of research in the mathematical community whose basic properties are still being discovered. Indeed, the computational and theoretical literature in this area move in lock-step: New theoretical constructions often are adapted by the computational community in a matter of months, and some key theoretical ideas in transport were inspired by computational considerations and constructions.

In these notes, we aim to provide some intuition about the relevance of OT to the discrete geometry pipeline. While a complete survey of work on OT or even just its computational aspects is worthy of a full textbook, here we focus on the narrower problem of how to make transport “work” on a shape represented as a simplicial complex or other discrete structure. The primary aim is to highlight the challenges in transitioning from smooth to discrete, to illustrate some basic constructions that have been proposed recently for this task, and—most importantly—to expose the plethora of open questions remaining in the relatively young discipline of computational OT. No-doubt incomplete references are provided to selected intriguing ideas in discrete OT, each of which is worthy of far more detailed discussion.

Disclaimer. These notes are intended as a short, intuitive, and *extremely* informal introduction to the specific problem of optimal transport on discrete domains like meshes. Optimal transport is a popular topic in mathematical research, and in-

Figure 33: A probability distribution (a) can be thought of as a “fuzzy” location of a point in \mathbb{R} . As the distribution sharpens about its mean to a δ -function, it encodes a classical piece of geometry: a point. This language, however, is fundamentally broader, including constructions like the superposition of two points (c) or of a point and a distribution (d).

terested readers should refer to surveys such as [13, 14] for more comprehensive discussion. The recent text [11] also provides discussion targeted to the applied world. A few recent surveys also are targeted to computational issues in optimal transport [8].

6.2 Motivation: From Probability to Discrete Geometry

To motivate the role of optimal transport in the context of geometry processing, we begin by considering the case of smooth probability distributions over the real numbers \mathbb{R} . Here, our geometry is extremely simple, described by values $x \in \mathbb{R}$ equipped with the distance metric $d(x, y) := |x - y|$. Then we expand to define the transport problem in full generality and state a few useful properties.

6.2.1 The Transport Problem

Define the space of probability measures over \mathbb{R} as $\text{Prob}(\mathbb{R})$; without delving into the formalities of measure theory, these are roughly the functions $\mu \in \text{Prob}(\mathbb{R})$ assigning probabilities to sets $S \subseteq \mathbb{R}$ such that $\mu(S) \geq 0$ for all measurable S , $\mu(\mathbb{R}) = 1$, and $\mu(\cup_i S_i) = \sum_i \mu(S_i)$ for disjoint sets $S_i \subseteq \mathbb{R}$. If μ is absolutely continuous, then it admits a *distribution function* $\rho(x) : \mathbb{R} \rightarrow \mathbb{R}$ assigning a probability density to every point:

$$\mu(S) = \int_S \rho(x) dx.$$

Measure theory, probability, and statistics all have their own interpretations of the set $\text{Prob}(\mathbb{R})$. Adding to the mix, we can think of optimal transport as giving a *geometric* interpretation to each $\mu \in \text{Prob}(\mathbb{R})$. In particular, as illustrated in Figure 33, roughly a probability distribution over \mathbb{R} can be thought of as a superposition of points in \mathbb{R} , whose weights are determined by $\rho(x)$. We can recover a (complicated) representation for a single point $x \in \mathbb{R}$ as a Dirac δ -measure centered at x .

From a physical perspective, we can think of distributions geometrically using a physical analogy. Suppose we are given a bucket of sand whose total mass is one

Figure 34: Two distributions ρ_0 and ρ_1 , nonzero in different places. No matter how far to the right ρ_1 is moved, the L_1 and KL divergence between these two distributions remains constant. The Wasserstein distance from optimal transport, however, increase linearly with distance over \mathbb{R} .

pound. We could distribute this pound of sand across the real numbers by stacking it all at a single point, concentrating it at a few points, or spreading it out more smoothly. Then, the height of the pile of sand is some expression of a geometric feature: Lots of sand at a point $x \in \mathbb{R}$ indicates we think a feature is located at x .

If we wish to lift basic notions from geometry to the more general space $\text{Prob}(\mathbb{R})$, perhaps the most basic object we must define is a notion of *distance* between two distributions $\mu_0, \mu_1 \in \text{Prob}(\mathbb{R})$. Supposing for now that μ_0 and μ_1 admit distribution functions ρ_0 and ρ_1 , respectively, a few candidate notions of divergence come to mind:

$$\begin{aligned} L_1 \text{ distance: } d_{L_1}(\rho_0, \rho_1) &:= \int_{-\infty}^{\infty} |\rho_0(x) - \rho_1(x)| dx \\ \text{KL divergence: } d_{\text{KL}}(\rho_0 \| \rho_1) &:= \int_{-\infty}^{\infty} \rho_0(x) \log \frac{\rho_0(x)}{\rho_1(x)} dx. \end{aligned}$$

These divergences are used widely in analysis and information theory, but they are insufficient for geometric computation. In particular, consider, the distributions ρ_0 and ρ_1 in Figure 34. As ρ_1 moves farther and farther to the right, the two distances above *do not change!* This is because they measure the overlap between ρ_0 and ρ_1 rather than their distance as functions over \mathbb{R} ; that is, the distance $d(x, y) = |x - y|$ is never used in the computation of these divergences.

Optimal transport resolves this issue by leveraging the physical analogy proposed above. In particular, suppose our sand is currently in arrangement ρ_0 and we wish to *reshape* it to a new distribution ρ_1 . We take a steam shovel and begin scooping up the sand in configuration ρ_0 where $\rho_0(x) > \rho_1(x)$ and dropping it places where $\rho_1(x) > \rho_0(x)$; eventually one distribution is transformed into the other.

There are many ways the steam shovel could approach its task: We could move sand efficiently, or we could drive it miles away and then drive back—wasting fuel in the process. But assuming $\rho_0 \neq \rho_1$, there is some amount of work inherent in the fact that at least one grain of sand must be moved. We can formalize this idea by solving for an unknown measure $\pi(x, y)$ determining how much mass gets moved from x to y by the steam shovel for each (x, y) pair. The minimum amount of work

is then

$$\mathcal{W}_1(\rho_0, \rho_1) := \begin{cases} \min_{\pi} & \iint_{\mathbb{R} \times \mathbb{R}} \pi(x, y) |x - y| dx dy & \text{Minimize total work} \\ \text{s.t.} & \pi \geq 0 \forall x, y \in \mathbb{R} & \text{Nonnegative mass} \\ & \int_{\mathbb{R}} \pi(x, y) dy = \rho_0(x) \forall x \in \mathbb{R} & \text{Starts from } \rho_0 \\ & \int_{\mathbb{R}} \pi(x, y) dx = \rho_1(y) \forall y \in \mathbb{R} & \text{Ends at } \rho_1. \end{cases} \quad (39)$$

This optimization problem quantifies the minimum amount of work—measured as mass $\pi(x, y)$ times distance traveled $|x - y|$ —required to transform ρ_0 into ρ_1 . We can think of the unknown function π as the instructions given to the laziest possible steam shovel tasked with dropping one distribution onto another. This amount of work is known as the *1-Wasserstein distance* in optimal transport; in one dimension, it equals the L_1 distance between the cumulative distribution functions of ρ_0 and ρ_1 . An example of ρ_0, ρ_1 , and the resulting π is shown in Figure [REF](#).

Generalizing slightly, we can define the p -Wasserstein distance:

$$[\mathcal{W}_p(\rho_0, \rho_1)]^p := \begin{cases} \min_{\pi} & \iint_{\mathbb{R} \times \mathbb{R}} \pi(x, y) |x - y|^p dx dy \\ \text{s.t.} & \pi \geq 0 \forall x, y \in \mathbb{R} \\ & \int_{\mathbb{R}} \pi(x, y) dy = \rho_0(x) \forall x \in \mathbb{R} \\ & \int_{\mathbb{R}} \pi(x, y) dx = \rho_1(y) \forall y \in \mathbb{R}. \end{cases} \quad (40)$$

In analogy to Euclidean space, many properties of \mathcal{W}_p are split into cases $p < 1$, $p = 1$, and $p > 1$; for instance, it is a distance any time $p \geq 1$. As we will see in § [REF](#), the $p = 2$ case is of particular interest in the literature and corresponds to a “least-squares” version of transport. Generalizing Eqn. 40 even more, if we replace $|x - y|^p$ with a generic cost function $c(x, y)$ we recover the *Kantorovich* problem.

It is important to note here an alternative formulation of the transport problem Eqn. 40. One could consider an alternative to optimizing for a function $\pi(x, y)$ that has an unknown for every possible (x, y) pair, in which instead a version in which the variable is a single function $\phi(x)$ that “pushes forward” ρ_0 onto ρ_1 ; this corresponds to choosing a single destination $\phi(x)$ for every source point x . In this case, the objective function would look like

$$\int_{-\infty}^{\infty} |\phi(x) - x|^p dx.$$

While this version corresponds to the original version of transport proposed by Monge, Figure [REF](#) shows what can go wrong in the general case: Sometimes it is necessary to split the mass at a single source point to multiple destinations. A triumph of theoretical optimal transport, however, shows that $\pi(x, y)$ is nonzero only on some set $\{(x, \phi(x))\}$ whenever ρ_0 is absolutely continuous, linking the two problems.

6.2.2 Discrete Problems in One Dimension

So far our definitions and discussion have not been amenable to numerical computation: Our unknowns are functions $\pi(x, y)$ with *infinite* numbers of variables (one value of π for each (x, y) pair in $\mathbb{R} \times \mathbb{R}$)—certainly more than can be stored on a computer with finite capacity. Continuing to work in one dimension, we suggest some special cases where we can solve the transport problem with a finite number of variables.

Rather than working with distribution functions $\rho(x)$, we will relax to the more general case of transport between measures $\mu_0, \mu_1 \in \text{Prob}(\mathbb{R})$. Define the Dirac δ -measure centered at $x \in \mathbb{R}$ via

$$\delta_x(S) := \begin{cases} 1 & \text{if } x \in S \\ 0 & \text{otherwise.} \end{cases}$$

It is easy to check that $\delta_x(\cdot)$ is a probability measure.

Suppose $\mu_0, \mu_1 \in \text{Prob}(R)$ can be written as *superpositions* of δ measures:

$$\mu_0 := \sum_{i=1}^{k_0} a_{0i} \delta_{x_{0i}} \quad \text{and} \quad \mu_1 := \sum_{i=1}^{k_1} a_{1i} \delta_{x_{1i}}, \quad (41)$$

where $1 = \sum_i a_{0i} = \sum_i a_{1i}$ and $a_{0i}, a_{1i} \geq 0$ for all i . Figure [REF](#) illustrates this case; all the mass of μ_0 and μ_1 is concentrated at a few isolated points.

In the case where the source and target distributions are composed of δ 's, we only can move mass between pairs of points $x_{0i} \mapsto x_{1j}$. Taking T_{ij} to be this total, we can solve for \mathcal{W}_p^p as

$$[\mathcal{W}_p(\mu_0, \mu_1)]^p = \left\{ \begin{array}{ll} \min_{T \in \mathbb{R}^{k_0 \times k_1}} & \sum_{ij} T_{ij} |x_{0i} - x_{1j}|^p \\ \text{s.t.} & T \geq 0 \\ & \sum_j T_{ij} = a_{0i} \\ & \sum_i T_{ij} = a_{1j}. \end{array} \right.$$

This is an optimization problem in $k_0 k_1$ variables T_{ij} : No need for an infinite number of $\pi(x, y)$'s! In fact, it is a *linear program* solvable using many classic algorithms, such as the simplex or interior point techniques [CITE](#). In fact, this provides a *convergent* means of approximating transport distances, in the sense that any measure can be well-approximated by a sum of the form Eqn. 41 in the Wasserstein metric [5].

There is a more subtle case where we can still represent the unknown in optimal transport using a finite number of variables. Suppose $\mu_0 \in \text{Prob}(\mathbb{R})$ is the superposition of δ measures and $\mu_1 \in \text{Prob}(\mathbb{R})$ is absolutely continuous, implying μ_1 admits

a distribution function $\rho_1(x)$:

$$\mu_0 := \sum_{i=1}^k a_i \delta_{x_i} \quad \text{and} \quad \mu_1(S) := \int_S \rho_1(x) dx. \quad (42)$$

This situation is illustrated in Figure [REF](#); it corresponds to transporting from a distribution whose mass is concentrated at a few points to a distribution whose distribution is more smooth. In the technical literature, this setup is known as *semidiscrete transport*.

Returning to the transport problem in Eqn. 40, in this semidiscrete case we can think of the coupling π as decomposing into a set of measures $\pi_1, \pi_2, \dots, \pi_k \in \text{Prob}(\mathbb{R})$ where each term in the sum Eqn. 42 has its own target distribution: $\delta_{x_i} \mapsto \pi_i$. As a sanity check, note that $\mu_1 = \sum_i a_i \pi_i(x)$.

Without loss of generality, we can assume the x_i 's are sorted, that is, $x_1 < x_2 < \dots < x_k$. Suppose $1 \leq i < j \leq k$, and hence $x_i < x_j$. In one dimension, it is easy to see that the optimal transport map π should never “leapfrog” mass, that is, the delivery target of the mass at x_i when transported to ρ_1 should be *to the left* of the target of mass at x_j , as illustrated in Figure [REF](#). This monotonicity property implies the existence of intervals $[a_1, b_1], [a_2, b_2], \dots, [a_k, b_k]$ such that π_i is supported in $[a_i, b_i]$ and $b_i < a_j$ whenever $i < j$; the mass $a_i \delta_{x_i}$ is distributed according to $\rho_1(x)$ in the interval $[a_i, b_i]$.

The semidiscrete transport problem corresponds to another case where we can solve a transport problem with a finite number of variables, the a_i 's and b_i 's. Of course, in one dimension these can be read off from the cumulative distribution function (CDF) of ρ_1 , but in higher dimensions this will not be the case.

While our discussion above gives two cases in which a computer could plausibly solve the transport problem, they do not correspond to the usual situation for DDG in which the geometry itself—in this case the real line \mathbb{R} —is discretized. As we will see in the discussion in future sections, there currently does not exist consensus about what to do in this case but several possible adaptations to this case have been proposed.

6.2.3 Moving to Higher Dimensions

We are now ready to state the optimal transport problem in full generality. Following [13, §1.1.1], take (X, μ) and (Y, ν) to be probability spaces, paired with a nonnegative measurable cost function $c(x, y)$. Define a *measure coupling* $\pi \in \Pi(\mu, \nu)$ as follows:

Definition 6 (Measure coupling). A *measure coupling* $\pi \in \text{Prob}(X \times Y)$ is a probability measure on $X \times Y$ satisfying

$$\begin{aligned}\pi(A \times Y) &= \mu(A) \\ \pi(X \times B) &= \nu(B)\end{aligned}$$

for all measurable $A \subseteq X$ and $B \subseteq Y$. The set of measure couplings between μ and ν is denoted $\Pi(\mu, \nu)$.

With this piece of notation, we can write the Kantorovich optimal transportation problem as follows:

$$\text{OT}(\mu, \nu; c) := \left\{ \begin{array}{ll} \min_{\pi \in \text{Prob}(X \times Y)} & \iint_{X \times Y} c(x, y) d\pi(x, y) \\ \text{s.t.} & \pi \in \Pi(\mu, \nu). \end{array} \right. \quad (43)$$

Here, we use some notation from measure theory: $d\pi(x, y)$ denotes integration against probability measure π . Note if π admits a distribution function $p(x, y)$ then we can write $d\pi(x, y) = p(x, y) dx dy$; the more general notation allows for δ measures and other objects that cannot be written as functions.

We note a few interesting special cases below:

Discrete transportation. Suppose $X = \{1, 2, \dots, k_1\}$ and $Y = \{1, 2, \dots, k_2\}$. Then, a probability measure $\mu \in \text{Prob}(X)$ can be written as a vector $v \in \mathbb{S}_n$, where \mathbb{S}_n denotes the n -dimensional probability simplex:

$$\mathbb{S}_n := \left\{ v \in \mathbb{R}^n : v \geq 0 \text{ and } \sum_i v_i = 1 \right\}. \quad (44)$$

Our cost function becomes discrete as well and can be written as a matrix $C = (c_{ij})$. After simplification, the transport problem between $v \in \mathbb{S}_{k_1}$ and $w \in \mathbb{S}_{k_2}$ given cost matrix C becomes

$$\text{OT}(v, w; C) = \left\{ \begin{array}{ll} \min_{T \in \mathbb{R}^{k_1 \times k_2}} & \sum_{ij} T_{ij} c_{ij} \\ \text{s.t.} & T \geq 0 \\ & \sum_j T_{ij} = v_i \forall i \in \{1, \dots, k_1\} \\ & \sum_i T_{ij} = w_j \forall j \in \{1, \dots, k_2\}. \end{array} \right.$$

This linear program is solvable computationally and is the most obvious way to make optimal transport work in a discrete context. It was proposed in the computational literature as the “earth mover’s distance” (EMD) [10]. When $k_1 = k_2 := k$ and C is symmetric, nonnegative, and satisfies the triangle inequality, one can check that $\text{OT}(\cdot, \cdot; C)$ is a distance on \mathbb{S}_k ; see [1] for a clear proof of this property.

Wasserstein distance. Next, suppose $X = Y = \mathbb{R}^n$, and take $c_{n,p}(x, y) := \|x - y\|_2^p$. Then, we recover the *Wasserstein distance* on $\text{Prob}(\mathbb{R}^n)$, defined via

$$\mathcal{W}_p(\mu, \nu) := [\text{OT}(\mu, \nu; c_{n,p})]^{1/p}.$$

\mathcal{W}_p is a distance when $p \geq 1$, and \mathcal{W}_p^p is a distance when $p \in [0, 1)$ [13, §7.1.1]. In fact, the Wasserstein distance can be extended to probability measures over manifold or even Polish spaces via the same formula.

6.2.4 One Problem, Many Forms

6.3 Motivating Applications

6.4 One Problem, Many Discretizations

6.5 Beyond Transport

REFERENCES

- [1] M. Cuturi and D. Avis. Ground metric learning. *Journal of Machine Learning Research*, 15(1):533–564, 2014.
- [2] R. L. Dobrushin. Definition of random variables by conditional distributions. *Teoriya Veroyatnostei i ee Primeneniya*, 15(3):469–497, 1970.
- [3] F. L. Hitchcock. The distribution of a product from several sources to numerous localities. *Studies in Applied Mathematics*, 20(1-4):224–230, 1941.
- [4] L. V. Kantorovich. On the translocation of masses. In *Dokl. Akad. Nauk SSSR*, volume 37, pages 199–201, 1942.
- [5] B. Kloeckner. Approximation by finitely supported measures. *ESAIM: Control, Optimisation and Calculus of Variations*, 18(2):343–359, 2012.
- [6] T. C. Koopmans. Exchange ratios between cargoes on various routes. 1941.
- [7] E. Levina and P. Bickel. The earth mover’s distance is the Mallows distance: Some insights from statistics. In *Proc. ICCV*, volume 2, pages 251–256. IEEE, 2001.
- [8] B. Levy and E. Schwindt. Notions of optimal transport theory and how to implement them on a computer. *arXiv:1710.02634*, 2017.
- [9] G. Monge. Mémoire sur la théorie des déblais et des remblais. *Histoire de l’Académie Royale des Sciences de Paris*, 1781.
- [10] Y. Rubner, C. Tomasi, and L. J. Guibas. The earth mover’s distance as a metric for image retrieval. *International journal of computer vision*, 40(2):99–121, 2000.
- [11] F. Santambrogio. *Optimal transport for applied mathematicians*. Springer, 2015.
- [12] L. N. Vaserštejn. Markov processes over denumerable products of spaces, describing large systems of automata. *Problemy Peredachi Informatsii*, 5(3):64–72, 1969.
- [13] C. Villani. *Topics in optimal transportation*. Number 58. American Mathematical Soc., 2003.
- [14] C. Villani. *Optimal transport: old and new*, volume 338. Springer Science & Business Media, 2008.